8-2020

Managing power system congestion and residential demand response considering uncertainty

Xiao Kou
University of Tennessee, xkou1@vols.utk.edu

To the Graduate Council:

I am submitting herewith a dissertation written by Xiao Kou entitled "Managing power system congestion and residential demand response considering uncertainty." I have examined the final electronic copy of this dissertation for form and content and recommend that it be accepted in partial fulfillment of the requirements for the degree of Doctor of Philosophy, with a major in Electrical Engineering.

Fangxing Li, Major Professor

We have read this dissertation and recommend its acceptance:

Mohammed Olama, Hector Pulgar, Mingzhou Jin

Accepted for the Council:

Dixie L. Thompson

Vice Provost and Dean of the Graduate School

(Original signatures are on file with official student records.)

Managing Power System Congestion and Residential Demand Response Considering Uncertainty

A Dissertation Presented for the

Doctor of Philosophy

Degree

The University of Tennessee, Knoxville

Xiao Kou

August 2020

Acknowledgment

First and foremost, I would like to express my deepest gratitude to my advisor, Dr. Fangxing (Fran) Li, for his continuous support of my work on this dissertation and all other research works during the course of my Ph.D. program at the University of Tennessee.

I am grateful to Dr. Mohammed Olama, Dr. Hector Pulgar, and Dr. Mingzhou Jin for devoting their time and effort to serve as my dissertation committee members.

I would like to thank the members of the Electric Network Laboratory for Intelligent Transactive ENergy (ENLITEN Lab), including Dr. Qinran Hu, Dr. Xue Li, Dr. Haoyu Yuan, Dr. Xin Fang, Dr. Can Huang, Dr. Riyasat Azim, Dr. Linquan Bai, Dr. Hantao Cui, Dr. Qingxin Shi, Mr. Wei Feng, Ms. Yan Du, Ms. Mariana Kamel, Mr. Qiwei Zhang, Mr. Ben Ollis, Mr. Xiaofei Wang, Mr. Haoyuan Sun, and Mr. Buxin She for their discussions of my research works.

My special thanks go to Ms. Helia Zandi and Dr. Mohammed Olama from the Oak Ridge National Laboratory (ORNL) for providing me with the opportunity to join their research teams. Without their precious support, it would have been impossible for me to finish this dissertation. In addition, I would like to thank other collaborators from the ORNL including Dr. Teja Kuruganti, Mr. Yaosuo Xue, Dr. Jin Dong, Dr. Yang Chen, Dr. Michael Starke, Dr. Ozgur Ozmen, Dr. James Nutaro, Dr. Piljae Im, and Mr. Larry Roberts.

Finally, I would like to thank my parents, whose love and encouragement has been with me throughout my life.

Abstract

Electric power grids are becoming increasingly stressed due to political and environmental difficulties in upgrading transmission capacity. This challenge receives even more interests with the paradigm change of increasing renewable energy sources and demand response (DR) programs. Among DR technologies, existing DR programs are primarily designed for industrial and commercial customers. However, household energy consumption accounts for 38% of total electricity consumption in the U.S., suggesting a significant missed opportunity. This dissertation presents an in-depth study to investigate managing power system congestion and residential DR program under uncertainty.

First, an interval optimization model is presented for available transfer capability (ATC) evaluation under uncertainties. The conventional approaches of ATC assessment include deterministic and probabilistic methods. However, the proposed interval optimization model can effectively reduce the accuracy requirements on the renewable forecasting, and lead to acceptable interval results by mitigating the impacts of wind forecasting and modeling errors.

Second, a distributed and scalable residential DR program is proposed for reducing the peak load at the utility level. The proposed control approach has the following features: 1) it has a distributed control scheme with limited data exchange among agents to ensure scalability and data privacy, and 2) it reduces the utility peak load and customers' electricity bills while considering household temperature dynamics and network flow.

Third, the impacts of weather and customers' behavior uncertainties on residential DR are also studied in this dissertation. A new stochastic programming-alternating direction method of multipliers (SP-ADMM) algorithm is proposed to solve problems related to

weather and uncertain customer behavior. The case study suggests that the performance of residential DR programs can be further improved by considering these stochastic parameters.

Finally, a deep deterministic policy gradient-based (DDPG-based) HVAC control strategy is presented for residential DR programs. Simulation results demonstrate that the DDPG-based approach can considerably reduce system peak load, and it requires much less input information than the model-based methods. Also, it only takes each agent less than 3 seconds to make HVAC control actions. Therefore, the proposed approach is applicable to online controls or the cases where accurate building models or weather forecast information are not available.

Keywords: alternating direction method of multipliers (ADMM), available transfer capability (ATC), congestion management, deep deterministic policy gradient (DDPG), demand response (DR), electricity market, interval optimization, reinforcement learning (RL), stochastic programming (SP).

Contents

List of Tables

List of Figures

List of Abbreviations

ADMM	Alternating direction method of multipliers
ATC	Available transfer capability
CBM	Capacity benefit margin
CPF	Continuous power flow
DDPG	Deep deterministic policy gradient
DERs	Distributed energy resources
DR	Demand response
DSO	Distribution system operator
DSRs	Demand response resources
ESS	Energy storage system
ETC	Existing transmission commitment
EV	Electric vehicle
EWH	Electric water heater
HEMS	Home energy management system
HVAC	Heating, ventilation, and air conditioning
ISO	Independent system operator
LAs	Load aggregators
LP	Linear programming
MCS	Monte Carlo simulation
MILP	Mixed integer linear programming
MSE	Mean square error
NERC	North American Electric Reliability Corporation
OASIS	Open Access Same-time Information System
OPF	Optimal power flow
PCC	Point of common coupling
PDF	Probability distribution function
PTDF	Power transfer distribution factor
PV	Photovoltaics
RC	Resistance-capacitance
RL	Reinforcement learning

RPF	Repeated power flow
SOC	State of charge
SP	Stochastic programming
TRM	Transmission reliability margin
TTC	Total transfer capability

Chapter 1 Introduction

Over the years, electric demand in the United States has increased significantly, and as a consequence, power system congestion has also been increased. However, few new transmission lines have been constructed to adapt to this change [1]. Power system congestion not only increases the locational marginal price at the congested load areas but also present severe threats to grid reliability by limiting the access to reserves [2]-[4]. Therefore, it is necessary to evaluate network congestion status and deploy demand response (DR) to reduce the system peak load as needed to maintain secure and economic operations of power grids.

1.1 Network congestion evaluation

Power system congestion happens when the transmission capacity is insufficient to simultaneously accommodate all requests for transmission service. To determine the congestion status, one of the most widely-used indices is the available transfer capability (ATC). In North America, transmission service providers (TSPs) are required to calculate the ATC and post it on the open access same-time information system (OASIS) to help the decision making of market participants [5]-[6]. ATC is defined as the remaining transfer capability in a transmission network for further commercial activities over already committed uses [7]. Underestimated ATC value may result in inadequate utilization of transmission system assets, while overestimated ATC value can cause overloading or system security issues [8]. There are two main types of ATC evaluation methods: deterministic and probabilistic [9].

In deterministic methods, the DC power transfer distribution factor (PTDF) has the fastest computation speed, but it ignores voltage limits and reactive power flow [10]. Repeated power flow (RPF) and continuous power flow (CPF) algorithms incrementally increase the power transaction until one of the operation limits is violated [11]-[12]. Even though the results from the RPF and CPF algorithms are more accurate than the results of the DC-PTDF algorithm, these approaches are time-consuming and thus cannot be used for online calculation. The optimal power flow (OPF) method first solves the economic dispatch, and then formulates an optimization problem to maximize the power transfer between the source and the sink areas [13].

Deterministic methods performed well when the uncertainty in power systems was small. However, with the increasing penetration of renewables, deterministic methods may fail to handle the large deviation between forecasted and actual values, limiting their potential for future power grid applications [14]. Therefore, growing attention has been paid to probabilistic methods, such as Monte Carlo simulation (MCS) and stochastic programming (SP) [15]-[16]. The fundamental idea is to convert the probabilistic problem into an equivalent deterministic problem. However, probabilistic methods heavily rely on weather forecasting technology. Much of the current literature assumes that uncertain parameters follow certain distributions, but this may not be aligned with the fact that the probabilistic distribution may not be readily available [17]-[19].

To overcome this challenge, interval optimization can be applied to ATC evaluation. The inputs of interval optimization are the bounds of the uncertain parameters, which reduces the requirements on input data and mitigates the impacts of wind modeling and forecasting errors. The outputs of interval optimization is also a range that contains possible ATC values.

1.2 Residential demand response

DR has been viewed as a lower-cost solution to reduce the peak load at the congested load area by changing the customers' electricity consumption behaviors [20]-[21]. Existing DR programs are primarily designed for industrial and commercial customers, since they tend to have larger electric loads that are much easier targeted. [22]. However, households account for 38% of the current total energy consumption in the United States, and over 212 million homes around the world are expected to join the utility DR programs by 2025, indicating the significance of conducting congestion management with residential DR [23]-[24]. Unlike the industrial or commercial load, the residential load is composed of numerous low-power home appliances. Further, the electricity consumption habits of customers are highly varied and dynamic. Therefore, residential DR algorithms must be scalable and consider customers' different preferences.

In literatures, there are two main residential DR management approaches: centralized methods and distributed methods [25].

Centralized methods apply to networks with customers' sharing the same control targets, e.g. maximizing the community social welfare. In this framework, operational data and constraints within residential buildings are needed to form an optimization problem at a centralized location. However, this limits the applications of centralized control approaches to small networks as the computational and communication needs can grow significantly with each additional entity.

In distributed schemes, optimization and controls are distributed to each residential building, leading to a reduced burden on the centralized system and a more scalable architecture. Moreover, as the information exchange between the centralized controller and

residential buildings is limited to economic signals and expected load responses, customers' can keep their device operation schedule information private.

Depending on the approach for driving the economic signal, residential DR can also be categorized into incentive-based or price-based [26]-[27].

In the incentive-based approach, the centralized system (often a load aggregator) make payments to the residential customers when the grid reliability is jeopardized or the market price is high. During the load reduction, the control center can either remotely control the residential load or penalize the residential customers who do not curtail their appliances. Examples of the incentive-based approaches include direct load control, curtailable service, and capacity market program [28].

In the price-based approach, the load aggregator offers Time of Use (ToU) rates to encourage customers to shift consumption. Price-based DR usually includes critical peak pricing, peak load pricing, and real-time pricing. Generally, residential customers can make their own choices on whether to change the load consumption for the 24-hour horizon or not [28].

The challenges for implementing large-scale optimization and controls of residential appliances are summarized as follows: 1) scalable algorithms to coordinate a large number of residential components, 2) data exchange mechanisms to protect customers' privacy, and 3) impacts of weather and customer behaviors uncertainties on system performance, and 4) model and parameter unavailability issues.

1.3 Dissertation outline

Chapter 2 presents the methodology for evaluating the ATC in transmission systems considering renewable integration. An interval optimization model is presented, which only requires the bounds of uncertainty without the precise data of wind power probabilistic distribution. Further, strong duality theory and artificial binary variables are introduced to convert the original combinatorial max-min problem to a single level maximization problem for efficient calculation.

Chapter 3 proposes a distributed and scalable algorithm for managing residential DR programs. First, a centralized optimization model is formulated to maximize community social welfare. Then, this model is solved in a distributed manner with the alternating direction method of multipliers (ADMM) by decomposing the original problem to a set of sub-problems. The advantages of this approach are 1) scalable and 2) only allows limited information exchange among agents to protect privacy.

Chapter 4 develops a stochastic programming based ADMM algorithm to study the impact of weather and customers' behavior uncertainties on residential DR programs. The proposed approach considers both the day-ahead and real-time electricity markets. In the first stage, residential customers determine the operating status of their devices (i.e. HVACs and electric water heaters (EWHs)), while the DSO calculates the needed amount of electricity to be purchased in the day-ahead market. In the second stage, the DSO participates in the real-time market to either purchase insufficient electricity or sell surplus electricity to maintain the supply-demand balance.

Chapter 5 presents a reinforcement learning based method to determine the HVAC operation status and realize the residential DR. The proposed deep deterministic policy

gradient (DDPG) algorithm does not require detailed building models or day-ahead weather forecast information. Rather, the control actions are calculated based on the current outdoor temperature, the current indoor temperature, the current time, and the non-responsive load in the system. The performance of the proposed approach is compared with the conventional thermostatic and model-based control approaches to demonstrate its performance.

Chapter 6 concludes the dissertation and provides directions for potential future work on network congestion management with residential DR.

1.4 Contributions

The contributions of this dissertation are as follows:

- This work proposes an interval optimization model to evaluate the congestion status of power systems under uncertainties.
- This work develops a scalable and distributed model-based approach to realize the residential DR with customers' privacy protected.
- This work studies the impacts of weather and customers' behavior uncertainties on model-based residential DR management programs.
- This work presents a DDPG based HVAC control strategy for residential DR programs and compares its performance with conventional thermostatic and model-based approaches.

Chapter 2 Interval Optimization for Available Transfer Capability (ATC) Evaluation Considering Wind Power Uncertainty

This chapter presents an interval optimization model for ATC evaluation to identify the power system congestion status. ATC is defined as the remaining amount of power that can be transferred between different areas over already committed capacity, and it provides valuable information for market participants. Under the paradigm of renewable power with uncertainty, it is reasonable to apply probabilistic ATC evaluation. However, the probabilistic distribution of uncertainty may not be readily available. In contrast, an interval optimization-based model only requires the bounds of uncertainty without the precise data of wind power probabilistic distribution. The purpose of introducing interval optimization is to determine the possible ATC range considering wind power uncertainty. In the proposed method, the original interval-based model is first decomposed into a lower boundary (optimistic) model and an upper boundary (pessimistic) model. Then, strong duality theory and artificial binary variables are applied to convert the combinatorial max-min problem in the pessimistic model to a single level maximization problem for efficient calculation.

Nomenclature

Sets and Indices

l	Index of transmission lines.
N / i	Set/index of buses.
T / t	Set/index of time intervals.

Parameters

c_i	Coefficients of the variables in the objective function.
$D_{i,t}$	Load demand at bus i during time interval t (MW).
$F_{l,t}$	The thermal limit of transmission line l during time interval t (MW).
$G_{i,t}^{min}$ / $G_{i,t}^{max}$	Minimum/maximum generation capacities of the thermal unit at bus i during time interval t (MW).
$gc_{i,t}$	Generation cost of the thermal unit at bus i during time interval t (\$/MWh).
$GSF_{i,l}$	Generation shift factor to line l from bus i.
L_i / U_i	Lower/upper bound of the variable x_i .
M	A large positive constant.
P_{CBM}	CBM (MW).
P_{TRM}	TRM (MW).
P_{TTC}	TTC (MW).
$R_{i,t}$	Ramping limits of the thermal units at bus i during time interval t (MW/h).
$\underline{W}_{i,t}$ / $\overline{W}_{i,t}$	Lower/upper bound of the predicted wind power generation at bus i during time interval t (MW).
α / β	Positive weight factors for the multi-objective function.

Variables

$D_{i,t}^{'}$	Load demand at bus i in the maximum transfer case during time interval t (MW).
$G_{i,t}$	Power generation at bus i in the base case during time interval t (MW).
$G_{i,t}^{'}$	Power generation at bus i in the maximum transfer case during time interval t (MW).
J	Multi-objective function value.
L	The Lagrange function.
P_{ATC}	Available transfer capability (MW).
P_{ETC}	Existing transmission commitment (MW).
x_i	The variables in the primal problem.
Z	The objective function value in the generalized LP model.
Z_{max}	Upper bound of the objective function value in the generalized LP model.

Z_{min}	Lower bound of the objective function value in the generalized LP model.
λ_i	The dual variable associated with the equality constraints in the primal problem.
λ_i^a	The dual variable associated with the power balance equation in the base case.
λ_b^i	The dual variable associated with the power balance equation in the maximum transfer case.
λ_c^i	The dual variable associated with the equality constraints other than the power balance equations in the primal problem.
γ_i^L / γ_i^U	The dual variable associated with the lower/upper bound of the variables in the primal problem.
v_i	The dual variable associated with the inequality constraints in the primal problem.
ω_i	Artificial binary variables.

2.1 Introduction

It is well known that many transmission infrastructures are becoming stressed due to the political and environmental difficulties in upgrading transmission capacity [29]. To solve this concern, the North American Electric Reliability Corporation (NERC) requires TSPs to evaluate ATC values of the transmission paths within their service regions [5]-[6]. Thus, operators can evaluate the congestion status of the grids and determine whether new power transaction requests can be approved. ATC also contributes to the identification and allocation of the transmission rights based on each TSP's risk tolerance for load shedding and their predictions of future conditions.

The conventional approaches to evaluate ATC are deterministic. For instance, a sensitivity-based DC power flow method is reported in [10]; a sensitivity-based AC power flow method is presented in [30]; in [31], the RPF method is implemented to evaluate the

ATC by gradually increasing the power transaction amount between the source and the sink areas; and in [9], a bi-level OPF approach is applied to calculate the ATC by formulating the ATC maximization problem in the upper level and the generation cost minimization problem in the lower level.

While deterministic methods have performed well in the past decade, the new paradigm change with more variable generations drives the need to address uncertainty in ATC evaluation. Thus, more attention has been paid to the probabilistic methods to model uncertainty and fluctuation in the renewable generation as non-constant values [32]-[34]. The fundamental idea is to apply statistical methods to convert the probabilistic problem into a deterministic problem [35]. In [36], a Monte Carlo based model is developed for ATC assessment, but it increases the computational burden since it needs to evaluate a large number of samples. In [37], a SP-based approach is used for ATC evaluation, and the generator availabilities, transmission line availabilities, and load variation are viewed as uncertain parameters, which comply with binomial distribution and normal distribution, respectively.

In summary, the uncertainty variables in previous works are usually assumed to follow certain pre-defined distributions, but this may not be aligned with the practical situations where probabilistic distribution may not be readily available [38]. Moreover, the performance of the previous research relies heavily on wind forecasting technology, which is subject to considerable errors or even data unavailability regarding wind probabilistic distribution, and therefore, it may further affect ATC calculations and the optimality of generation scheduling. To better address this challenge, an interval optimization-based approach is proposed in this chapter to evaluate ATC in power systems with renewables.

Interval optimization utilizes upper and lower boundaries to represent the uncertainty of random variables, and does not require the probability distribution function (PDF) of uncertain variables (e.g., wind power) [38]-[40]. In other words, the uncertain variables are modeled within a specific range, rather than via detailed and accurate probabilistic distribution. Further, the optimization result is also an interval, which is composed of a lower (optimistic) bound and an upper (pessimistic) bound. Therefore, interval optimization has a low requirement of input data regarding uncertainty without a PDF, but it can still give a range for the output variable. The interval optimization method is especially applicable to the cases where the PDF of uncertain factors is less accessible since it is much easier to obtain the boundaries of uncertain variables than their specific probabilistic description. Consequently, interval optimization is more practicable compared with other probability-based methods.

The main contributions of this chapter are summarized as the following:

1) The inputs for the proposed algorithm are the bounds of uncertain wind generation, rather than the PDF of wind generation. The introduction of interval optimization leads to acceptable interval results by mitigating the negative impacts of wind forecasting and modeling errors.

2) The pessimistic model in interval optimization is a combinatorial max-min optimization problem, which cannot be solved within polynomial time. This chapter improves the conventional solving algorithm by applying strong duality theory and introducing artificial binary variables for interval ATC evaluation. Finally, the pessimistic model is converted to a one-step maximization problem for efficient calculation.

3) As the system size grows, the solver for solving the pessimistic model may lead to unacceptable results. In this chapter, the power balance equation in the base case is relaxed to an inequality constraint to ensure the solvability of the solutions. Simulation results validate its effectiveness.

The rest of this chapter is structured as follows: Section 2.2 formulates the mathematical model for ATC evaluation, Section 2.3 presents the algorithm for solving interval optimization models, Section 2.4 demonstrates case studies to validate the proposed method, and Section 2.5 concludes the chapter.

2.2 The mathematical formulation for ATC evaluation

The generic mathematical formulation for ATC is usually presented as:

$$P_{ATC} = P_{TTC} - P_{ETC} - P_{CBM} - P_{TRM} \tag{2.1}$$

where total transfer capability (TTC) indicates the maximum transfer capability of a transmission path before violating constraints or causing security issues; existing transfer commitment (ETC) denotes the sum of expected capacity to be used, which in many cases is represented by the line flow in the base case; capacity benefit margin (CBM) gives load serving entities access to energy generation from elsewhere in the interconnected systems to lower the need of installed generating capacity, and it is only supposed to be used in times of emergency generation shortages; transmission reliability margin (TRM) accommodates the inherent uncertainties (e.g., aggregate load forecast uncertainties, load distribution uncertainty, transmission system topology uncertainty, generation dispatch variations) to enable reliable system operations.

In North America, the capacities of CBM and TRM are usually treated as fixed values and determined by independent system operators (ISOs) based on their specific system condition and reliability requirements [41]-[42]. Therefore, TSPs may only need to focus on the TTC and ETC values of each transmission path/flowgate to calculate the ATC values. In this chapter, the effects of CBM and TRM on ATC are also neglected for simplicity.

Meanwhile, with the increasing penetration of variable wind generation, it is more popular to consider uncertain factors in ATC evaluation. Currently, most existing probabilistic methods are iteration-based. For example, the configuration of a typical Monte-Carlo based ATC evaluation method is illustrated in Figure 2.1 [43].

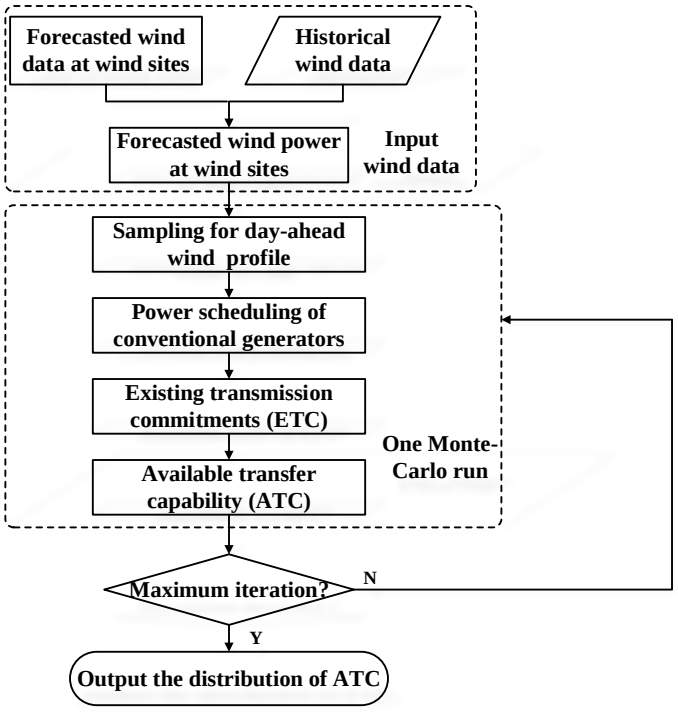

Figure 2.1 Probabilistic-based ATC evaluation algorithm.

Since probabilistic methods require tremendous amounts of calculation, the computational time limits their potential applications in practice. In addition, as the current wind forecasting technology is still immature, the uncertainty and variability of renewables may become unmanageable with high wind power penetration or simply unavailable in terms of the PDF of wind power. It is also worth mentioning that the interval solution from the Monte Carlo method is only a subset of the actual interval [44], which is verified by the case study. Therefore, results from a Monte Carlo simulation underestimate the actual interval range, and may not provide good references under extreme conditions.

To address these problems, the interval optimization method is applied in this chapter to evaluate the ATC considering uncertain wind power. The goal is to identify the objective function values in extreme cases and assess the potential impact of wind uncertainty on ATC calculations as well as generation cost. Unlike previous methods, interval optimization provides a superset of the actual interval, which provides a better option for applications that require the information of full ranges [44]. The detailed mathematical formulations are given next. Note, the geographical distance between the generation center and the load pocket is assumed to be far enough such that the load and wind generation at different buses may not influence each other.

2.2.1 Objective function

The objective function minimizes the overall generation cost while maximizing the ATC between different areas. The modeling process is based on two prerequisites: 1) since the ATC and generation cost under the current electricity market framework is usually modeled as linear functions, DC power flow is applied to conduct power scheduling ([9],[36],[45]); and 2) even though existing technology still has difficulties in obtaining the accurate PDF

of wind, it is much easier to predict future wind power output intervals from historical wind data. Hence, wind generation is modeled as an uncertain variable fluctuating in a specific range.

The objective function is represented by:

$$\min J = \sum_{t=1}^{T}\left[\alpha\sum_{i=1}^{N} gc_{i,t}G_{i,t} - \beta \sum_{i\in source}\left(G_{i,t}^{'} - G_{i,t}\right)\right] \tag{2.2}$$

where the first term denotes minimizing generation cost, and the second term aims to maximize the ATC between the source and sink areas.

2.2.2 Constraints

The constraints are composed of power balance equations, generation capacity limits, generator ramping limits, transmission line thermal limits, generation constraints for source/sink areas, and demand constraints for source/sink areas, as expressed in formulas (2.3)-(2.14):

$$\sum_{i=1}^{N} G_{i,t} + \sum_{i=1}^{N}[\underline{W}_{i,t}, \bar{W}_{i,t}] = \sum_{i=1}^{N} D_{i,t}, \forall t \tag{2.3}$$

$$G_{i,t}^{\min} \le G_{i,t} \le G_{i,t}^{\max}, \ \forall i, \forall t \tag{2.4}$$

$$-R_{i,t} \le G_{i,t} - G_{i,t-1} \le R_{i,t}, \forall i, \forall t \tag{2.5}$$

$$-R_{i,t} \le G_{i,t-1} - G_{i,t} \le R_{i,t}, \forall i, \forall t \tag{2.6}$$

$$-F_{l,t} \le \sum_{i=1}^{N} GSF_{i,l}^{T} \cdot (G_{i,t} + [\underline{W}_{i,t}, \bar{W}_{i,t}] - D_{i,t}) \le F_{l,t}, \forall l, \forall t \tag{2.7}$$

$$\sum_{i=1}^{N} G_{i,t}^{'} + \sum_{i=1}^{N}[\underline{W}_{i,t}, \bar{W}_{i,t}] = \sum_{i=1}^{N} D_{i,t}^{'}, \forall i, \forall t \tag{2.8}$$

$$G_{i,t}^{\min} \le G_{i,t}^{'} \le G_{i,t}^{\max}, \forall i, \forall t \tag{2.9}$$

$$G_{i,t} \le G_{i,t}^{'}, \forall i \in source, \forall t \tag{2.10}$$

$$G_{i,t} = G_{i,t}^{'}, \ \forall i \in sink, \forall t \tag{2.11}$$

$$D_{i,t} = D_{i,t}^{'}, \forall i \in source, \forall t \tag{2.12}$$

$$D_{i,t} \le D_{i,t}^{'}, \quad \forall i \in sink, \forall t \tag{2.13}$$

$$-F_{l,t} \le \sum_{i=1}^{N} GSF_{i,l}^{T} \cdot \left(G_{i,t}^{'} + [\underline{W}_{i,t}, \overline{W}_{i,t}] - D_{i,t}^{'} \right) \le F_{l,t}, \forall l, \forall t \tag{2.14}$$

where (2.3) is the power balance constraint in the base case; (2.4) is the generation capacity limits in the base case; (2.5) and (2.6) are the generator ramp-up and ramp-down constraints; (2.7) is the transmission line limits in the base case; (2.8) is the power balance constraints in the maximum transfer case; (2.9) is the generator capacity limits in the maximum transfer case; (2.10) is the generation constraints in the source area; (2.11) is the generation constraints in the sink area; (2.12) is the demand constraints in the source area; (2.13) is the demand constraints in the sink area; and (2.14) is the transmission line limits in the maximum transfer case.

It is worth mentioning that reactive power is neglected in the problem formulation. It is known that wind generators may consume reactive power, which may cause reactive power deficiency if not adequately compensated. To address this problem, the Federal Regulatory Commission issued Order 827 in 2016 to set reactive power compensation requirements for non-synchronous generators [46]. Order 827 requires that wind turbines must maintain a power factor within the range of 0.95 leading to 0.95 lagging at the point of interconnection as a prerequisite for interconnection. Therefore, under this regulation, wind power plants will not absorb much reactive power from the main grid. Based on these considerations, the reactive power issue is ignored and wind generators are treated as conventional units with uncertainties.

Since both the objective function and the constraints in equations (2.2)-(2.14) are linear functions, the mathematical formulation for the interval optimization-based model can be generalized by:

$$Z = \min_{x} \ c^T x \tag{2.15}$$

$$s.t.\ A_i x_i = [\underline{b}_i, \bar{b}_i] : \lambda_i \tag{2.16}$$

$$E_i x_i \le [\underline{d}_i, \bar{d}_i] : \nu_i \tag{2.17}$$

$$L_i \le x_i \le U_i \ : \gamma_i^L, \gamma_i^U \tag{2.18}$$

Note that in the ATC calculation model, the wind power generation is expressed as an interval in eq. (2.16), which leads to indeterminate constraints that cannot be processed directly. Therefore, the original interval optimization problem needs to be converted to its equivalent deterministic form to be solved.

2.3 Interval optimization algorithm

In the previous section, the model of ATC with uncertain wind power integration is first introduced, where the uncertain wind power is treated as interval variables and brings indeterminate constraints in the problem formulation. In this section, the interval optimization algorithm is further converted to its equivalent deterministic forms by introducing both strong duality theory and artificial binary variables.

According to [47], the optimization models for solving the optimistic and pessimistic values can be expressed in (2.19)-(2.22), and (2.23)-(2.26), respectively:

The optimistic model:

$$Z_{\min} = \min_{x} \ c^T x \tag{2.19}$$

$$s.t.\ \underline{b}_i \le A_i x_i \le \bar{b}_i \tag{2.20}$$

$$E_i x_i \le \bar{d}_i \tag{2.21}$$

$$L_i \le x_i \le U_i \tag{2.22}$$

The pessimistic model:

$$Z_{\max} = \max \min_{x} \; c^T x \tag{2.23}$$

$$s.t.\,(Ax)_i = \underline{b}_i \; or \; \overline{b}_i \; : \lambda_i \tag{2.24}$$

$$E_i x_i \le \underline{d}_i \; : \nu_i \tag{2.25}$$

$$L_i \le x_i \le U_i \; : \gamma_i^L, \gamma_i^U \tag{2.26}$$

After substituting the interval-based constraints into the optimistic model, the lower bound of the objective function (optimistic) value can be calculated from (2.4)-(2.6), (2.9)-(2.13), and (2.27)-(2.31):

$$J_{\min} = \min \sum_{t=1}^{T} \left[\alpha \sum_{i=1}^{N} gc_{i,t} G_{i,t} - \beta \sum_{i \in source} \left(G_{i,t}^{'} - G_{i,t} \right) \right] \tag{2.27}$$

$$s.t. \sum_{i=1}^{N} D_{i,t} - \sum_{i=1}^{N} \overline{W}_{i,t} \le \sum_{i=1}^{N} G_{i,t} \le \sum_{i=1}^{N} D_{i,t} - \sum_{i=1}^{N} \underline{W}_{i,t}, \forall t \tag{2.28}$$

$$\left.\begin{aligned} -\max\left(\sum_{i=1}^{N} GSF_{i,l}{}^{T} \cdot \underline{W}_{i,t}, \sum_{i=1}^{N} GSF_{i,l}{}^{T} \cdot \overline{W}_{i,t} \right) \\ -F_{l,t} \le \sum_{i=1}^{N} GSF_{i,l}{}^{T} \cdot (G_{i,t} - D_{i,t}) \le F_{l,t} \\ -\min\left(\sum_{i=1}^{N} GSF_{i,l}{}^{T} \cdot \underline{W}_{i,t}, \sum_{i=1}^{N} GSF_{i,l}{}^{T} \cdot \overline{W}_{i,t} \right) \end{aligned}\right\}, \forall l, \forall t \tag{2.29}$$

$$\sum_{i=1}^{N} D_{i,t}^{'} - \sum_{i=1}^{N} \overline{W}_{i,t} \le \sum_{i=1}^{N} G_{i,t}^{'} \le \sum_{i=1}^{N} D_{i,t}^{'} - \sum_{i=1}^{N} \underline{W}_{i,t}, \forall t \tag{2.30}$$

$$\left.\begin{aligned} -\max\left(\sum_{i=1}^{N} GSF_{i,l}{}^{T} \cdot \underline{W}_{i,t}, \sum_{i=1}^{N} GSF_{i,l}{}^{T} \cdot \overline{W}_{i,t} \right) \\ -F_{l,t} \le \sum_{i=1}^{N} GSF_{i,l}{}^{T} \cdot (G_{i,t}^{'} - D_{i,t}^{'}) \le F_{l,t} \\ -\min\left(\sum_{i=1}^{N} GSF_{i,l}{}^{T} \cdot \underline{W}_{i,t}, \sum_{i=1}^{N} GSF_{i,l}{}^{T} \cdot \overline{W}_{i,t} \right) \end{aligned}\right\}, \forall l, \forall t \tag{2.31}$$

While substituting the interval-based constraints into the pessimistic model, the upper bound of the objective function (pessimistic) value can be obtained from (2.4)-(2.6), (2.9)-(2.13), and (2.32)-(2.36):

$$J_{\max} = \max \min \sum_{t=1}^{T} \left[\alpha \sum_{i=1}^{N} gc_{i,t} G_{i,t} - \beta \sum_{i \in source} \left(G_{i,t}^{'} - G_{i,t} \right) \right] \tag{2.32}$$

$$s.t.\ \sum_{i=1}^{N} G_{i,t} - \sum_{i=1}^{N} D_{i,t} = -\sum_{i=1}^{N} \underline{W}_{i,t} \ or \ \sum_{i=1}^{N} G_{i,t} - \sum_{i=1}^{N} D_{i,t} = -\sum_{i=1}^{N} \bar{W}_{i,t}, \forall t \tag{2.33}$$

$$\left.\begin{aligned} &-\min\left(\sum_{i=1}^{N} GSF_{i,l}{}^{T} \cdot \underline{W}_{i,t}, \sum_{i=1}^{N} GSF_{i,l}{}^{T} \cdot \bar{W}_{i,t}\right) \\ &-F_{l,t} \le \sum_{i=1}^{N} GSF_{i,l}{}^{T} \cdot (G_{i,t} - D_{i,t}) \le F_{l,t} \\ &-\max\left(\sum_{i=1}^{N} GSF_{i,l}{}^{T} \cdot \underline{W}_{i,t}, \sum_{i=1}^{N} GSF_{i,l}{}^{T} \cdot \bar{W}_{i,t}\right) \end{aligned}\right\}, \forall l, \forall t \tag{2.34}$$

$$\sum_{i=1}^{N} G_{i,t}^{'} - \sum_{i=1}^{N} D_{i,t}^{'} = -\sum_{i=1}^{N} \underline{W}_{i,t} \ or \ \sum_{i=1}^{N} G_{i,t}^{'} - \sum_{i=1}^{N} D_{i,t}^{'} = -\sum_{i=1}^{N} \bar{W}_{i,t}, \forall t \tag{2.35}$$

$$\left.\begin{aligned} &-\min\left(\sum_{i=1}^{N} GSF_{i,l}{}^{T} \cdot \underline{W}_{i,t}, \sum_{i=1}^{N} GSF_{i,l}{}^{T} \cdot \bar{W}_{i,t}\right) \\ &-F_{l,t} \le \sum_{i=1}^{N} GSF_{i,l}{}^{T} \cdot (G_{i,t}^{'} - D_{i,t}^{'}) \le F_{l,t} \\ &-\max\left(\sum_{i=1}^{N} GSF_{i,l}{}^{T} \cdot \underline{W}_{i,t}, \sum_{i=1}^{N} GSF_{i,l}{}^{T} \cdot \bar{W}_{i,t}\right) \end{aligned}\right\}, \forall l, \forall t \tag{2.36}$$

From the above formulas, it is observed that the optimistic model is a trivial linear programming (LP) problem that can be easily solved. However, the pessimistic model is a combinatorial max-min problem with indeterminate parameters in the equality constraints. It is not known in advance whether the optimal value of the pessimistic model is obtained at the lower bound or the upper bound of the uncertain variables in (2.33) and (2.35). Therefore, the pessimistic model turns out to be an NP-hard problem and cannot be solved within polynomial time. The conventional method for finding the optimal solution for the pessimistic model needs to list all the possible combinations of wind generation, then individually solve each sub LP problem and select the maximum objective function value [48]. A flowchart of this algorithm is given in Figure 2.2. The total computational effort is to solve $2^{T \cdot NW}$ LP optimization problems.

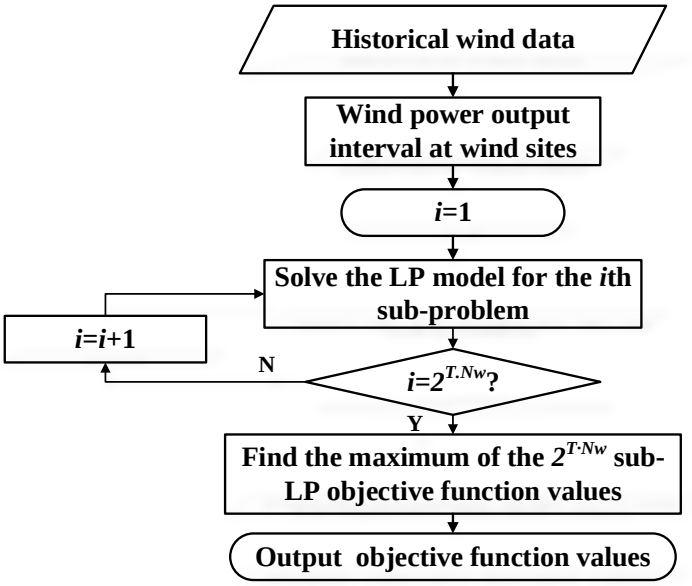

Figure 2.2 Flowchart of the conventional algorithm.

The conventional approach functions efficiently only when both the number of wind generators and the total time period are small. However, as the numbers of wind generators and time interval increase, the computational time also grows exponentially. For instance, if the system has two wind turbines, the computation effort for finding the global optimum will be solving $2^{24\times2}$ (more than 2.8×10^{14}) LP problems. Such a computational time is unacceptable for practical applications.

To overcome the above-mentioned combinatorial explosion problem, in this chapter the strong duality theory is utilized to convert the original max-min problem to its equivalent dual problem form, and then introduce the artificial binary variables to eliminate indeterminate constraints, thus making the proposed algorithm a one-step method and avoiding iterations [49]. The flowchart of the proposed algorithm is illustrated in Figure 2.3.

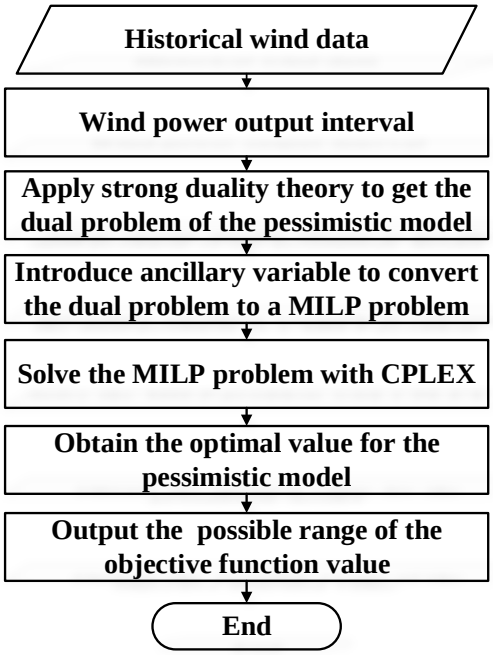

Figure 2.3 Diagram of the proposed method.

The detailed algorithm of each step is summarized as follows: Step 1: Apply strong duality theory to convert the inner minimization problem to a maximization problem. The proof of the models using the strong duality theory can be found in Appendix A.

$$\max_{\lambda,\nu,\gamma^L,\gamma^U} \quad -[\underline{b},\bar{b}]^T\lambda-\underline{d}^T\nu+L^T\gamma^L-U^T\gamma^U \tag{2.37}$$

$$s.t. \quad A_i^T\lambda+E_i^T\nu-\gamma_i^L+\gamma_i^U=-c_i \tag{2.38}$$

$$\nu_i\geq 0;\ \gamma_i^L\geq 0;\ \gamma_i^U\geq 0 \tag{2.39}$$

The new pessimistic model is shown in (2.40)-(2.43). Note that in the dual problem, the indeterminate parameter ξ_i is switched from the constraints to the objective function.

$$Z_{\max}=\max_{\lambda,\nu,\gamma^L,\gamma^U,\xi} \quad -\xi^T\lambda-\underline{d}^T\nu+L^T\gamma^L-U^T\gamma^U \tag{2.40}$$

$$s.t. \quad A_i^T\lambda+E_i^T\nu-\gamma_i^L+\gamma_i^U=-c_i \tag{2.41}$$

$$\nu_i\geq 0;\ \gamma_i^L\geq 0;\ \gamma_i^U\geq 0 \tag{2.42}$$

$$\xi_i = \underline{b}_i \text{ or } \overline{b}_i \tag{2.43}$$

Step 2: Since the value of coefficient ξ in the equation (37) is still indeterminate, binary variables ω_i and a large constant M are introduced to further transform the combinatorial problems into a mixed-integer linear programming (MILP) problem, as described in (2.44)-(2.48):

$$Z_{\max} = \max_{\lambda,\nu,\gamma^L,\gamma^U,\omega} \; -\underline{b}^T\lambda - (\overline{b}-\underline{b})^T \cdot \delta - \underline{d}^T\nu + L^T\gamma^L - U^T\gamma^U \tag{2.44}$$

$$s.t. \;\; A_i^T\lambda + E_i^T\nu - \gamma_i^L + \gamma_i^U = -c_i \tag{2.45}$$

$$-M \cdot \omega_i \le \delta_i \le M \cdot \omega_i \tag{2.46}$$

$$\lambda_i - M \cdot (1-\omega_i) \le \delta_i \le \lambda_i + M \cdot (1-\omega_i) \tag{2.47}$$

$$\nu_i \ge 0;\; \gamma_i^L \ge 0;\; \gamma_i^U \ge 0 \tag{2.48}$$

Constraints (2.46)-(2.47) guarantee that the value of δ_i is limited to 0 or λ_i. When ω_i = 0, constraint (2.46) becomes binding and constraint (2.47) becomes redundant. At this point, δ_i is equal to 0, which means the worst case is obtained at the lower bound of the uncertainty variable in hour *i*. Likewise, when ω_i = 1, constraint (2.47) becomes binding and constraint (2.46) becomes redundant. At this point, $\delta_i = \lambda_i$, which means that the worst case is obtained at the upper bound of the uncertainty variable in hour *i*.

Step 3: The pessimistic problem has now been converted to a MILP with deterministic parameters, which can be further solved by the General Algebraic Modeling System (GAMS) or any other MILP solver.

Therefore, instead of solving and comparing the results of $2^{T \cdot NW}$ sub-problems, the proposed method only needs to address one MILP problem to obtain the globally optimal solution, which considerably improves computational efficiency. However, as the number

of variables becomes larger, the solver may have unbounded results. To solve this problem, the following assumptions are made to relax the original model.

Assumption 1: the sum of power generation in the base case is relaxed to no less than the sum of the load at all times.

From eq. (2.15)–(2.18), the Lagrange function of the generalized LP problem is formulated as below:

$$L = c^T x + \lambda^T \left(Ax - b\right) + \nu^T \left(Ex - d\right) - \left(\gamma^L\right)^T (x - L) + \left(\gamma^U\right)^T (x - U) \tag{2.49}$$

In eq. (2.49), the second term is associated with equality constraints, which can be further decomposed into power balance constraints for the base case, power balance constraints for the maximum transfer case, and other equality constraints. After the relaxation, since $\sum P \geq \sum D - \sum W$, and λ^a is non-negative, the Lagrangian function is represented by eq. (2.50).

$$\begin{aligned} L = {} & c^T x - \left(\lambda^a\right)^T \left(A^a x - b^a\right) + \left(\lambda^b\right)^T \left(A^b x - b^b\right) + \left(\lambda^c\right)^T \left(A^c x - b^c\right) \\ & + \nu^T \left(Ex - d\right) - \left(\gamma^L\right)^T (x - L) + \left(\gamma^U\right)^T (x - U) \end{aligned} \tag{2.50}$$

Therefore, the pessimistic model becomes:

$$Z_{\max} = \max_{\lambda, \nu, \gamma^L, \gamma^U, \omega} \begin{bmatrix} \left(\underline{b}^a\right)^T \lambda^a + (\bar{b}^a - \underline{b}^a)^T \delta^a - \left(\underline{b}^b\right)^T \lambda^b \\ -(\bar{b}^b - \underline{b}^b)^T \delta^b - \left(\underline{b}^c\right)^T \lambda^c - \underline{d}^T \nu \\ + L^T \gamma^L - U^T \gamma^U \end{bmatrix} \tag{2.51}$$

$$-\left(A_i^a\right)^T \lambda^a + \left(A_i^b\right)^T \lambda^b + \left(A_i^c\right)^T \lambda^c + E_i^T \nu - \gamma_i^L + \gamma_i^U = -c_i \tag{2.52}$$

$$-M \cdot \omega_i \leq \delta_i^a \leq M \cdot \omega_i \tag{2.53}$$

$$-M \cdot \omega_i \leq \delta_i^b \leq M \cdot \omega_i \tag{2.54}$$

$$\lambda_i^a - M \cdot \left(1 - \omega_i\right) \leq \delta_i^a \leq \lambda_i^a + M \cdot \left(1 - \omega_i\right) \tag{2.55}$$

$$\lambda_i^b - M \cdot \left(1 - \omega_i\right) \leq \delta_i^b \leq \lambda_i^b + M \cdot \left(1 - \omega_i\right) \tag{2.56}$$

$$\nu_i \geq 0; \lambda_i^a \geq 0; \gamma_i^L \geq 0; \gamma_i^U \geq 0 \tag{2.57}$$

Since the sum of generation is assumed to be greater than the sum of the load, the power balance equation in the base case may not be held in some cases when the ramping capacity of all the generators is insufficient. Therefore, another assumption is introduced in this chapter.

Assumption 2: the ramping capacity of all the generators is always greater than the rate of load change during all the time intervals, but the ramping of a single generator can be smaller than the rate of load change.

As a matter of fact, even though the power balance constraint in Assumption 1 is relaxed, the sum of generation is always equal to the sum of the load, because the optimal solutions are always obtained at the vertices in LP problems. As the goal is to minimize the sum of generation cost and subtract ATC, excess generation yields worse optimization results. Therefore, the sum of the generation should be equal to the sum of the load.

2.4 Case study

The proposed algorithm is implemented on the PJM 5-bus system and the IEEE 118-bus system through a hybrid platform, MATLAB 2016a and GAMS 24.7, where MATLAB is used for creating input data profiles and storing computation results. The MILP problem is solved by CPLEX in GAMS. The hardware environment is a laptop with Intel i7 2.5 GHz CPU, and 8.00 GB RAM.

2.4.1 Case study on the PJM 5-bus test system

The configuration of the 5-bus system is depicted in Figure 2.4. The test system is composed of two areas: the generation center (including Bus A and Bus E) and the load center (including Bus B, Bus C, and Bus D). There are two aggregated wind farms connected to the system at Bus A and Bus D, respectively. The maximum power output of each wind farm is 100 MW.

The forecasted day-ahead wind generation for the two wind farms is plotted in Figure 2.5. The forecasting error is 5%. The line parameter settings are the same as in [9]. Since tie lines A-B and D-E have already reached their capacity limits under the regular economic dispatch condition, the goal is to find the maximum ATC between the generation center and load center.

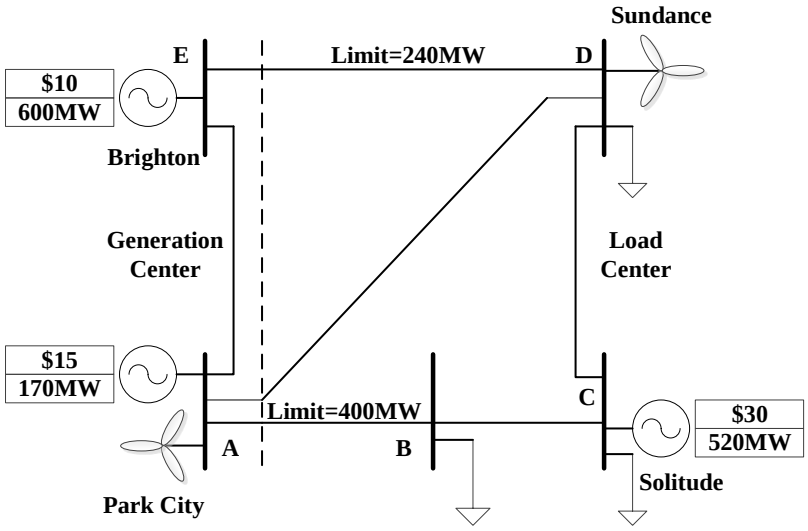

Figure 2.4 The configuration of the PJM 5 bus system.

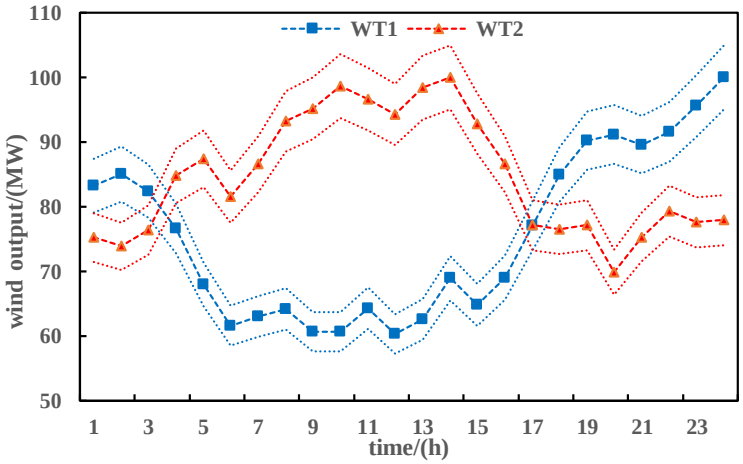

Figure 2.5 Forecasted upper and lower boundaries for wind power generation.

As mentioned in the previous section, the original interval optimization-based model is first decomposed into an optimistic model and a pessimistic model. In the optimistic model, there are 432 decision variables, 144 equality constraints, and 996 inequality constraints. In the pessimistic model, there are 1,860 decision variables, 48 binary variables, 432 equality constraints, and 384 inequality constraints. The value of α is set to zero to achieve the maximum ATC for the PJM 5-bus system. The results for a day-ahead ATC interval are illustrated in Figure 2.6.

In Figure 2.6, the maximum ATC value is 437.0 MW, obtained from the optimistic model. The minimum ATC value is 380.9 MW, obtained from the pessimistic model. It is also observed that the optimistic ATC values and the pessimistic ATC values follow the same trend over time. Both the optimistic model and the pessimistic model obtain the maximum ATC values at 3 p.m. and the minimum ATC values at 9 p.m.

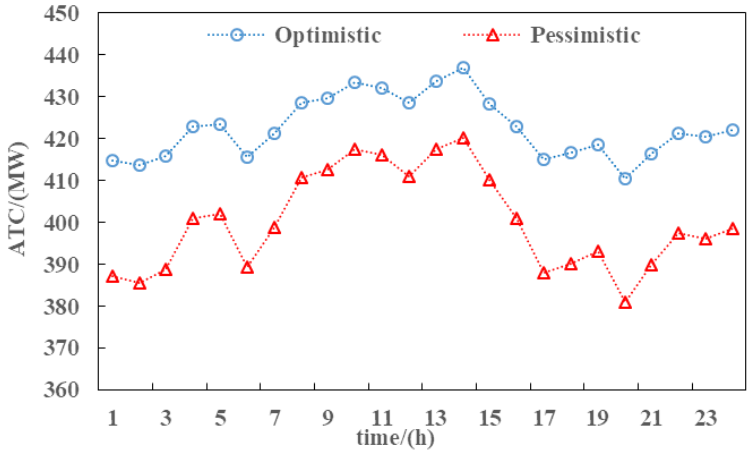

Figure 2.6 Day-ahead ATC intervals for the PJM 5 bus system.

Table 2.1 Computational time of the optimistic and pessimistic model.

Duration/(h)	Optimistic/(s)	Pessimistic/(s)
3	0.326	0.638
6	0.335	0.665
9	0.338	0.689
12	0.339	0.851
15	0.342	0.893
18	0.352	1.051
21	0.367	1.062
24	0.375	1.126

Table 2.1 compares the computational speed of the optimistic model and the pessimistic model for different time scales. Even though the length of test hours increases from 3 to 24, the computational time of the pessimistic model is still around one second. Further, the computational speed of the optimistic model is always faster than that of the pessimistic

model, because the optimal value for the optimistic model is a linear optimization problem with deterministic constraints, whereas for the pessimistic model it is a MILP problem.

2.4.2 Impact of wind forecasting error on ATC calculations

In this section, the effect of wind forecasting error on generation cost and maximum ATC values is studied. The test system is the same as the PJM 5-bus system from the previous subsection except that the wind forecasting error increases from 10% to 30%, for illustrative purposes.

When the forecasting error is 10%, the minimum generation cost ranges from $467,674.90 to $475,370.30, and the maximum ATC interval ranges from 391.1 MW to 433.8 MW. When the forecasting error is 30%, the minimum generation cost ranges from $459,979.40 to $483,065.80, and the maximum ATC interval is from 353.7 MW to 478.4 MW. Once the wind forecasting error becomes larger, the optimistic objective function value decreases, whereas the pessimistic objective function value increases. As the error becomes larger, the objective function values in both optimistic and pessimistic models deviate further from the actual ATC and generation cost. Therefore, accurate wind power forecasting data yields to narrower ranges of both generation cost and ATC, which reasonably supports the better decision-making for the grid operators.

2.4.3 Efficiency and accuracy of the proposed algorithm

The performance of the proposed algorithm is compared with that of the conventional approach and MCS using the same test system as shown in Figure 2.4. Due to the combinatorial explosion issue, it is impossible to evaluate the 24-hour ATC using the

conventional approach with a regular laptop (as discussed in section III). Therefore, for illustrative purposes, the number of time intervals is set to 3.

With the conventional approach, the computational burden is to solve 64 LP problems and then select the minimum ATC value as the pessimistic solution. The computational time is 27.14 *sec*, and the average ATC over 3 hours is from 387.13 MW to 407.87 MW.

With the MCS, the wind power in different scenarios is assumed to be uniformly distributed between the lower and upper boundaries, and the number of scenarios is 1000. The computational time for MCS is 860.01 *sec*, and the range of ATC over 3 hours is between 399.66 MW and 406.56 MW.

With the proposed interval optimization-based algorithm, it needs to solve the optimistic value and the pessimistic value, respectively. The proposed algorithm spends 0.33 sec to solve the optimistic model and 0.63 sec to solve the pessimistic model. The total computational time is *0.96* sec. The result of the average ATC interval is from 387.13 MW to 414.78 MW.

The case studies verify that both MCS and the proposed method are very close to the conventional approach. However, the proposed interval optimization-based approach is much faster than the other approaches. The conventional approach needs to consider all possible combinations of the upper and lower bounds of all uncertain variables, and the MCS needs to evaluate a large number of random samples. Both require a significant amount of optimization runs. The proposed interval optimization-based approach is much faster. This demonstrates the great efficiency of the proposed interval optimization-based algorithm.

It is also observed that both the MCS and the proposed interval approach give very close results to the actual range (calculated from the conventional approach considering all possible combinations). While the result from the MCS is a subset of the actual ATC interval, the result from the proposed algorithm is a slight superset of the actual ATC interval. This observation is aligned with the discussion in Section 2.2.

2.4.4 Case study on the IEEE 118-bus test system

To validate the performance of the proposed method in large systems, the proposed algorithm is further deployed on a modified IEEE 118-bus system. The configuration of the system is shown in Figure 2.7. The test system is composed of three areas, where Area 1 and Area 3 are the generation centers, and Area 2 is the load center.

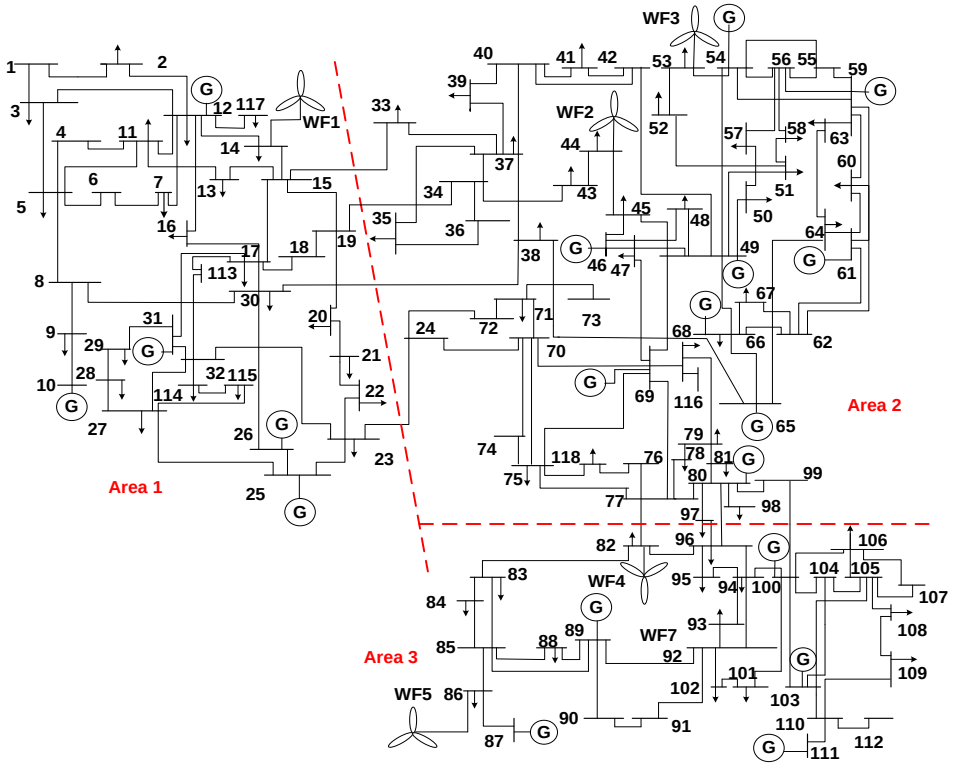

Figure 2.7 The configuration of the IEEE 118 bus system.

There are five aggregated wind farms in this system, located on bus 17, bus 44, bus 54, bus 82, and bus 86, respectively. The generation capacity of all the wind farms is set to 50 MW. The forecasted day-ahead wind generation for the wind turbines is plotted in Figure 2.8. The forecast error in this case study is 10%. Other transmission line parameters settings are the same as in [9].

In the optimistic model, there are 8,496 decision variables, 14,596 equality constraints, and 2,832 inequality constraints. In the pessimistic model, there are 29,524 decision variables, 120 binary variables, 8,496 equality constraints, and 960 inequality constraints. The goal is to minimize the generation cost while maximizing the ATC. The ratio between the weight factors β and α is set to five. The results of the day-ahead ATC interval for the IEEE 118-bus system are given in Figure 2.9.

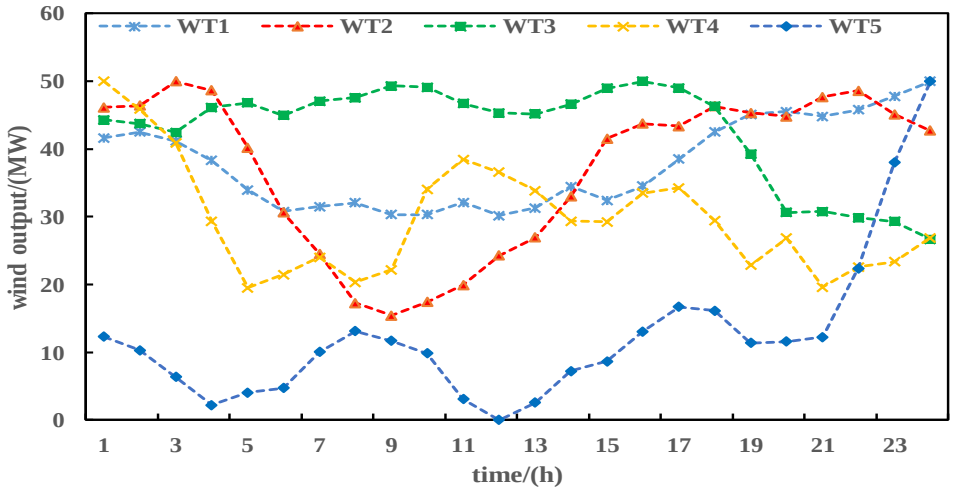

Figure 2.8 Forecasted wind power generation.

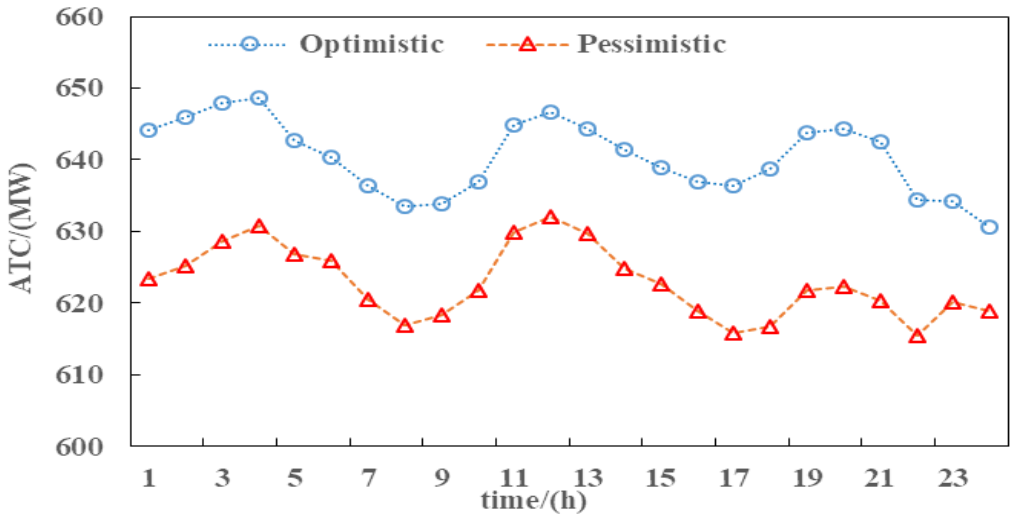

Figure 2.9 Day-ahead ATC intervals for IEEE 118 system.

Unlike the previous case, the minimum/maximum ATC values of the optimistic and pessimistic models in the IEEE 118-bus system are not acquired at the same time. In the optimistic model, the maximum ATC value is obtained at 4 a.m., while the minimum ATC value is obtained at 12 midnight. However, in the pessimistic model, the maximum ATC value is obtained at 12 noon and the minimum ATC value is obtained at 5 p.m.

2.4.5 Impact of weighting factors of generation cost and ATC

Since both of the weight factors are non-negative numbers, increasing the value of α will result in generation cost reduction, while raising the value of β leads to ATC increase. Therefore, the influence of weight factors on generation costs and ATC values can be explored by changing the ratio between β and α. The results are shown in Figure 2.10 and Figure 2.11.

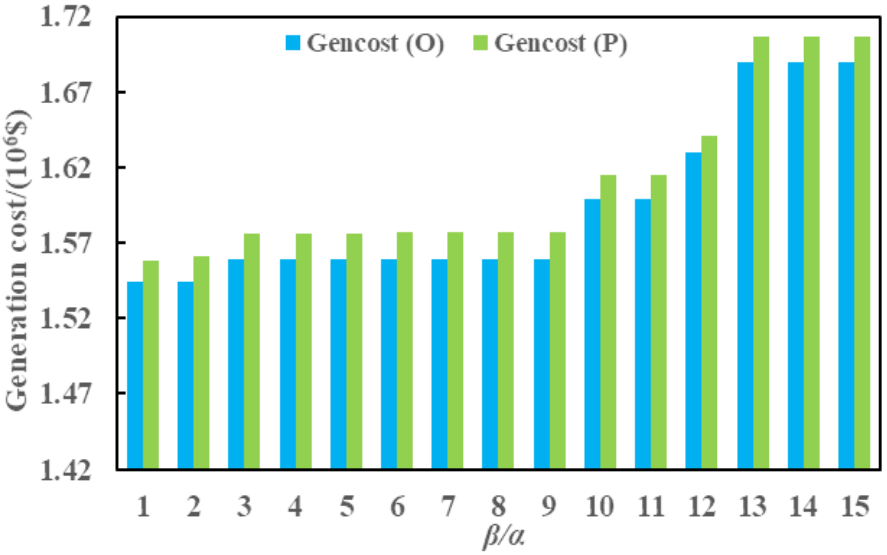

Figure 2.10 Influence of weight parameters on the generation cost range.

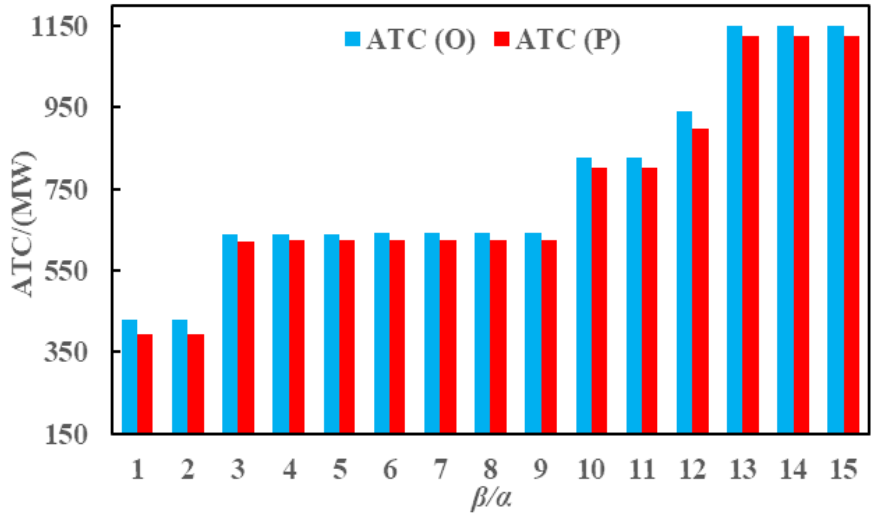

Figure 2.11Influence of weight parameters on the ATC range.

From Figure 2.10, the generation cost is shown as being positively correlated with the ratio of β/α. In the beginning, the generation cost does not change much as the ratio value increases. When the value of β/α equals to ten, the generation cost starts to increase sharply. Finally, by continuously increasing the ratio, the generation cost curve tends to be flat again.

In Figure 2.11, the values of ATC become greater when the value of β/α increases. It is observed that when increasing the weighting factor ratio from one to ten, the amount of ATC is doubled. In addition, similar to Figure 2.10, the ATC value will also remain unchanged at the very end, because the transmission capacity between the different areas must obey physical laws, and it has already reached the saturated capacity.

Furthermore, from Figure 2.10 and Figure 2.11, it is observed that the ATC value in the optimistic model is always greater than that in the pessimistic model, while the generation cost in the optimistic model is always less than that in the pessimistic model.

In deregulated electricity markets, the goal of ISOs is to maximize social welfare. Therefore, the impact of generation cost on power scheduling should always be considered (i.e., the weight factor α must always be greater than 0). The physical interpretation of the ratio of weights can be viewed as the tolerance for line congestion, which may be determined by ISOs' own reliability requirements. As the strategies of reserving transmission corridors deserve another full-fledged chapter, they will not be further discussed in this chapter.

2.5 Chapter Summary

In this chapter, an interval optimization-based algorithm for ATC calculations is proposed. Uncertain wind power is modeled as a variable varying within a specific range. Then, the original interval-based model is decomposed into an optimistic model and a pessimistic model to calculate the lower bound and the upper bound of the objective function value, respectively. The optimistic model is a regular LP problem, while the pessimistic model is a difficult combinatorial max-min problem. To solve the pessimistic problem, strong duality theory and artificial binary variables are introduced to convert the NP-hard

pessimistic model to a single-level maximization problem for efficient calculation. Furthermore, the power balance equation in the base case is relaxed to an inequality constraint to ensure the solvability of the proposed algorithm in large systems. Case studies demonstrate that the computational speed of the proposed interval-based algorithm is insensitive to the number of variables. Increasing the number of time intervals or system size will not significantly affect the computational time, hence validating the feasibility of the proposed algorithm in real-world applications. Also, the impacts of forecasting error and weighting factors are studied. Accurate wind forecasting yields more accurate ATC values, thus providing a better reference for grid operators and market participants.

Chapter 3 A Scalable and Distributed Algorithm for Managing Residential Demand Response Programs Using Alternating Direction Method of Multipliers

For effective engagement of residential demand-side resources (DSRs) and to ensure efficient operation of distribution networks, the challenges of controlling and coordinating residential components and devices at scale must be overcome. This chapter presents a distributed and scalable algorithm with a three-level hierarchical information exchange architecture for managing residential DR programs. First, a centralized optimization model is formulated to maximize community social welfare. Then, this centralized model is solved in a distributed manner with the ADMM by decomposing the original problem into utility-level and house-level problems. The information exchange between the different layers is limited to the primary residual (i.e., supply-demand mismatch), Lagrangian multipliers, and the total load of each house to protect each customer's privacy. Simulation studies are performed on the IEEE 33 bus test system with 605 residential customers. The results demonstrate that the proposed approach can reduce both customers' electricity bills and the peak load at the utility level without much-affecting customers' comfort and privacy. Finally, a quantitative comparison of the distributed and centralized algorithms shows the scalability advantage of the proposed ADMM-based approach, and it gives benchmarking results for future research works.

Nomenclature

Sets and Indices

d	Index of iterations.
N_L / l	Set / index of distribution lines.
N_M / j, k	Set / index of buses (aggregators).
C_k	Set of child buses of bus k
N_N / i	Set / index of residential customers.
N_T / t	Set / index of time.

Parameters

a / b	Electricity cost coefficients (\$/kW^2, \$/kW).
C_i^{house}	Thermal capacitance of house i (J/°C).
C_i^{wh}	Thermal capacitance of the EWH in house i (J/°C).
$\underline{ESS}_i^C$ / $\overline{ESS}_i^C$	Minimum/maximum charging power capacity of the ESS in house i (kW).
$\underline{ESS}_i^D$ / $\overline{ESS}_i^D$	Minimum/maximum discharging power capacity of the ESS in house i (kW).
E_i^{ESS}	Energy capacity of the ESS in house i (kWh).
p_i^{hvac} / q_i^{hvac}	Real/reactive power rating of the HVAC in house i (kW/kVar).
$p_{i,t}^{nr}$ / $q_{i,t}^{nr}$	Real/reactive power consumption of the non-responsive devices in house i at time t (kW/kVar).
$p_{i,t}^{pv}$	PV power output of house i at time t (kW).
$\overline{p}^{pcc}$	Maximum contracted load limit at the PCC (kW).
p_i^{wh} / q_i^{wh}	Real/reactive power rating of the EWH in house i (kW/kVar).
$r_{j\text{-}k}^{line}$ / $x_{j\text{-}k}^{line}$	Resistance/reactance of the distribution line connecting bus j and bus k (Ω).
R_i^{house}	Thermal resistance of house i (°C/kW).
R_i^{wh}	Thermal resistance of the EWH in house i (°C/kW).
$\underline{SOC}_i$ / $\overline{SOC}_i$	Minimum/maximum ESS state-of-charge in house i at time t.

$\underline{T}_i^{in}$ / $\overline{T}_i^{in}$	Minimum/maximum indoor temperature of house *i* (°C).
$T_i^{in,set}$	Indoor temperature setpoint of house *i* (°C).
T_t^{out}	Day-ahead outdoor temperature forecast (°C).
$\underline{T}_i^{wh}$ / $\overline{T}_i^{wh}$	Minimum/maximum water temperature of the EWH in house *i* (°C).
$T_i^{wh,set}$	Water temperature setpoint of house *i* (°C).
α / β	Weight factors ($/°C).
ε^R / ε^S	Primary/secondary feasibility tolerance value.
η_i^C / η_i^D	Charging/discharging efficiency of the ESS in house *i* at time *t*.
λ^{vio}	Peak load violation rate ($/kW).
ρ	Penalty factor of the augmented Lagrangian term.

Continuous variables

$dis_{i,t}^{hvac}$	Indoor temperature discomfort of customer *i* at time *t* (°C).
$dis_{i,t}^{wh}$	Water temperature discomfort of customer *i* at time *t* (°C).
$ESS_{i,t}^C$ / $ESS_{i,t}^D$	Charging/discharging power of the ESS in house *i* at time *t* (kW).
$I_{j\text{-}k,t}^{line}$	Power flow of line *j*-*k* at time *t* (kW).
$p_{i,t}^{cus}$ / $q_{i,t}^{cus}$	Net real/reactive load of house *i* at time *t* (kW/kVar).
$p_{k,t}^{agg}$ / $q_{k,t}^{agg}$	Net real/reactive load of aggregator *k* at time *t* (kW/kVar).
$p_{j\text{-}k,t}^{line}$ / $q_{j\text{-}k,t}^{line}$	Real/reactive power flowing in distribution line *j*-*k* at time *t* (kW/kVar).
p_t^{pcc}	Amount of electricity purchased from the PCC at time *t* (kW).
p^{vio}	Maximum amount of load that exceeds the maximum load limit at the utility level (kW).
R_t	Primal residual of ADMM at time *t*.
$S_{i,t}$	Secondary residual of ADMM at time *t*.
$SOC_{i,t}$	State-of-charge of the ESS in house *i* at time *t*.
$T_{i,t}^{in}$	Indoor temperature of house *i* at time *t* (°C).
$T_{i,t}^{wh}$	Water temperature of the EWH in house *i* at time *t* (°C).
$V_{j,t}$ / $V_{k,t}$	Voltage magnitude of bus *j* / *k* at time *t*.
λ_t	Lagrangian multiplier.

Binary Variables

$b_{i,t}^{hvac}$	Operating status of the HVAC in house *i* at time *t*.
$b_{i,t}^{wh}$	Operating status of the EWH in house *i* at time *t*.
$\mu_{i,t}^{C}$ / $\mu_{i,t}^{D}$	Charging/discharging status of the ESS in house *i* at time *t*.

3.1 Introduction

DR research and demonstration projects have been ongoing for several decades. New communication infrastructure and methodologies along with more distributed intelligence have led to an increase in research and development for DSRs and distributed energy resources (DERs). More recently, a substantial focus was placed on the quantity and capability of DSR and DER assets needed to provide ancillary services [50]-[52]. In 2012 and 2013, an extensive study evaluated the potential quantity and quality of DSRs and DERs, potential market value, and barriers to technology maturation [53]-[54]. While the study noted that the residential sector appeared to have significant resource potential, the available communication and computation infrastructure was not sufficient to coordinate large numbers of low-power devices and customers' highly diverse electricity consumption patterns [55]. Therefore, these resources were often deemed cost-prohibitive to implement when compared to larger providers, such as commercial buildings and industrial loads. Hence, an effective approach that can manage and integrate residential DSRs and DERs remains critical to the use of these loads in the long-term.

The changing landscape of communication technology and the development of the Internet have led to the interconnection of many intelligent devices and have provided a wealth of opportunities to control and optimize energy use in ways that were not previously possible. Communication systems such as Wi-Fi and Zigbee via smart home energy management systems (HEMS) provide access to controllable end-use systems [56]-[57] and

can securely bridge house-level components to utility-level applications [58]. For example, new smart heating, ventilation, and air conditioning (HVAC) systems and EWHs have been identified as promising candidates for DR. The large power ratings and thermal inertia (changing device operating status does not have a significant impact on customers' comfort in the short term) make HVAC systems and EWHs opportune resources [59]-[61].

Currently, available control algorithms for managing DSRs are categorized as either centralized or distributed [25]. In the centralized control approach, the models and control actions are computed and issued by the control center according to collected measurement inputs from sub-systems. In [62], a centralized energy management model is proposed for determining the operation schedules of plug-in hybrid electric vehicles (EVs), HVAC systems, EWHs, and pool pumps in residential buildings. The simulation results from this work demonstrated that coordinated DER scheduling could increase net benefits to the customer. In similar research [63], a centralized model is formulated to minimize the power purchasing cost of residential customers in a dynamic pricing market. The results suggest that centralized scheduling can substantially improve customers' cost benefits. The centralized approach, when it is applied at a small-scale and utilizes customers with common goals, is straightforward and functional. However, customers in the centralized structure have to release device operating information and allow the utility to directly control the devices. Moreover, as the number of customers grows, the computational complexity increases significantly.

In the distributed control approach, customers independently conduct local optimizations to determine the optimal scheduling of devices. In [64], a distributed direct load control approach is presented to shave the peak load in a low-voltage unbalanced distribution

network. Simulation results indicate that the proposed approach is scalable and can maximize the welfare of both the utility and customers. In [65], the authors compare the performance of three control methods (centralized, decentralized, and distributed) on mitigating the impact of solar generation on the distribution network. The results show that the centralized approach has the best performance but is non-scalable, while the distributed approach does scale well. In the distributed approach, the major part of the calculation is performed by local HEMS, distributing the intelligence and reducing the centralized computational requirements. Since each HEMS is independent, calculations are all run in parallel reducing the needed computational time. Customer privacy is also better protected as minimal information is shared with a central system. However, the distributed control algorithms often suffer from convergence challenges and do not always reach the optimal solution.

Additional literature discusses the residential DR management topic further. In [66], a Stackelberg game-based model is presented to study competition among utility and multiple load aggregators (LAs), but this algorithm is not scalable since as the number of aggregators increases, the number of dual variables and Karush-Kuhn-Tucker (KKT) constraints also increases significantly. In [67], Benders decomposition is proposed to solve the optimal scheduling problem for EV drivers to swap their depleted batteries at battery stations. The drawbacks are that the algorithm requires global information and cannot be scaled for large applications. The work in [68] improves the algorithm in [67] by relaxing the binary decisions to continuous variables and then naively rounding the results to discretize the solutions. However, such relaxation may cause an infeasible solution or constraint violations [69]. In [70], dual decomposition is applied to solve the residential load control problem, but

the algorithm may suffer from slow convergence [71]. In [72], a robust algorithm is presented for residential DR applications. While the results demonstrate the proposed approach is scalable and can protect customers' privacy, the household temperature dynamics and the network flow are neglected.

In recent years, the ADMM, which is a robust iteration-based algorithm that solves arbitrary-scale optimization problems and supports distributed computation, has gained growing popularity in solving DR problems [73]. The basic idea of the ADMM is to formulate a centralized model, decompose the model into a set of small sub-problems, and solve each sub-problem independently [71]. In [74], a dual census ADMM algorithm is developed for asynchronous distributed DR, but this work does not consider the distribution network flow model. In [75], the ADMM is applied to solve the DC-OPF problem with DR, but the system power loss is ignored. A similar issue exists in [76], where the ADMM is used for solving optimal tracking problems. In [77], both the Frank-Wolfe method and the ADMM are applied to solve EV charging coordination problems. However, the Frank-Wolfe method may not work for the proposed problem in this chapter since some of the decision variables are binary.

To address these challenges, a three-level hierarchical DR algorithm is proposed for vertically integrated monopoly utilities to coordinate the scheduling of residential DSRs and shave the peak load at the utility level. In the proposed DR program, customers are allowed to customize their preferred indoor and water temperature ranges, and only report the total load information to the aggregators. The resistance-capacitance (RC) thermal model is used to simulate household temperature dynamics, and DistFlow equations are introduced to calculate network power flow [78]-[79]. Further, the ADMM has been selected as the

solution methodology. Even with a large number of binary variables (ON/OFF status variables of HVAC systems and EWHs, and the binary charge/discharge status variables of energy storage systems (ESSs)), the computational complexity is distributed through the use of ADMM.

The main contributions of this chapter are summarized as follows: 1) a distributed control scheme with limited data exchange among agents to ensure feasibility for large-scale applications and maintain data privacy, and 2) a DR management approach that reduces the utility peak load and reduces customers' electricity bills while considering household temperature dynamics and network flow equations.

This chapter is organized as follows: Section 3.2 presents the three-level hierarchical architecture of the distribution networks, Section 3.3 formulates the mathematical model of the centralized DR management system, Section 3.4 decomposes the centralized model to a utility-level sub-problem and a set of house-level sub-problems, Section 3.5 presents case studies, and Section 3.6 concludes the chapter.

Notation conventions: superscript ^{hvac} refers to HVAC, superscript ^{wh} refers to EWH, superscript ^{cus} refers to residential customers, superscript ^{agg} refers to LAs, and superscript ^{line} refers to distribution lines.

3.2 The architecture of the hierarchical distribution networks

In this chapter, a comprehensive three-level hierarchical architecture for managing residential DR programs is proposed. The detailed configuration is shown in Figure 3.1. The three levels are composed of the utility, LAs, and end-use customers which form the top, middle, and bottom levels, respectively.

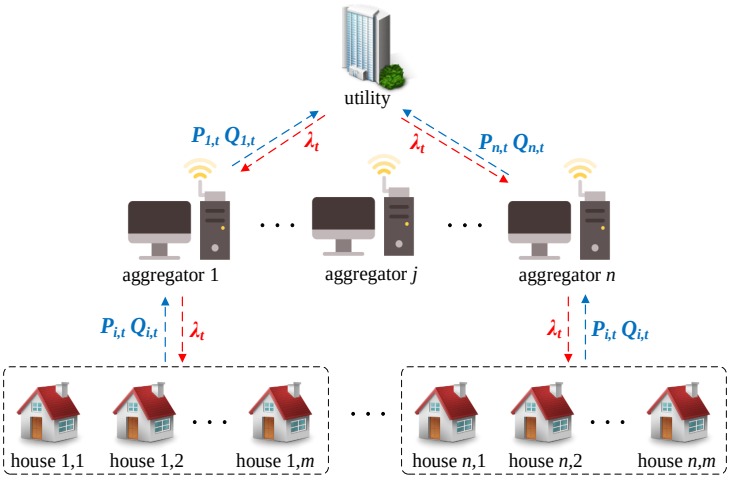

Figure 3.1 Hierarchical distribution network architecture.

Notice that the LAs act as intermediates between the vertically integrated utility and customers, and they provide a means to support end-user participation in these markets [80]-[82]. In addition, aggregators reduce the utility communication requirements since communication needs are now reduced to a single entity instead of many assets.

The aggregators in this chapter are assumed to be profit neutral (i.e., the revenue and the operation cost of the aggregators should be equal). The revenue of aggregators comes from the customers who participate in the DR program. Each customer is required to pay a fixed amount of membership fee to its corresponding aggregator. Any excess payment will be refunded and deficiency will be repaid at the end of each month or year, which is very similar to the business model of ISOs [83]. However, since the operation cost of aggregators is beyond the scope of this chapter, the details are omitted.

Furthermore, residential customers are clustered by geographical locations and interconnection to the distribution system for each aggregator. From the network flow viewpoint, aggregators are treated as buses and interconnected to form a distribution network.

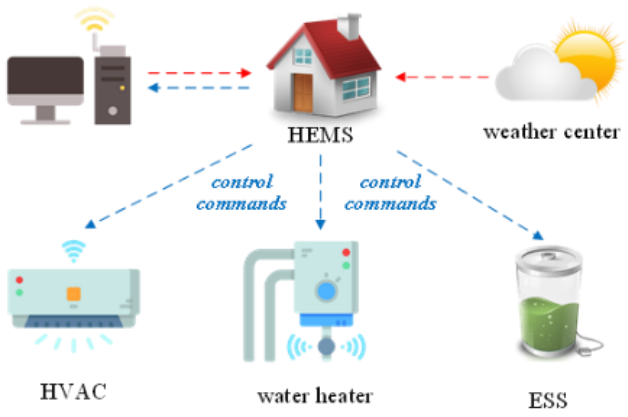

Figure 3.2 Home energy management system.

At the house level, HEMSs are responsible for receiving data from aggregators and local weather service centers to perform optimization and decision-making on behalf of customers. The diagram of the HEMS is illustrated in Figure 3.2.

3.3 Modeling of the centralized residential DR management systems

In this section, the residential DR management optimization problem is formulated as a centralized model to maximize the social welfare of the community. The objective is to minimize the power purchasing cost of the community, customer discomfort, and the peak load violation cost. Then in the next section, this centralized model is decomposed and solved distributively to improve computational efficiency.

3.3.1 Objective function

The objective function of the centralized model is given by:

$$\min \sum_{t \in N_T} \left[a \cdot \left(p_t^{pcc} \right)^2 + b \cdot p_t^{pcc} + \sum_{i \in N_M} \left(\alpha \cdot dis_{i,t}^{hvac} + \beta \cdot dis_{i,t}^{wh} \right) \right] + \lambda^{vio} \cdot P^{vio} \tag{3.1}$$

where the first two terms represent the utility's power purchasing cost from the grid, the third term represents the customers' discomfort cost due to indoor temperature deviating from the setpoint, the fourth term represents the customers' discomfort cost due to water temperature deviating from the setpoint, and the last term represents the peak load violation charge.

Notice that the utility's power purchasing cost is represented by a quadratic function [84]-[86]. In this chapter, quadratic terms are used to model dynamic pricing and to encourage customers to shift the load from peak to off-peak hours. In eq. (3.1), the peak load violation charge is defined as the product of a "peak load violation" rate and the maximum amount of load that exceeds the allowable load limit at the point of common coupling (PCC). The load violation amount can be calculated from eq. (3.2). In this chapter, the peak load violation charge is set to \$5/kW.

$$p^{vio} = \max\left(p_t^{pcc} - \overline{p}^{pcc}, 0 \right) \quad \text{for all } t \in N_T \tag{3.2}$$

3.3.2 HVAC model

In this chapter, a simplified version of the RC model in [79] is used to calculate the indoor temperature dynamics. Details on HVAC modeling are provided in Appendix B. The input parameter for the HVAC model is the day-ahead forecasted outdoor temperature, and the HVAC model is represented by:

$$T_{i,t}^{in} = T_{i,t-1}^{in} + [(T_t^{out} - T_{i,t-1}^{in}) / R_i^{house} - b_{i,t}^{hvac} \cdot p_i^{hvac} \cdot \Delta t] / C_i^{house} \tag{3.3}$$

$$\underline{T}_i^{in} \le T_{i,t}^{in} \le \overline{T}_i^{in} \tag{3.4}$$

$$dis_{i,t}^{hvac} = \left| T_{i,t}^{in} - T_i^{ins} \right| \tag{3.5}$$

where eq. (3.3) is used for calculating the indoor temperature of house *i* at each time step *t*, eq. (3.4) is the minimum/maximum indoor temperature limit constraint for each house, and eq. (3.5) represents customers' discomfort due to indoor temperature deviating from the setpoint. The detailed parameter settings of HVAC units are given in Table 3.1, and the power factor of HVAC is set to 0.81.

3.3.3 EWH model

Similar to the HVAC model, the EWH model is represented by:

$$T_{i,t}^{wh} = T_{i,t-1}^{wh} + [(T_{i,t}^{in} - T_{i,t-1}^{wh}) / R_i^{wh} + b_{i,t}^{wh} \cdot p_i^{wh} \cdot \Delta t] / C_i^{wh} \tag{3.6}$$

$$\underline{T}_i^{wh} \le T_{i,t}^{wh} \le \overline{T}_i^{wh} \tag{3.7}$$

$$dis_{i,t}^{wh} = \left| T_{i,t}^{wh} - T_i^{whs} \right| \tag{3.8}$$

where eq. (3.6) calculates the water temperature of house *i* at each time step *t*, eq. (3.7) is the minimum/maximum water temperature limit constraint for each house, and eq. (3.8) calculates customers' discomfort due to water temperature deviating from the setpoint. The detailed parameter settings of EWHs are given in Table 3.2, and the EWH power factor is set to 1.0.

Table 3.1 HVAC parameter settings.

C_i^{house}	U[1.0, 1.5] J/℃	R_i^{house}	U[25.6, 38.4] J/℃
P^{hvac}	3.5 kW	T_i^{ins}	21~23 ℃
$\underline{T}_i^{in}$	$T_{i,t}^{ins}$ -1 ℃	$\overline{T}_i^{in}$	$T_{i,t}^{ins}$ +1 ℃

Table 3.2 EWH parameter settings.

C_i^{wh}	U[0.1, 0.15] J/℃	R_i^{wh}	U[48.0, 72.0] J/℃
P^{wh}	2.5 kW	$T_{i,t}^{whs}$	55.0~57.5 ℃
$\underline{T}_i^{in}$	$T_{i,t}^{whs}$ -5℃	$\overline{T}_i^{wh}$	$T_{i,t}^{whs}$ +5℃

3.3.4 ESS model

The ESS model is represented by:

$$\mu_{i,t}^{C} + \mu_{i,t}^{D} = 1 \tag{3.9}$$

$$\mu_{i,t}^{C} \cdot \overline{ESS}_i^{C} \le ESS_{i,t}^{C} \le \mu_{i,t}^{C} \cdot \underline{ESS}_i^{C} \tag{3.10}$$

$$\mu_{i,t}^{D} \cdot \underline{ESS}_i^{D} \le ESS_{i,t}^{D} \le \mu_{i,t}^{D} \cdot \overline{ESS}_i^{D} \tag{3.11}$$

$$SOC_{i,t} = SOC_{i,t-1} + \eta \cdot ESS_{i,t}^{C} / E_i^{ESS} - ESS_{i,t}^{D} / \left(\eta \cdot E_i^{ESS}\right) \tag{3.12}$$

$$\underline{SOC}_i \le SOC_{i,t} \le \overline{SOC}_i, \forall t \tag{3.13}$$

$$ESS_{i,t} = ESS_{i,t}^{D} - ESS_{i,t}^{C} \tag{3.14}$$

$$SOC_{i,t=1} = SOC_{i,t=N_T} \tag{3.15}$$

where eq. (3.9) limits the ESS such that it cannot be charged and discharged at the same time, eq. (3.10) is the charging power capacity constraint of the ESS, eq. (3.11) is the discharging power capacity constraint of the ESS, eq. (3.12) calculates the state-of-charge (SOC) of the ESS at each time, eq. (3.13) is the minimum/maximum SOC limit constraint, eq. (3.14) calculates the power output of the ESS at each time, and eq. (3.15) is the final SOC status constraint for the ESS. The detailed parameter settings of ESSs are given in Table 3.3, and the initial SOC of ESSs is set to 50%.

Table 3.3 ESS parameter settings.

$\underline{ESS}_i^C, \underline{ESS}_i^D$	0 kW	$\overline{ESS}_i^C, \overline{ESS}_i^D$	5 kW
E_i^{ESS}	15 kWh	η^C, η^D	95%
$\underline{SOC}_i$	20%	$\overline{SOC}_i$	90%

3.3.5 Load model

In this chapter, power output from a solar panel is viewed as a negative load. Therefore, the load of each house is equal to the sum of the responsive load (including HVAC and EWH) and the non-responsive load minus solar generation. The load model is given by:

$$p_{i,t}^{cus} = p_i^{hvac} \cdot b_{i,t}^{hvac} + p_i^{wh} \cdot b_{i,t}^{wh} + p_{i,t}^{nr} - ESS_{i,t} - p_{i,t}^{pv} \tag{3.16}$$

$$q_{i,t}^{cus} = q_i^{hvac} \cdot b_{i,t}^{hvac} + q_i^{wh} \cdot b_{i,t}^{wh} + q_{i,t}^{nr} \tag{3.17}$$

where eq. (3.16) calculates the real power load of each house, and eq. (3.17) calculates the reactive power load of each house. The power factor of the non-responsive load is set to 0.89.

3.3.6 Network flow model

The DistFlow model in [87] is applied to model power flow in the balanced radial network. An illustration of the network structure is given in Figure 3.3. The detailed mathematical formulations are given by eqs. (3.18)-(3.24).

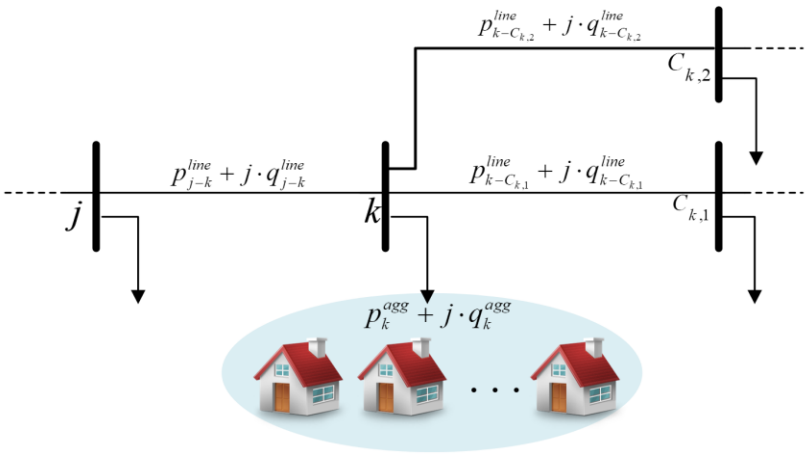

Figure 3.3 Illustration of the DistFlow model.

$$p_{k,t}^{agg} = \sum_{i \in k} p_{i,t}^{cus} \tag{3.18}$$

$$q_{k,t}^{agg} = \sum_{i \in k} q_{i,t}^{cus} \tag{3.19}$$

$$p_{j-k,t}^{line} = \sum_{\forall k-C_k} p_{k-C_k,t}^{line} + p_{k,t}^{agg} + \left(I_{j-k,t}^{line}\right)^2 \cdot r_{j-k}^{line} \tag{3.20}$$

$$q_{j-k,t}^{line} = \sum_{\forall k-C_k} q_{k-C_k,t}^{line} + q_{k,t}^{agg} + \left(I_{j-k,t}^{line}\right)^2 \cdot x_{j-k}^{line} \tag{3.21}$$

$$\left(V_{k,t}\right)^2 = \left(V_{j,t}\right)^2 - 2\left(r_{j-k}^{line} \cdot p_{j-k,t}^{line} + x_{j-k}^{line} \cdot q_{j-k,t}^{line}\right) + \left(I_{j-k,t}^{line}\right)^2 \cdot \left[\left(r_{j-k}^{line}\right)^2 + \left(x_{j-k}^{line}\right)^2\right] \tag{3.22}$$

$$\left(p_{j-k,t}^{line}\right)^2 + \left(q_{j-k,t}^{line}\right)^2 \le \left(V_{j,t}\right)^2 \cdot \left(I_{j-k,t}^{line}\right)^2 \tag{2.23}$$

$$p_t^{pcc} = p_{0-1,t}^{line} \tag{3.24}$$

where eqs. (3.18) and (3.19) are the net real and reactive load of aggregator k at time t respectively, eqs. (3.20) and (3.21) are the real and reactive power flow of line j-k at time t respectively, eq. (3.22) calculates the voltage magnitude of bus k at time t, eq. (2.23) is the branch flow constraint, and eq. (3.24) is the supply-demand balance constraint at the PCC.

Notice that constraints (3.20)-(3.22) are linear if $(V_{j,t})^2$, $(V_{k,t})^2$, and $(I_{j-k,t}^{line})^2$ are viewed as variables, and eq. (2.23) becomes a second-order cone constraint after relaxing the "equal" sign to the "less than or equal to" sign.

3.4 Decomposing the centralized model with ADMM

Despite the fact that many off-the-shelf packages (e.g. CPLEX, SCIP, BARON) can handle mixed-integer problems, they cannot be directly applied to solve the proposed centralized model due to the model's large number of binary variables and constraints. To address this challenge, the ADMM is introduced to decompose the original model into sub-problems and solve the residential DR problem in a distributed manner to ensure the scalability of the proposed method. The ADMM applies to optimization problems with separable objective functions. It was initially designed for convex problems (e.g. [88]), but has also demonstrated its effectiveness in solving non-convex problems with binary variables (e.g. [89]). In [72], the ADMM is used to decompose a large mixed-integer nonconvex problem into multiple sub-problems to distribute the computational complexity. Also, in [90] the ADMM is applied to determine the ON/OFF operation schedules of the HVACs in residential houses. The general ADMM problem formulation is given as follows [71]:

$$\min\ f(x)+g(z) \tag{3.25}$$

$$A\cdot x+B\cdot z=c \tag{3.26}$$

where x and z are two sets of variables, and $f(x)$ and $g(z)$ are two separable objectives. Also, eq. (3.26) is the equality coupling constraint, which contains both variable x and variable z.

The augmented Lagrangian form of ADMM can be represented as:

$$L_p\left(x,z,y\right)=f(x)+g(z)+y^T\cdot(Ax+Bz-c)+\rho/2\cdot\left\|Ax+Bz-c\right\|_2^2 \tag{3.27}$$

where y is the dual variable associated with the equality coupling constraint, and ρ is the penalty factor of the augmented Lagrangian term. In general, there is no unique standard on the selection of the penalty factor [90]. In this chapter, the value of ρ is set to 2.

Also, the primary and secondary residuals of ADMM in the dth iteration are defined by eqs. (3.28) and (3.29) as:

$$R^{(d)} = Ax^{(d)} + Bz^{(d)} - c \tag{3.28}$$

$$S^{(d)} = \rho A^T B\left(z^{(d)} - z^{(d-1)}\right) \tag{3.29}$$

To split the objectives, within each iteration, eq. (3.27) is minimized over x with z fixed and vice versa. Therefore, the equations for updating the values of x, z and y can be represented by eqs. (3.30)-(3.32):

$$x^{(d)} = \arg\min_x L_p(x, z^{(d-1)}, y^{(d-1)}) \tag{3.30}$$

$$z^{(d)} = \arg\min_z L_p(x^{(d)}, z, y^{(d-1)}) \tag{3.31}$$

$$y^{(d)} = y^{(d-1)} + \rho\left(Ax^{(d)} + Bz^{(d)} - c\right) \tag{3.32}$$

The iteration will stop when both $||R^{(d)}||_2$ and $||S^{(d)}||_2$ are respectively less than the primary and secondary feasibility tolerance values [91]-[92].

In the proposed model, the primary residual and the secondary residual are defined in eqs. (3.33) and (3.34) as:

$$R^{(d)} = p_{0-1}^{line(d)} - p^{pcc(d)} \tag{3.33}$$

$$S_i^{(d)} = \rho \cdot \left(p_i^{cus(d)} - p_i^{cus(d-1)}\right) \tag{3.34}$$

Moreover, $f(x)$ represents the customers' objective that aims to minimize the indoor and hot water temperature discomfort costs. The decision variable x includes the operating schedules of HVAC units, EWHs, and ESSs for the next day. $g(z)$ represents the utility's

objective function that aims to minimize electricity cost and peak load violation charge. The decision variable z is the amount of electricity supply at each time. Further, the coupling constraint is the supply-demand balance constraint in eq. (3.24), which contains variables from both the utility-level and house-level (since the aggregators do not have objective functions and are only responsible for aggregating house-level load). Therefore, the proposed centralized model can be decomposed into a utility-level optimization problem, aggregator-level calculation, and a set of house-level optimization problems.

3.4.1 House-level sub-problem

In the x-update step, each residential customer minimizes his/her discomfort cost and primary residual (i.e. power mismatch). The house-level objective function is represented as:

$$\min \sum_{t\in N_T} \left\{ \begin{array}{l} \alpha \cdot dis_{i,t}^{hvac} + \beta \cdot dis_{i,t}^{wh} + \lambda_t \cdot \left[R_t^{(d)} / N_N - P_{i,t}^{(d-1)} + P_{i,t}^{(d)} \right] \\ + \dfrac{\rho}{2} \cdot \left\| R_t^{(d)} / N_N - P_{i,t}^{(d-1)} + P_{i,t}^{(d)} \right\|_2^2 \end{array} \right\} \tag{3.35}$$

According to the solution algorithm in eqs. (3.30)-(3.32), the augmented Lagrangian form of the ADMM in eq. (3.27) is first minimized over x with z fixed. Therefore, the first two terms in eq. (3.35) are essentially the $f(x)$ in eq. (3.27). Further, since the value of z is fixed in the x-update step, the $g(z)$ term in eq. (3.27) becomes a constant and is excluded from the objective function in eq. (3.35). Finally, the remaining terms in eq. (3.35) are the penalties for violating the coupling constraints in eq. (3.24).

The constraints for the house-level optimization problem are eqs. (3.3)-(3.17).

The aggregators then collect local load information and report it to the utility:

$$p_{k,t}^{agg(d)} = \sum_{i \in k} p_{i,t}^{cus(d)} \tag{3.36}$$

$$q_{k,t}^{agg(d)} = \sum_{i \in k} q_{i,t}^{cus(d)} \tag{3.37}$$

In the *x*-update step, the information flows from the bottom hierarchy (i.e. houses) to the top hierarchy (i.e. utility). The messages sent from customers to their corresponding aggregators are arrays that contain the total real and reactive load usage data ($p_{i,t}^{cus}$ and $q_{i,t}^{cus}$) of each house at different times. After receiving the data, aggregators calculate the total load consumption within their service region ($p_{k,t}^{agg}$ and $q_{k,t}^{agg}$) and report it to the utility. An illustration of the information exchange among different agents in this step is shown in Figure 3.4(a).

(a) *x*-update step.

(b) *z*-update step.

Figure 3.4 Information exchange among agents.

3.4.2 Utility-level sub-problem

In the *z*-update step, the information flows from the top hierarchy (i.e. utility) to the bottom hierarchy (i.e. houses). The utility minimizes the electricity cost, the peak load violation cost, and the primary residual. The objective function of the utility-level optimization problem at the *d*th iteration is given by (3.38).

$$\min \sum_{t \in N_T} \left\{ a \cdot \left[p_t^{pcc(d)} \right]^2 + b \cdot p_t^{pcc(d)} + \lambda_t \cdot R_t^{(d)} + \left\| R_t^{(d)} \right\|_2^2 \right\} + \lambda^{vio} \cdot p^{vio} \tag{3.38}$$

The first two terms and the last term in eq. (3.38) are essentially the $g(z)$ in eq. (3.27). Further, since the value of x is fixed in the z-update step, the $f(x)$ term in eq. (3.27) becomes a constant and is excluded from the objective function in eq. (3.38). Finally, the remaining terms in eq. (3.38) are the penalties for violating the coupling constraints in eq. (3.24).

The constraints for the utility level optimization problem are eqs. (3.2), (3.20)-(2.23), and (3.33).

Also, the utility updates the dual variable associated with the supply-demand balance equation (y-update) after solving the utility-level problem:

$$\lambda_t^{(d)} = \lambda_t^{(d-1)} + \rho \cdot R_t^{(d)} \tag{2.39}$$

The messages sent from the utility through aggregators to customers are the primary residual (R_t) and the dual variable associated with the supply-demand balance equation (λ_t) at each time. An illustration of the information exchange in the z-update step between different agents is shown in Figure 3.4(b).

3.4.3 Solving process of the proposed algorithm

In summary, the process of using the ADMM to solve the scalable residential DR management problem is provided in Algorithm 1.

Algorithm 1. ADMM for scalable residential DR management systems

1. Each HEMS pulls the day-ahead weather forecast information from the local weather service center.
2. Initialize λ_t, R_t, $p_{i,t}^{cus}$ and $q_{i,t}^{cus}$
3. **while** $\left\|R^{(d)}\right\|_2 > \varepsilon_R$ or $\left\|S_i^{(d)}\right\|_2 > \varepsilon_S$ **do**
4. Each HEMS updates the operation schedule of the responsive devices based on the λ_t and R_t, then sends the $p_{i,t}^{cus}$ and $q_{i,t}^{cus}$ to its corresponding aggregator (*x*-update).
5. Each aggregator collects the load information of customers within its service region and reports $p_{k,t}^{agg}$ and $q_{k,t}^{agg}$ to the utility.
6. Utility updates R_t and λ_t, and broadcasts the information to all the aggregators (*z*-update and y-update).
7. Aggregators broadcast the R_t and λ_t information to their customers.
8. **End**

During the iteration process, the house-level HEMS receives the arrays of the dual variables associated with the power balance equations and the primal residual of the ADMM, then updates the real/reactive load consumption data at each time accordingly. The aggregator is responsible for calculating the total load within its service region and passing through information between customers and the utility. Finally, the utility receives the real/reactive load information from aggregators and updates the primary residual and dual variable information at each time.

3.5 Case study

The proposed approach is tested on a radial distribution network through a hybrid simulation platform, MATLAB 2018a and GAMS 24.7, where MATLAB is used for creating input data files for GAMS and storing the results. The hardware environment is a laptop with Intel (R) Core^{TM} i7-8650U 1.90GHz CPU, and 16.00GB RAM. The utility-level

sub-problem is solved by CPLEX, and the house-level sub-problems are solved by BARON and SCIP [93].

3.5.1 Input data

The configuration of the test system is shown in Figure 3.5 [94]. The time step is 15 minutes, and the time horizon is 24 hours. The total number of houses is 605. There are 606 agents in the system, one agent for each house plus one agent for the utility. Also, the residential houses are allocated to different aggregators based on the original load at each bus in the IEEE 33-bus system. There are 31 homes that have HVACs, EWHs, ESSs, and solar installed; 31 homes have HVACs, EWHs, and ESSs installed; 93 homes have HVACs, EWHs, and solar installed; and the remaining homes only have HVACs and EWHs installed.

The outdoor temperature and standard solar output forecast information are plotted in Figure 3.6 [95]-[96]. The discomfort weight factor for indoor temperature is \$0.05/℃, while the discomfort weight factor for water temperature is \$0.01/℃.

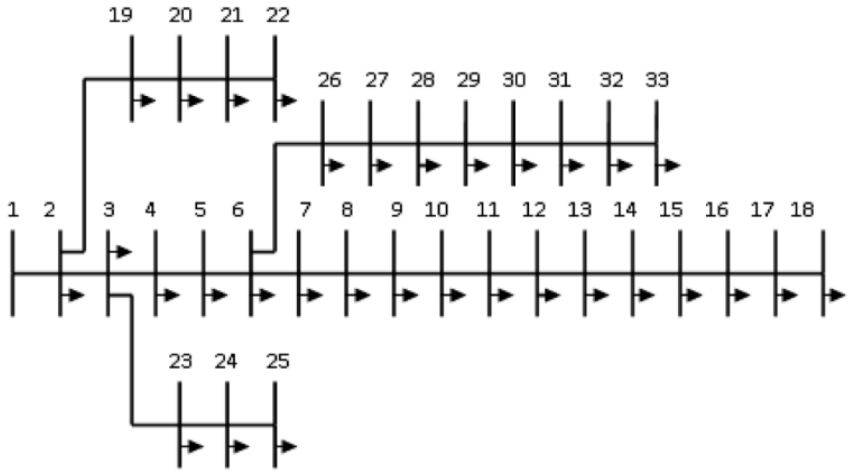

Figure 3.5 The IEEE 33 bus system configuration.

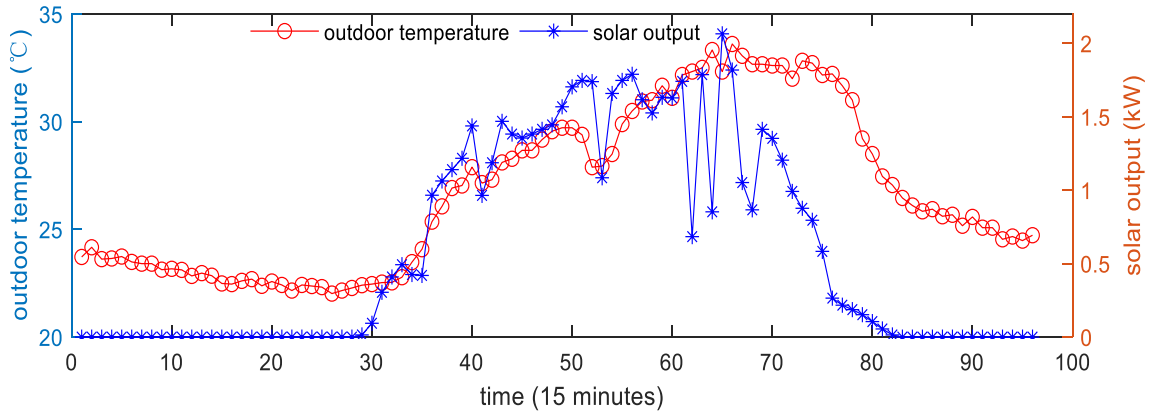

Figure 3.6 Outdoor temperature and solar generation data.

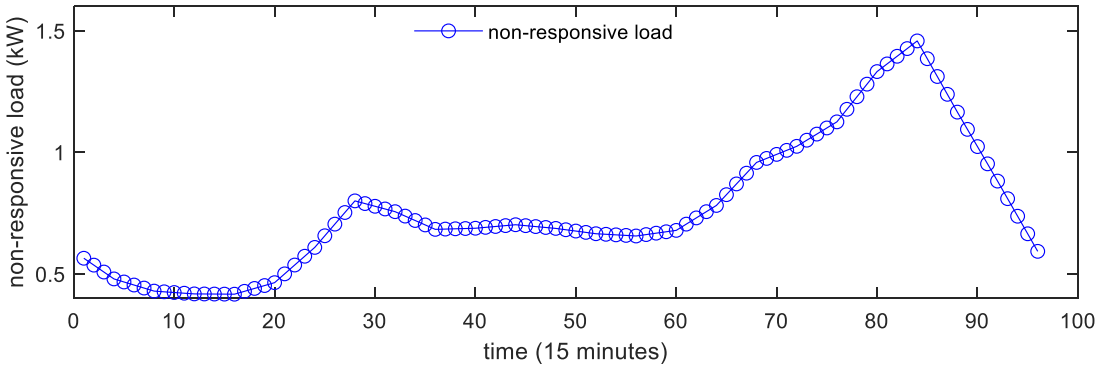

Figure 3.7 Non-responsive load data.

The non-responsive load profile is given in Figure 3.7 [97]. Random samples from normal distributions of solar power outputs and non-responsive loads are considered for each house to provide variation [98].

Three cases were designed to compare the performance of different scenarios, as explained in Table 3.4. Note that in Case 1 (conventional thermostatic-based control), the responsive devices will not change their operating status unless the indoor/water temperature falls out of the pre-specified boundaries.

Table 3.4 Different cases for testing the performance.

Case #	# of houses	Responsive devices	Control approach
1	605	HVAC, EWH	Conventional
2	605	HVAC, EWH	ADMM
3	605	HVAC, EWH, ESS	ADMM

The mathematical formulations for this conventional thermostatic control logic are described as [99]:

$$b_{i,t+1}^{hvac} = \begin{cases} 1 & \text{if } T_{i,t}^{in} \geq \overline{T}_i^{in} \\ 0 & \text{if } T_{i,t}^{in} \leq \underline{T}_i^{in} \\ b_t^{hvac} & \text{otherwise} \end{cases} \quad b_{i,t+1}^{wh} = \begin{cases} 0 & \text{if } T_{i,t}^{wh} \geq \overline{T}_i^{wh} \\ 1 & \text{if } T_{i,t}^{wh} \leq \underline{T}_i^{wh} \\ b_{i,t}^{wh} & \text{otherwise} \end{cases} \tag{3.40}$$

3.5.2 Simulation results

Since the proposed centralized model is a nonlinear programming problem with 116,160 binary variables, 364,417 continuous variables and 712,897 constraints, the ADMM is applied to solve the model in Case 2 and Case 3. Figure 3.8 compares the resulting load profiles for the different cases. In Case 1, the peak load of the utility appears at 7:00 pm and is 1853.25 kW, which exceeds the 1700 kW maximum load limit. In Case 2, the peak load is reduced to 1699.70 kW, and the maximum load appears at 5:00 pm. In Case 3, the maximum load is 1662.71 kW, and it appears at 6:15 pm. From this graph, it is concluded that the proposed model significantly reduces the peak load at the utility level with respect to conventional control.

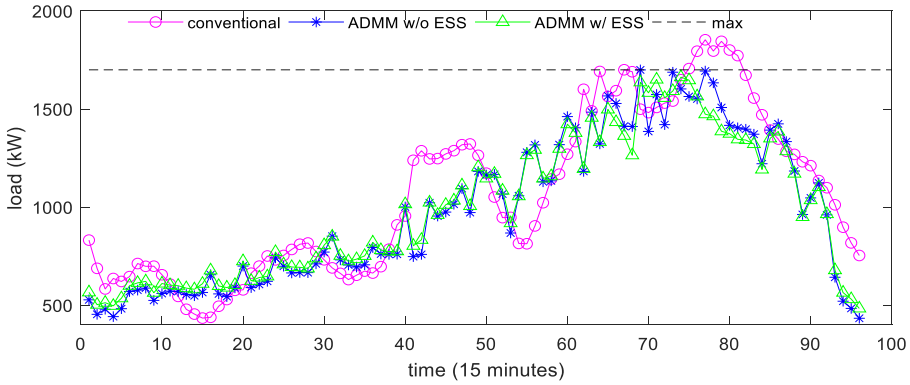

Figure 3.8 Comparison of the load profiles at the PCC for different cases.

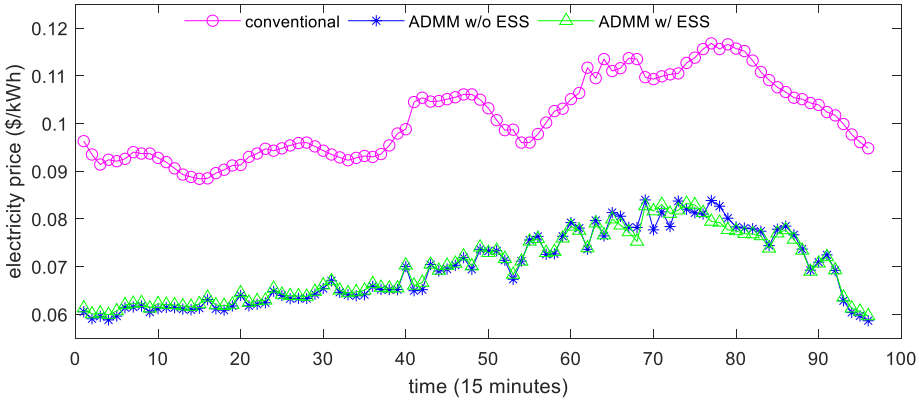

Figure 3.9 Comparison of the electricity prices for different cases.

Figure 3.9 shows the electricity prices for different cases. Since the Lagrangian multiplier in non-convex optimization problems may not reflect the real change in the objective function value when the parameter on the right side of the coupling equation changes, λ (which is the dual variable associated with the supply-demand balance equation) is not used for calculating electricity prices [100]. In this chapter, the electricity price is composed of two parts: the first part is determined by the electricity purchasing cost at the PCC, while the second part is determined by the peak load violation charge. The peak load violation cost is then distributed to all the residential customers and added to the electricity

price on a pro-rata basis. From Figure 3.9, it is observed that due to the peak load violation charge, the electricity price in Case 1 (purple curve) is always higher than the other cases. Further, the electricity prices in Case 2 (blue curve) and Case 3 (green curve) are similar.

Table 3.5 provides the average cost of each house for different cases. It can be concluded that due to the high discomfort cost and peak load violation charge, the average customer's cost in Case 1 is the highest. In Case 2, both the regular electricity cost and peak violation cost are lower than in Case 1. The total cost is reduced to $6.71, which is only about 67.98% of the cost in Case 1. In Case 3, the regular electricity cost is almost equal to that in Case 2, but the discomfort cost is further decreased. Therefore, the customers in Case 3 have the best performance.

Figure 3.10 and Figure 3.11 compare the indoor and water temperatures in house 1 for different cases. It is observed that Case 3 has the least deviations from the setpoints. Also, as the thermostatic control in Case 1 can only change the operating status of HVACs and EWHs when the temperatures fall out of the boundaries, Case 1 has the largest temperature deviations.

Table 3.5 The average cost of each house for different cases.

Cost	Case 1	Case 2	Case 3
Discomfort ($)	5.50	3.92	3.80
Electricity ($)	3.10	2.79	2.80
Peak Violation ($)	1.27	0	0
Total ($)	9.87	6.71	6.60

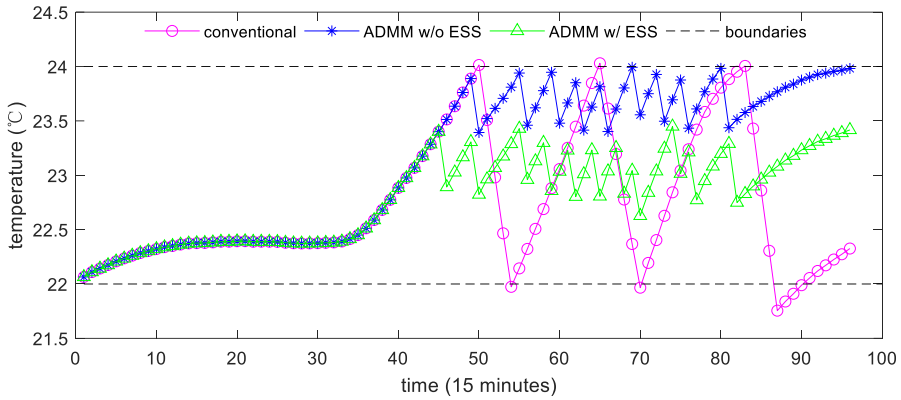

Figure 3.10 Comparison of the indoor temperature in house 1 for different cases.

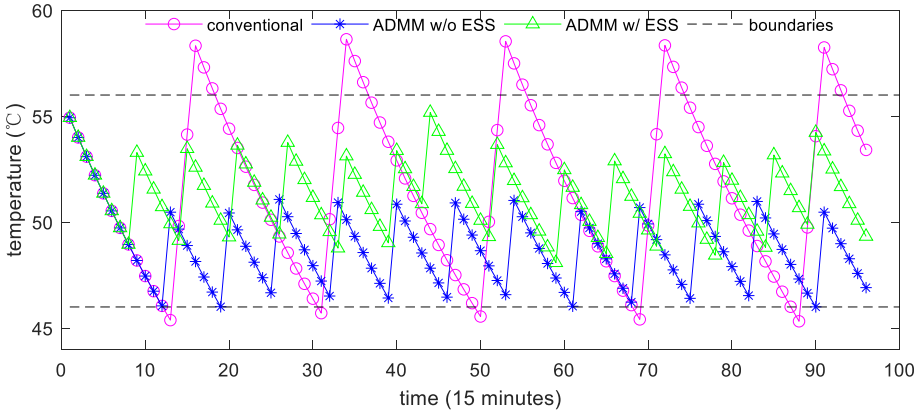

Figure 3.11 Comparison of the water temperature in house 1 for different cases.

Figure 3.12 and Figure 3.13 show the operating status of the HVAC and EWH in house 1 over time. It is observed that the operating status of the HVAC and EWH in Case 2 and Case 3 changes more frequently than in Case 1. Notice that in this chapter, it is assumed that the HVACs and EWHs cannot change their operation status within the time cycle to avoid the short-cycling issue. Although some literature considers startup and shutdown costs, adding these costs will introduce extra binary variables to the house-level sub-problems and further increase the computation time. Moreover, considering that the lifespans of HVACs and EWHs are usually longer than 15 years, the startup and shutdown costs are considered

marginal and would not significantly affect the optimization results. Therefore, the startup/shutdown costs of HVACs and EWHs are not considered in this chapter.

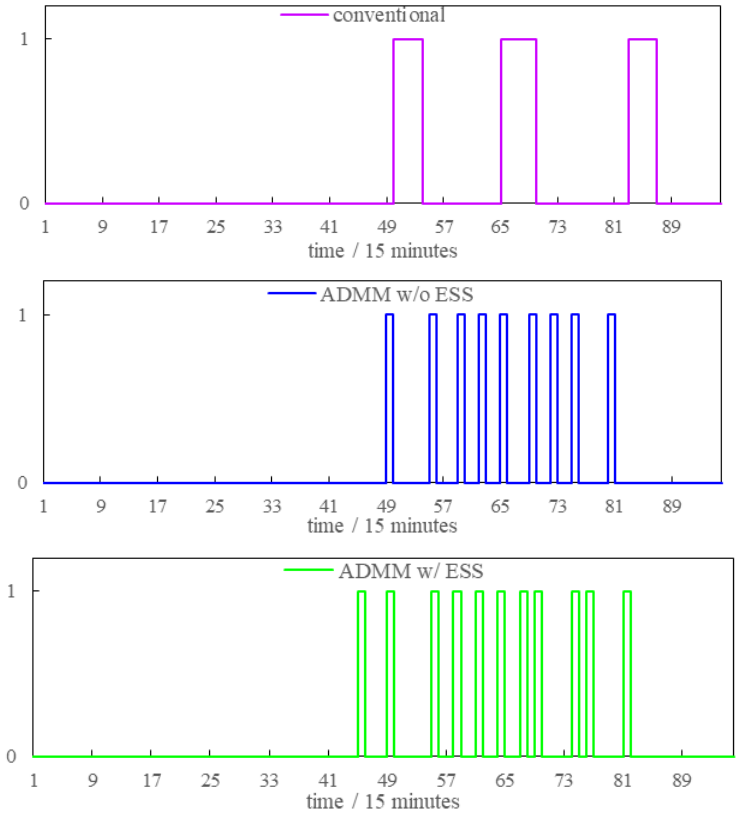

Figure 3.12 HVAC operation schedule in house 1 for different cases.

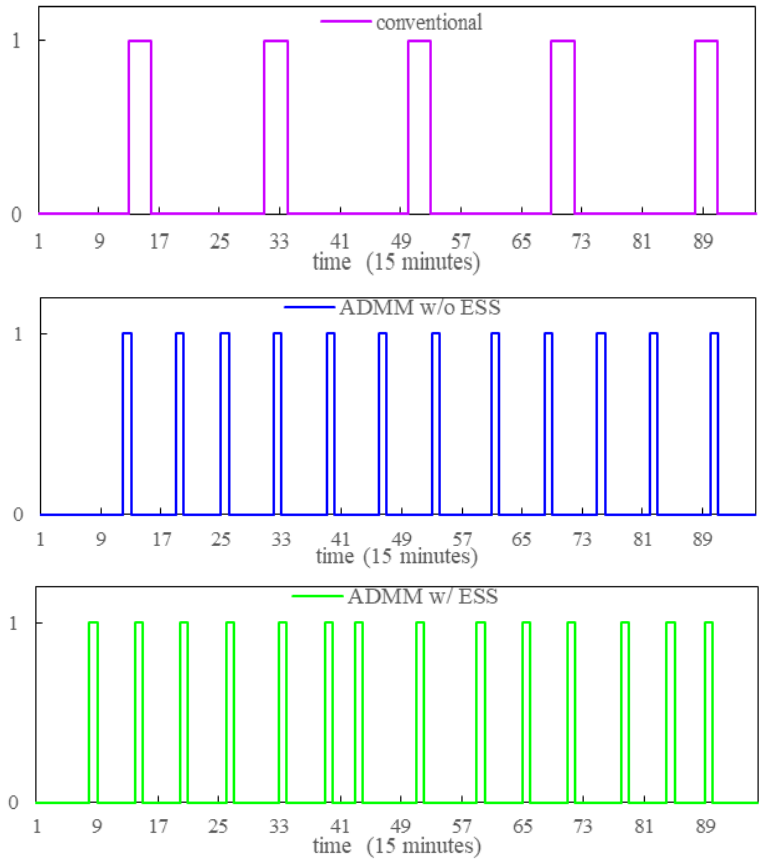

Figure 3.13 EWH operation schedule in house 1 for different cases.

3.5.3 Discussions

Figure 3.14 illustrates the convergence process of the ADMM in Case 2. The graph shows that the proposed solution algorithm takes 23 iterations to converge. It is worth mentioning that the number of iterations depends on specific problems and varies case by case. However, the iteration number is also closely related to the value of the penalty factor ρ. Generally, a smaller ρ yields better optimization results, but it comes with the risk of convergence issues. On the other hand, a larger ρ may give a sub-optimal solution, but it makes the algorithm easier to converge.

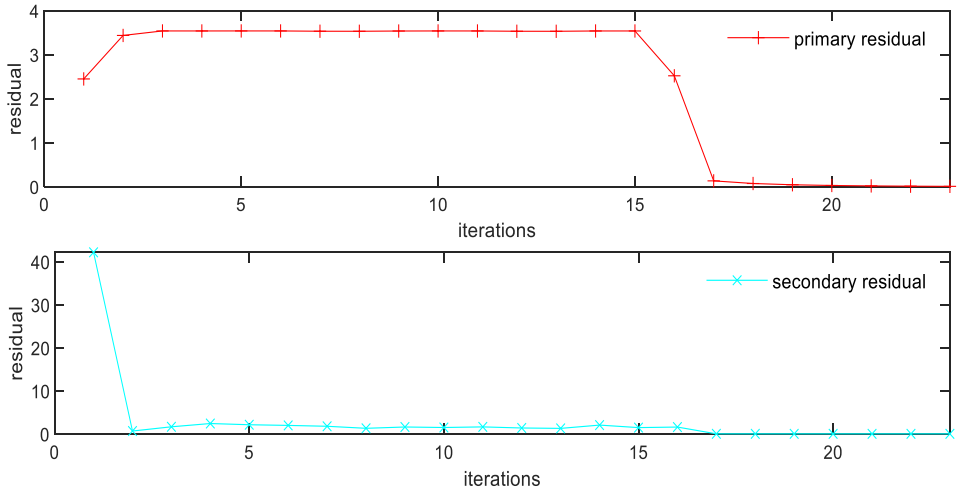

Figure 3.14 The primary and secondary residuals in each iteration.

The ρ value may also be tuned automatically by using adaptive ADMM algorithm, as discussed in [101]. However, in this chapter, only the conventional ADMM is used to solve the residential device management problems.

The computational time of the proposed approach for the different cases are also studied. In Case 2, the total computational time is 187.76 *sec*. In practice, since the house-level optimizations will run in parallel, the house that has the largest computational time determines the computational time of each iteration. The house-level model is a mixed-integer quadratic programming problem, and the first iteration has the longest computational time (88.25 *sec*), while the maximum utility-level model computational time in each iteration is 0.57 *sec*. In Case 3, the proposed approach takes 403.78 *sec* to converge, and the maximum computational time of the utility-level problem in each iteration is 0.34 *sec*.

In this chapter, the communication delays among different agents are not considered. Therefore, the time consumption in practical applications should be slightly longer than the

time mentioned previously. From the results, it is concluded that the proposed algorithm can satisfy the computational time requirements for managing residential DR programs.

Finally, Table 3.6 compares the optimization results from the centralized and distributed (ADMM-based) solution algorithms. The CPLEX solver in GAMS is used to solve the centralized problem, and the maximum computational time is specified as one hour.

As the table shows, in the distributed algorithm, the computational time does not increase with the number of houses because the iteration numbers of the ADMM for solving nonconvex problems are not positively correlated with the problem size. When the number of houses equals 15 or 20, it takes more iterations for the proposed approach to converge, thus making computational time slightly longer than the other three cases. Nevertheless, it is clearly shown that the ADMM approach is highly scalable and much faster than the centralized approach.

Table 3.6 Comparison of centralized and distributed algorithms.

	No. of houses	15	20	25	30	35
Centralized	Electricity cost ($)	2.48	2.53	3.26	3.66	n/a
	Discomfort cost ($)	2.02	2.06	1.99	1.99	n/a
	Total cost ($)	**4.50**	**4.59**	**5.25**	**5.65**	**n/a**
	Time (*sec*)	**3600**	**3600**	**3600**	**3600**	**3600**
Distributed (ADMM-based)	Electricity cost ($)	1.93	1.97	1.90	1.94	1.98
	Discomfort cost ($)	3.03	3.14	3.01	3.19	3.04
	Total cost ($)	**4.96**	**5.11**	**4.91**	**5.13**	**5.02**
	Time (*sec*)	**68.63**	**68.10**	**31.21**	**24.31**	**34.35**

Note: The computing time limit for the centralized approach is 1 hour (3600 sec), and the centralized approach cannot converge to a solution with 35 houses or more.

Further, Table 3.6 shows that the centralized solution approach performs slightly better than the distributed ADMM algorithm when the total number of houses is 20 or less, which is reasonable; when the house number grows to 25 or 30, the ADMM outperforms the centralized approach because the problem scale is large and the centralized solver essentially gives a sub-optimal solution; further, when the house number is 35 or more, the centralized approach cannot converge. This clearly demonstrates that the centralized approach is not scalable, while the distributed ADMM shows a very consistent performance.

Thus, the comparative study results in Table 3.6 present a benchmarking performance of centralized and distributed algorithms at increasing system scales, and these results have achievable values for future research works.

3.6 Chapter Summary

In this chapter, a scalable residential DR management solution is proposed for a hierarchical network structure, which is composed of a utility, LAs, and residential customers, to maximize community social welfare. However, this centralized model is neither directly solvable nor feasible due to the problem size and data privacy issues. Therefore, the ADMM is applied to decompose the centralized model into a utility-level sub-problem and a set of house-level sub-problems to reduce computational complexity.

Since the optimization model can be solved in a distributed manner, the proposed approach is especially applicable to distribution networks with large numbers of houses. The information exchange among the utility, LAs, and customers is limited to power consumption, the dual variable of the power balance equation, and the primary residual, which considerably protects customer privacy and makes the approach more practical.

Further, a comparative study is given in the case study section to present a benchmarking performance of the centralized and distributed ADMM algorithms with increasing system scales, and it provides references for future research works.

The limitation of this chapter is that the proposed DR management approach assumes the utility has the full information of the electricity cost function. However, in an open-market environment, the impact of day-ahead locational marginal price and real-time pricing signals on residential DR program performance should also be considered.

Chapter 4 A Comprehensive Scheduling Framework using Stochastic Programming-Alternating Direction Method of Multipliers for Residential Demand Response with Weather and Customer Uncertainties

This chapter presents a comprehensive scheduling framework for residential DR programs considering both the day-ahead and real-time electricity markets. In the first stage, residential customers determine the operating status of their responsive devices such as HVAC systems and EWHs, while the distribution system operator (DSO) computes the amount of electricity to be purchased in the day-ahead electricity market. In the second stage, the DSO purchases insufficient (or sells surplus) electricity in the real-time electricity market to maintain the supply-demand balance. Due to computational complexity and data privacy issues, the proposed model cannot be directly solved in a centralized manner, especially with a large number of uncertain scenarios. Therefore, this chapter proposes a combination of the SP and the ADMM algorithms, called SP-ADMM algorithm, to decompose the original model and then solve each sub-problem in a distributed manner while considering multiple uncertain scenarios. The simulation study is performed on the IEEE 33-bus system including 121 residential houses. The results demonstrate the effectiveness of the proposed approach for large-scale residential DR applications under weather and customer uncertainties.

Nomenclature

Sets and Indices

d	Index of iterations.
N_M / j, k	Set / index of buses (aggregators).
C_k	Set of child buses of bus k.
N_N / i	Set / index of residential customers.
Ns / s	Set / index of scenarios.
N_T / t	Set / index of time.

Parameters

a / b	Electricity cost coefficients.
c^{water}	Specific heat capacity of water (J/(kg·℃)).
C_i^{house}	Thermal capacitance of house i (J/℃).
C_i^{wh}	Thermal capacitance of the EWH in house i (J/℃).
$m_{i,t,s}^{water}$	Hot water consumption of house i at time t in scenario s (kg).
p_i^{hvac} / q_i^{hvac}	Real/reactive power rating of the HVAC in house i (kW).
$p_{i,t,s}^{nr}$ / $q_{i,t,s}^{nr}$	Real/reactive load of the non-responsive devices in house i at time t in scenario s (kW).
$\overline{P}^{pcc}$	Maximum contracted load limit at the PCC (kW).
$p_{i,t,s}^{pv}$	PV generation of house i at time t in scenario s (kW).
p_i^{wh} / q_i^{wh}	Real/reactive power rating of the EWH in house i (kW).
$r_{j\text{-}k}^{line}$ / $x_{j\text{-}k}^{line}$	Resistance/reactance of the distribution line connecting bus j and bus k (Ω).
R_i^{house}	Thermal resistance of house i (℃/kW).
R_i^{wh}	Thermal resistance of the EWH in house i (℃/kW).
$\underline{T}_i^{in}$ / $\overline{T}_i^{in}$	Minimum/maximum indoor temperature limit of house i (℃).
T_i^{ins}	Indoor temperature setpoint of house i (℃).
$T_{i,t,s}^{out}$	Outdoor temperature forecast at time t in scenario s (℃).

$\underline{T}_i^{wh}$ / $\overline{T}_i^{wh}$	Minimum/maximum water temperature limit of the EWH in house i (℃).
T_i^{whs}	Hot water temperature setpoint of house i (℃).
V^{pcc}	Voltage magnitude at the PCC.
α / β	Weight factors ($/℃).
ε^R / ε^S	Primary/secondary tolerance value.
Δt	Length of the time interval.
λ^{rtp} / λ^{rts}	Electricity purchasing/selling price in the real-time market ($/kW).
λ^{vio}	Peak load violation rate ($/kW).
ρ	Penalty factor of the augmented Lagrangian term.

Continuous Variables

$dis_{i,t,s}^{hvac}$	Indoor temperature discomfort of customer i at time t in scenario s (℃).
$dis_{i,t,s}^{wh}$	Water temperature discomfort of customer i at time t in scenario s (℃).
$p_{i,t,s}^{cus}$ / $q_{i,t,s}^{cus}$	Real/reactive load of house i at time t in scenario s (kW / kVar).
$p_{j,t,s}^{agg}$ / $q_{j,t,s}^{agg}$	Real/reactive load of aggregator j at time t in scenario s (kW / kVar).
$p_{j\text{-}k,t,s}^{line}$ / $q_{j\text{-}k,t,s}^{line}$	Real/reactive power flowing from node j to node k at time t in scenario s (kW / kVar).
$p_{t,s}^{da}$	The amount of electricity purchased from the day-ahead market at time t in scenario s (kW).
$p_{t,s}^{pcc}$	Actual load at the PCC at time t in scenario s (kW).
$p_{t,s}^{rtp}$ / $p_{t,s}^{rts}$	The amount of electricity purchased from/sold to the real-time market at time t in scenario s (kW).
p_s^{vio}	The maximum amount of load that exceeds the contracted load limit in scenario s (kW).
$R_{t,s}$	Primal residual of the ADMM at time t in scenario s.
$S_{i,t,s}$	Secondary residual of house i at time t in scenario s.
$T_{i,t,s}^{in}$	Indoor temperature of house i at time t in scenario s (℃).
$T_{i,t,s}^{wh}$	Water temperature of the EWH in house i at time t in scenario s (℃).
$V_{j,t,s}$	Voltage magnitude of bus j at time t in scenario s.

$\lambda_{t,s}$	Dual variable associated with the power balance equation at time t in scenario s.

Binary Variables

$b_{i,t}^{hvac}$	Operating status of the HVAC in house i at time t.
$b_{i,t}^{wh}$	Operating status of the EWH in house i at time t.

4.1 Introduction

The ever-increasing electric load and renewable integration have posed severe threats to the secure and economic operations of power grids [102]-[103]. One solution to address this challenge is implementing the DR [104]. Existing DR programs are primarily designed for industrial and commercial customers, who tend to have larger electric loads that are more easily targetable [54]. However, residential loads account for 38% of the total energy consumption in the United States, indicating the significant potential in this sector [105]. Since residential loads are composed of numerous low-capacity home appliances, it is imperative to have an effective algorithm that can coordinate the operating schedules of residential components and devices at scale to improve DR impact and performance [55].

In recent years, advances in communication technology have provided tremendous opportunities for grid operators to send messages to (or receive messages from) residential customers through secured two-way communication channels [57]. With the support of HEMSs, DSOs can connect with customers to realize system-wide control objectives, e.g., DR. Existing control structures for residential DR programs are categorized into centralized and distributed approaches [25]. In [62] and [63], residential DR management problems are formulated as centralized models, where the control actions are computed and executed by the control center according to the measurements from sub-systems. Centralized approaches

are straightforward and applicable to small-scale networks with customers sharing common goals. However, end-users may have to release their device operation information and allow the utility to control their appliances. Moreover, as the number of customers grows, the computational complexity will be significantly increased. In [64] and [65], distributed residential DR models are proposed, where customers independently conduct local optimizations to determine the optimal scheduling of devices. The major part of the calculation is performed by local HEMSs, distributing the intelligence and reducing the centralized computational requirements. Since each HEMS is independent, calculations are all run in parallel, reducing the needed computational time. Meanwhile, privacy can also be better protected, as only minimal information is shared with the electric utility company.

In addition to scalability and privacy issues, DR programs may also confront challenges of handling uncertain parameters, e.g., weather and customer uncertainties [106]-[108]. The conventional approach is to treat uncertain parameters as fixed values. However, as forecasting technology is still immature, extra spinning reserve capacity and supplemental reserve have to be ensured, which increases the electricity cost [109]. To address this challenge, attention has been paid to optimization methods that model uncertainty and fluctuation as non-constant values [110]. In [111], a robust optimization model is proposed to shave the system peak load and reduce residential customers' electricity bills while considering weather and occupancy uncertainties. The results indicate that the aggregator can still reduce the peak load even in the worst case where none of the customers agree with the system-level objectives. Generally, the inputs for robust optimization are the bounds of the uncertain parameters. This allows robust optimization to avoid the risks of constraint violations in extreme conditions. In [112], a SP model for HEMSs is presented, which aims

to reduce customers' electricity costs while considering the uncertainties of the availability of electric vehicles (EVs) and renewable generation. The results demonstrate that residential customers can save up to 31% as compared to the deterministic approach. Unlike robust optimization, SP assumes the uncertain parameters comply with certain probabilistic distributions, such that it can be converted to an equivalent deterministic problem. In [113], SP and robust optimization are applied to solve a real-time price-based DR management problem. The results suggest that both approaches can mitigate the financial risk introduced by the price uncertainty. Another observation is that SP has higher computational requirements but yields a lower electricity cost solution as compared to robust optimization.

To conclude, even though previous works have already explored the parameter uncertainty problems in DR, there is still a lack of a comprehensive scheduling framework to coordinate the operating schedules of numerous home devices at scale while considering the weather and customer uncertainties. The main contributions of this chapter are summarized as follows:

1) a comprehensive scheduling framework that considers both the day-ahead and real-time electricity markets is proposed to mitigate the impacts of weather and customers' behavior uncertainties on residential DR performance;

2) a limited information exchange mechanism is developed among the DSO, LAs, and customers to better protect residential customers' privacy; and

3) a new solution algorithm called SP-ADMM is proposed which combines the SP and ADMM algorithms. The proposed SP-ADMM model decomposes the original model into sub-problems to ensure the feasibility of the proposed algorithm for large-scale applications while considering a large number of uncertain scenarios.

The rest of this chapter is structured as follows: Section 4.2 presents the architecture of the residential distribution networks, Section 4.3 formulates the proposed comprehensive framework for residential DR, Section 4.4 discusses the solution algorithm, Section 4.5 conducts the case studies, and Section 4.6 concludes the chapter.

Notation conventions: superscript ^{hvac} refers to HVAC, superscript ^{wh} refers to EWH, superscript ^{cus} refers to residential customers, superscript ^{agg} refers to LAs, and superscript ^{line} refers to distribution lines.

4.2 Distribution network architecture

Four types of uncertain parameters are studied in this chapter, including 1) outdoor temperature, 2) solar generation, 3) non-responsive load, and 4) hot water consumption. To reduce the impact of uncertain parameters on residential DR, a two-stage scheduling model has been formulated. In the first stage, residential customers determine the operating status of responsive devices, while the DSO computes the amount of electricity to be purchased in the day-ahead market. In the second stage, the DSO purchases insufficient (or sells surplus) electricity in the real-time market to maintain the supply-demand balance. A graph illustrating this process is provided in Figure 4.1.

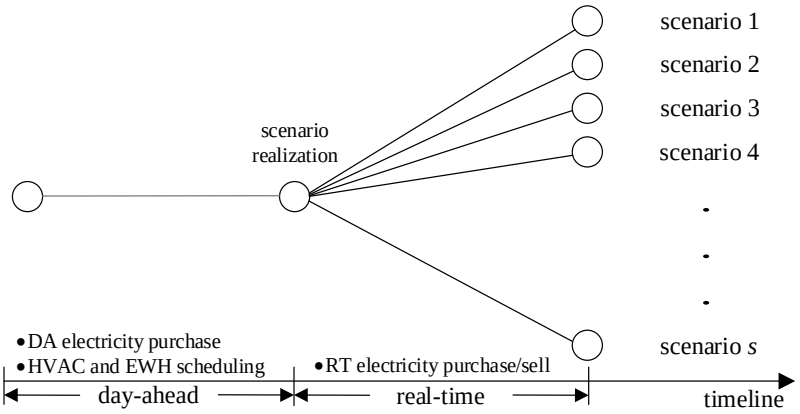

Figure 4.1 The proposed two-stage residential management approach.

4.3 Problem formulation

The proposed residential distribution network has a three-level hierarchical architecture, including the DSO, LAs, and residential customers, which are the top, middle, and bottom levels, respectively. In this study, LAs are the intermediates between the DSO and customers. The reason for introducing LAs is that the flexible load resource of a single residential customer is far less than the DSO's minimum capacity threshold. LAs can collect small load resources for the DSO and help residential customers to participate in the electricity market [80]-[82]. Moreover, LAs reduce DSO communication requirements since communication needs are now reduced to a single entity instead of many assets.

Further, it is assumed that the residential customers are clustered by geographical locations and interconnected to the distribution system through LAs. From the power flow viewpoint, LAs are treated as buses and interconnected to form a distribution network. At the house level, HEMSs are responsible for receiving data from LAs and local weather service centers to perform optimization and decision-making on behalf of customers. The responsive devices considered in this study are HVACs systems and EWHs.

4.3.1 Objective function

The objective of the residential DR program is to maximize community social welfare, as described by:

$$\min f(x) + E\left[Q(x,\xi)\right] \tag{4.1}$$

$$f(x) = \sum_{t \in N_T} \left[a \cdot \left(p_t^{da} \right)^2 + b \cdot p_t^{da} \right] \tag{4.2}$$

$$Q(x,\xi) = \lambda^{vio} \cdot p_s^{vio} + \sum_{t \in N_T} \left(\lambda^{rtp} \cdot p_{t,s}^{rtp} - \lambda^{rts} \cdot p_{t,s}^{rts} \right) + \sum_{t \in N_T} \sum_{i \in N_N} \left(\alpha \cdot dis_{i,t,s}^{hvac} + \beta \cdot dis_{i,t,s}^{wh} \right) \tag{4.3}$$

where $f(x)$ represents the first-stage objective, $Q(x, \xi)$ represents the second-stage objective, (4.2) calculates the DSO's electricity purchasing cost in the day-ahead market represented by a quadratic function [84], (4.3) calculates the sum of peak load violation charge, electricity trading cost in the real-time market, and customers' discomfort cost. Note that in (4.3), the peak load violation charge is defined as the product of a peak load violation rate and the maximum amount of load that exceeds the contracted load limit at the PCC [114]. The load violation amount can be calculated from (4.4) and (4.5). In this chapter, the peak load violation rate is set to \$10/kW.

$$p_{t,s}^{pcc} = p_t^{da} + p_{t,s}^{rtp} - p_{t,s}^{rts} \tag{4.4}$$

$$p_s^{vio} = \max\left(p_{t,s}^{pcc} - \overline{p}^{pcc}, 0 \right) \quad \text{for all } t \in N_T \tag{4.5}$$

4.3.2 HVAC model

The input parameter for the HVAC model is the day-ahead outdoor temperature forecast in each scenario. The HVAC model is represented by:

$$T_{i,t,s}^{in} = T_{i,t-1,s}^{in} + [(T_{i,t,s}^{out} - T_{i,t-1,s}^{in}) / R_i^{house} - b_{i,t}^{hvac} \cdot p_i^{hvac}] \cdot \Delta t / C_i^{house} \quad (4.6)$$

$$\underline{T}_i^{in} \le T_{i,t,s}^{in} \le \overline{T}_i^{in} \quad (4.7)$$

$$dis_{i,t,s}^{hvac} = \left| T_{i,t,s}^{in} - T_i^{ins} \right| \quad (4.8)$$

where (4.6) calculates the indoor temperature of house *i* at each time in different scenarios, (4.7) is the minimum/maximum indoor temperature limit constraint for each house, and (4.8) calculates customers' discomfort due to indoor temperature deviating from the setpoint in different scenarios. The detailed parameter settings of HVAC are given in Table 4.1, and the power factor of HVAC is set to 0.81.

4.3.3 EWH model

Similar to the HVAC model, the input parameter for the EWH model is the indoor temperature and the amount of hot water consumption in each scenario. The discrete-time form of the EWHs model is represented by:

$$T_{i,t,s}^{wh} = T_{i,t-1,s}^{wh} + [(T_{i,t,s}^{in} - T_{i,t-1,s}^{wh}) / R_i^{wh} - c^{water} \cdot m_{i,t,s}^{water} \left(T_{i,t-1,s}^{wh} - T_{i,t,s}^{in} \right) + b_{i,t}^{wh} \cdot p_i^{wh}] \cdot \Delta t / C_i^{wh} \quad (4.9)$$

$$\underline{T}_i^{wh} \le T_{i,t,s}^{wh} \le \overline{T}_i^{wh} \quad (4.10)$$

$$dis_{i,t,s}^{wh} = \left| T_{i,t,s}^{wh} - T_i^{whs} \right| \quad (4.11)$$

where (4.9) calculates the water temperature of house *i* at each time in different scenarios, (4.10) is the minimum/maximum water temperature limit constraint for each house, and (4.11) calculates customers' discomfort due to water temperature deviating from the setpoint in different scenarios. The detailed parameter settings of EWH are given in Table 4.2, and the power factor of EWH is set to 1.0.

Table 4.1 Parameter settings of the HVAC.

C_i^{house}	U[1.0, 1.5] J/℃	R_i^{house}	U[6.4, 9.6] J/℃
P_i^{hvac}	3.5 kW	T_i^{ins}	U[21, 23] ℃
$\underline{T}_i^{in}$	T_i^{ins} -1℃	$\overline{T}_i^{in}$	T_i^{ins} +1℃

Table 4.2 Parameter settings of the EWH.

C_i^{wh}	U[0.1, 0.15] J/℃	R_i^{wh}	U[48.0, 72.0] J/℃
P_i^{wh}	2.5 kW	T_i^{whs}	U[55.0, 57.5] ℃
$\underline{T}_i^{wh}$	T_i^{whs} -5℃	$\overline{T}_i^{wh}$	T_i^{whs} +5℃

4.3.4 Load model

In this chapter, the power output of the solar PV is viewed as a negative load. Therefore, the load of each house is equal to the sum of the responsive load (including HVAC and EWH) and the non-responsive load minus the solar generation. The load model is given by:

$$p_{i,t,s} = p_i^{hvac} \cdot b_{i,t}^{hvac} + p_i^{wh} \cdot b_{i,t}^{wh} + p_{i,t,s}^{nr} - p_{i,t,s}^{pv} \tag{4.12}$$

$$q_{i,t,s} = q_i^{hvac} \cdot b_{i,t}^{hvac} + q_i^{wh} \cdot b_{i,t}^{wh} + q_{i,t,s}^{nr} \tag{4.13}$$

where (4.12) calculates the real power load of each house in different scenarios, and (4.13) calculates the reactive power load of each house in different scenarios.

4.3.5 Network model

The DistFlow equations in [87] are applied to solve the network flow problem in the distribution network. The detailed mathematical formulations for distribution network flow are given as follows:

$$p_{k,t,s}^{agg} = \sum_{i \in k} p_{i,t,s}^{cus} \tag{4.14}$$

$$q_{k,t,s}^{agg} = \sum_{i \in k} q_{i,t,s}^{cus} \tag{4.15}$$

$$p_{j-k,t,s}^{line} = \sum_{\forall k-C_k} p_{k-C_k,t,s}^{line} + p_{k,t,s}^{agg} + \left(I_{j-k,t,s}^{line}\right)^2 \cdot r_{j-k}^{line} \tag{3.16}$$

$$q_{j-k,t,s}^{line} = \sum_{\forall k-C_k} q_{k-C_k,t,s}^{line} + q_{k,t,s}^{agg} + \left(I_{j-k,t,s}^{line}\right)^2 \cdot x_{j-k}^{line} \tag{3.17}$$

$$\left(V_{k,t,s}\right)^2 = \left(V_{j,t,s}\right)^2 - 2\left(r_{j-k}^{line} \cdot p_{j-k,t,s}^{line} + x_{j-k}^{line} \cdot q_{j-k,t,s}^{line}\right) + \left(I_{j-k,t,s}^{line}\right)^2 \cdot \left[\left(r_{j-k}^{line}\right)^2 + \left(x_{j-k}^{line}\right)^2\right] \tag{3.18}$$

$$\left(p_{j-k,t,s}^{line}\right)^2 + \left(q_{j-k,t,s}^{line}\right)^2 \le \left(V_{j,t,s}\right)^2 \cdot \left(I_{j-k,t,s}^{line}\right)^2 \tag{3.19}$$

$$p_{t,s}^{pcc} = p_{0-1,t,s}^{line} \tag{3.20}$$

where (4.14) calculates the net real load at aggregator *k* in different scenarios, (4.15) calculates the net reactive load at aggregator *k* in different scenarios, (3.16) and (3.17) respectively represent the real and reactive branch power flow of line *j*-*k* at time *t* in different scenarios, (3.18) calculates the voltage magnitude of each bus *k* at each time in different scenarios, (3.19) is the conic constraints, and (3.20) is the power balance constraint at the PCC.

Notice that constraints (3.16)-(3.18) are linear if $(V_{j,t,s})^2$, $(V_{k,t,s})^2$, and $(I_{j-k,t,s}^{line})^2$ are viewed as variables, and eq. (3.19) becomes a second-order cone constraint after relaxing the "equal" sign to the "less than or equal to" sign.

4.4 Solution methodology

The above model involves a large amount of variables if a centralized optimization algorithm is applied. For example, in the next section of case studies, the IEEE 33-bus system including 121 residential houses will be used as the test system, where the optimization problem has 887,040 continuous variables, 23,232 binary variables, 654,720 equality constraints, and 1,059,168 inequality constraints.

Due to the massive problem size, it would be difficult to directly solve this model with available solvers. Therefore, the ADMM is introduced to decompose the original problem into a DSO-level problem and a set of house-level sub-problems to reduce the computational complexity. Meanwhile, there are multiple uncertain scenarios in the residential DR behavior, so a mathematical model considering such uncertainties must be addressed as well. Therefore, a solution algorithm called SP-ADMM, which combines SP and ADMM to solve the model in section 4.3 is proposed. The proposed SP-ADMM algorithm for solving comprehensive DR scheduling is illustrated next.

In this chapter, $f(x)$ represents the customers' objective that aims to minimize the indoor temperature and water temperature discomfort cost. The decision variable x includes the operating schedules of HVACs and EWHs for the next day. $g(z)$ represents the utility's objective function that aims to minimize the contracted load violation charge plus the electricity purchasing cost in both the day-ahead and real-time electricity markets. The decision variable z is the amount of electricity purchased from (or sold to) the electricity markets. Moreover, the coupling constraint is the supply-demand balance constraint in (3.20), which contains variables from both the utility-level and house-level (since the LAs do not have objective functions and are only responsible for aggregating the house-level load). Therefore, the proposed centralized model can be decomposed into a utility-level optimization problem and a set of house-level optimization problems. The primary residual and the secondary residual are calculated by (4.21) and (4.22), respectively:

$$R_s^{(d)} = p_s^{pcc,(d)} - p_{0-1,s}^{line,(d)} \tag{4.21}$$

$$S_{i,s}^{(k)} = \rho \cdot \left(p_{i,s}^{cus,(d)} - p_{i,s}^{cus,(d-1)} \right) \tag{4.22}$$

The dual variable associated with the coupling constraint is calculated by:

$$\lambda_s^{(d)} = \lambda_s^{(d-1)} + \rho \cdot R_s^{(d)} \tag{4.23}$$

After the decomposition, the deterministic equivalent of the house-level optimization problem can be represented by:

$$\begin{aligned} &\min \sum_{t\in N_T}\sum_{s\in N_S}\left(\alpha \cdot dis_{i,t,s}^{hvac} + \beta \cdot dis_{i,t,s}^{wh}\right) \\ &+\sum_{t\in N_T}\sum_{s\in N_S}\rho_s \cdot \left\{\lambda_t\left[R_{t,s}^{(d)}/N_N - p_{i,t,s}^{cus,(d-1)} + p_{i,t,s}^{cus}\right]\right\} \\ &+\sum_{t\in N_T}\sum_{s\in N_S}\rho_s \cdot \left\{\frac{\rho}{2}\cdot\left\|R_{t,s}^{(d)}/N_N - p_{i,t,s}^{cus,(d-1)} + p_{i,t,s}^{cus}\right\|_2^2\right\} \end{aligned} \tag{4.24}$$

where the first two terms minimize the customers' discomfort cost, and the remaining terms present the penalty for violating the power balance constraints.

The constraints for the house-level optimization problem are (4.6)-(4.13), and (4.22).

The aggregator-level calculation collects local real and reactive load information and reports it to the DSO, as given by (4.14)-(4.15).

The deterministic equivalent of the DSO-level objective function becomes:

$$\begin{aligned} &\min \sum_{t\in N_T}\left[a\cdot\left(p_t^{da}\right)^2 + b\cdot p_t^{da}\right] + \sum_{s\in N_S}\rho_s\cdot\lambda^{vio}\cdot p_s^{vio} \\ &+\sum_{t\in N_T}\sum_{s\in N_S}\rho_s\cdot\left(\lambda_s^{rtp}\cdot p_{t,s}^{rtp} - \lambda_s^{rts}\cdot p_{t,s}^{rts}\right) + \sum_{t\in N_T}\sum_{s\in N_S}\rho_s\cdot\left(\lambda_{t,s}\cdot R_{t,s}^{(d)} + \frac{\rho}{2}\cdot\left\|R_{t,s}^{(d)}\right\|_2^2\right) \end{aligned} \tag{4.25}$$

where the first two terms represent the electricity purchasing cost in the day-ahead market, the third term is the peak load violation charge, the fourth and fifth terms are the cost/revenue for trading electricity in the real-time electricity market, and the rest represents the penalty terms for violating the power balance constraints.

The constraints for the DSO level optimization problem are (4.4)-(4.5), (3.16)-(3.19), (4.21), and (4.23).

In summary, the messages sent from the DSO through LAs to all the customers are arrays that contain the dual variable associated with the power balance equation and the primary residual of the ADMM in each scenario. The messages sent from customers to their corresponding LAs are arrays that contain the total real and reactive load usage data in each scenario. Finally, the messages sent from LAs to the DSO are the total real and reactive power consumption within their service region in each scenario.

The flowchart of using SP-ADMM to solve the two-stage residential DR management problems is given in Figure 4.2.

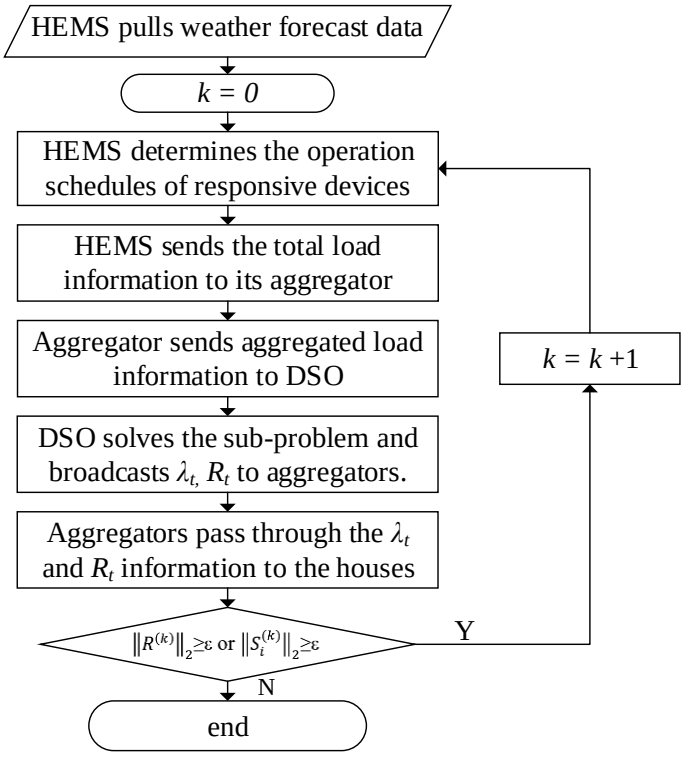

Figure 4.2 Flowchart of the proposed algorithm.

During the iteration process, the house-level HEMS receives the arrays of the dual variables associated with the power balance equations and the primal residual of the ADMM in each scenario, then it updates the real/reactive load consumption data in each scenario accordingly. The aggregator is responsible for calculating the total load within its service region and passing the information to the DSO. Finally, the DSO receives the real/reactive load information from each aggregator and updates the primal residuals and dual variables associated with the coupling constraints in each scenario. The iteration will stop when both $||R_s^{(k)}||^2$ and $||S_i^{(d)}||^2$ satisfy the tolerance criteria.

4.5 Case study

The proposed algorithm is tested on the IEEE 33-bus system including 121 residential houses. As previously mentioned in the beginning paragraph in Section 4.4, the optimization model has 887,040 continuous variables, 23,232 binary variables, 654,720 equality constraints, and 1,059,168 inequality constraints. This level of complexity, as well as the privacy protection and uncertain scenarios, motivates the proposal of the SP-ADMM approach. The solution is done through a hybrid simulation platform, MATLAB and GAMS. The hardware environment is a laptop with Intel i7 1.90GHz CPU and 16.00GB RAM. The utility-level sub-problem is solved by CPLEX and MINOS, and the house-level sub-problems are solved by SCIP.

4.5.1 Parameter settings

The time resolution of the case study is 15 minutes, and the total time horizon is 24 hours. The total number of houses is 121. The number of residential houses allocated to different LAs are based on the original load at each bus in the IEEE 33-bus system [94].

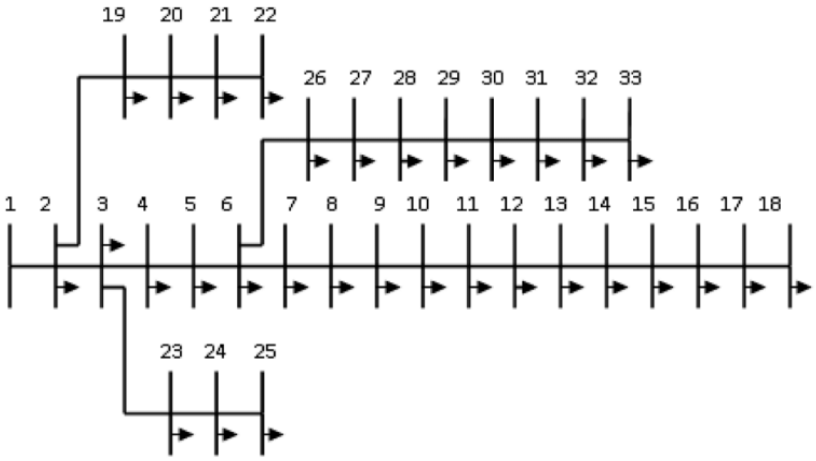

Figure 4.3 Configuration of the IEEE 33-bus test system.

There are 31 houses that have HVAC, EWH, and PV installed, while the other 90 houses only have HVACs and EWHs installed. The discomfort weight factor for indoor temperature is \$0.05/℃, and the discomfort weight factor for water temperature is \$0.01/℃. These weights are empirically chosen and also aligned with the parameters in the previous work [115].

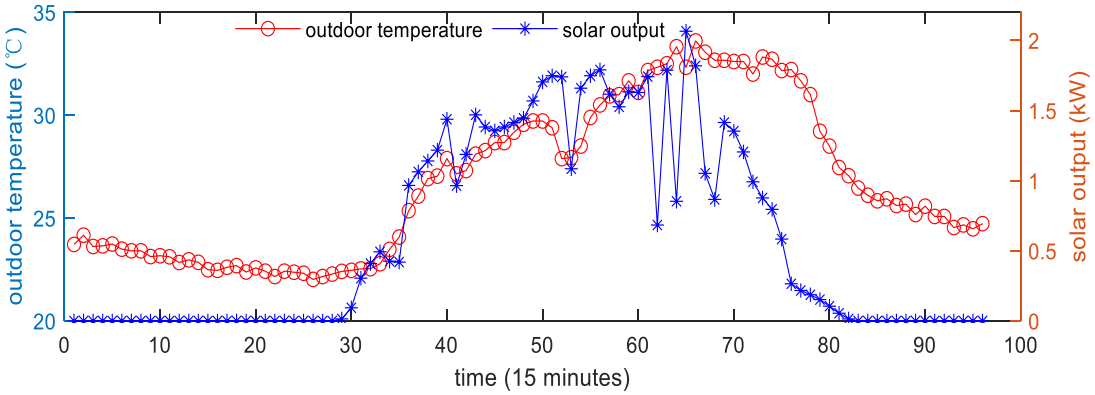

Figure 4.4 Outdoor temperature and solar generation data for generating samples.

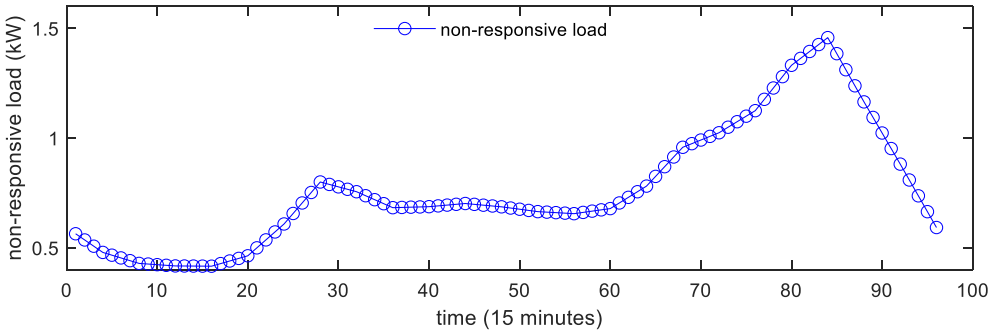

Figure 4.5 Non-responsive load data for generating samples.

Table 4.3 Range of uncertain parameters.

Parameter	Lower range	Upper range
Outdoor temperature	-20%	+20%
Solar output	-20%	+20%
Non-responsive load	-20%	+20%
Water consumption	-20%	+20%

Table 4.4 Probability of each scenario.

Scenario	1	2	3	4	5	6	7	8	9	10
Probability	0.08	0.11	0.04	0.16	0.11	0.07	0.13	0.16	0.07	0.07

The outdoor temperature and standard solar output forecast information data for generating the test scenarios are plotted in Figure 4.4, and the non-responsive load data for generating the test scenarios is given in Figure 4.5. Moreover, Monte Carlo sampling is employed to provide variation and uncertainty in different scenarios. The ranges of the

uncertain parameters are given in Table 4.3. Consequently, 100 samples are generated according to the PDF of the uncertain parameters.

Since it is intractable and time-consuming to include all the samples into considerations, scenario reduction is conducted to reduce the computational burden [116]. First, the min-max normalization is applied to rescale different uncertain parameters, then used the SCENRED tool in GAMS to reduce the number of scenarios [93][117]-[118]. By applying the fast-backward algorithm, a subset of scenarios is selected from the initial samples and each of them is assigned with a new probability. Thus, the initial 100 samples are reduced to 10 scenarios considering the tradeoff between accuracy and computational time. The resulting probabilities of the reduced scenarios are given in Table 4.4.

Also, three test cases are designed to compare the performance of different DR management approaches. In Case 1, the responsive devices do not change their operating status unless the indoor/water temperature falls out of the pre-specified boundaries (i.e., conventional thermostatic control). In Case 2, the DSO treats uncertain parameters as fixed values and applies the deterministic ADMM to coordinate the operating schedule of responsive devices. Finally, Case 3 implements the SP-ADMM algorithm to manage the operating schedules of residential components.

4.5.2 Simulation results

Figure 4.6 and Table 4.5 compare the resulted load profiles in different cases. In Case 1, the peak load of the DSO is 445.50 kW and appears in Scenario 10 after the scenario reduction. The weighted average peak load of the DSO for all the scenarios is 416.97 kW. Therefore, both the peak and average loads exceed the 390-kW contracted load limit. In Case

2, the peak load of the DSO is 422.63 kW and appears in Scenario 5 after the scenario reduction. The weighted average peak load of the DSO for all the scenarios is 403.70 kW. In Case 3, the peak load of the DSO is further reduced to 386.28 kW and it appears in Scenario 10 after the scenario reduction. The weighted average peak load of the DSO for all the scenarios is 374.42 kW.

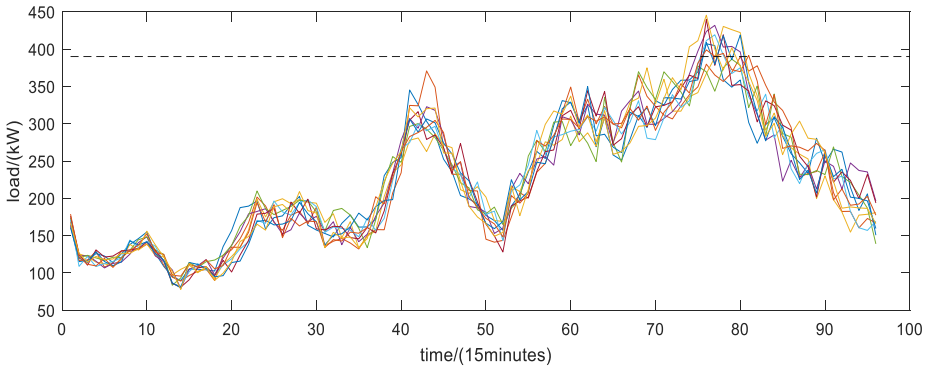

(a) Case 1

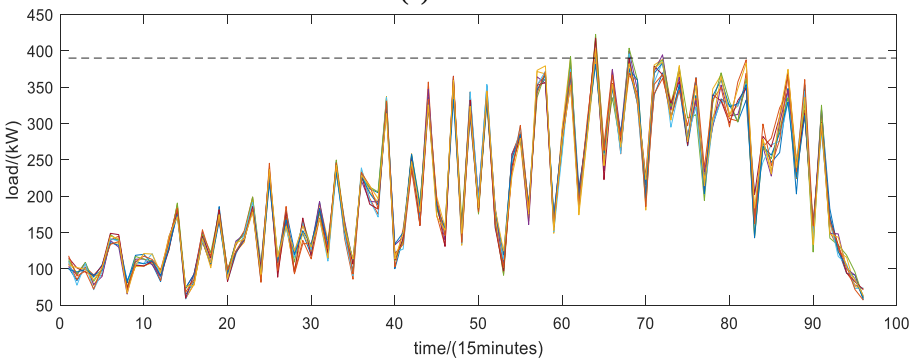

(b) Case 2

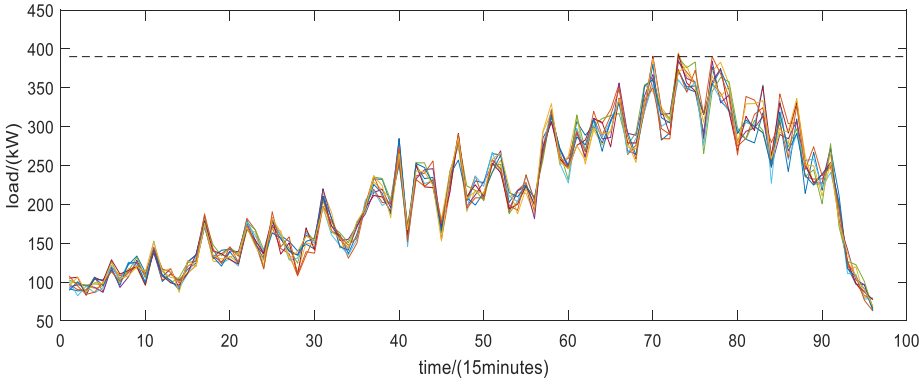

(c) Case 3

Figure 4.6 Load profiles in different test cases.

Table 4.5 Peak load in different cases.

Scenarios	1	2	3	4	5	6	7	8	9	10
Case1 (kW)	407.18	389.67	430.41	431.84	386.58	419.25	440.00	418.93	399.05	445.50
Case2 (kW)	390.88	416.38	390.86	399.86	422.63	398.24	417.49	388.22	400.98	402.75
Case3 (kW)	372.21	378.26	384.74	375.10	383.96	353.56	383.06	361.31	371.44	386.28

Table 4.6 Peak load violation in different cases.

Scenarios	1	2	3	4	5	6	7	8	9	10
Case1 (kW)	17.18	0	40.41	41.84	0	29.25	50	28.93	9.05	55.50
Case2 (kW)	0.88	26.38	0.86	9.86	32.64	8.24	27.49	0	10.98	10.75
Case3 (kW)	0	0	0	0	0	0	0	0	0	0

Table 4.6 provides the peak load violation in different cases. It is observed that the highest average peak load charge appears in Case 1, which is $27.38. By applying the deterministic ADMM approach, the average peak load charge can be reduced to $13.85. The proposed SP-ADMM algorithm can further decrease the peak load charge to $0. From the graph and tables, it can be concluded that SP-ADMM significantly reduces the peak load and peak demand violation charge compared to the conventional control and deterministic ADMM control.

Table 4.7 and Table 4.8 provide the average discomfort cost and average electricity cost of residential customers in different scenarios. It is observed that the customers in Case 1 are expected to have more discomfort and pay higher costs than the customers in the other two cases. The sum of the discomfort and electricity costs in Case 1 is $13.64. In Case 2, either the discomfort or electricity cost is lower than that in Case 1. The total cost is reduced to $9.15, which is only about 67.08% of the cost in Case 1. In Case 3, the sum of the discomfort and electricity cost is $8.49, which is 62.24% of the cost in Case 1. Therefore, Case 3 gives the best performance.

Table 4.7 Average discomfort cost in different cases.

Scenarios	1	2	3	4	5	6	7	8	9	10
Case1 ($)	5.62	5.66	5.64	5.72	5.72	5.67	5.66	5.66	5.69	5.67
Case2 ($)	4.02	3.88	3.99	3.78	3.93	3.83	3.67	3.62	3.75	3.83
Case3 ($)	3.72	3.63	3.70	3.53	3.65	3.57	3.46	3.44	3.52	3.57

Table 4.8 Average electricity cost in different cases.

Scenarios	1	2	3	4	5	6	7	8	9	10
Case1 ($)	12.23	11.23	14.31	5.32	8.67	5.10	4.69	6.39	10.67	9.06
Case2 ($)	5.57	7.79	5.45	6.08	8.05	6.32	7.58	4.20	6.27	6.27
Case3 ($)	4.93	4.91	4.82	4.80	4.89	4.78	4.95	4.98	5.15	5.18

The impact of uncertainties on indoor temperature is also investigated, as shown in Figure 4.7. The minimum and maximum indoor temperature limits for house 1 are 20.50℃ and 22.50℃, respectively. In Case 1, the indoor temperature range of house 1 in all the scenarios is from 19.91℃ to 22.80℃. In Case 2, the indoor temperature range of house 1 in all the scenarios is from 20.78℃ to 22.76℃. In Case 3, the indoor temperature range of house 1 in all the scenarios is from 20.51℃ to 22.47℃. From Figure 4.7, it is observed that the indoor temperature deviation in Case 1 is much larger than that in the other two cases. Further, due to the outdoor temperature uncertainty, the indoor temperature in Case 2 may violate the temperature constraints. By contrast, the indoor temperature in Case 3 is always within the pre-defined limits.

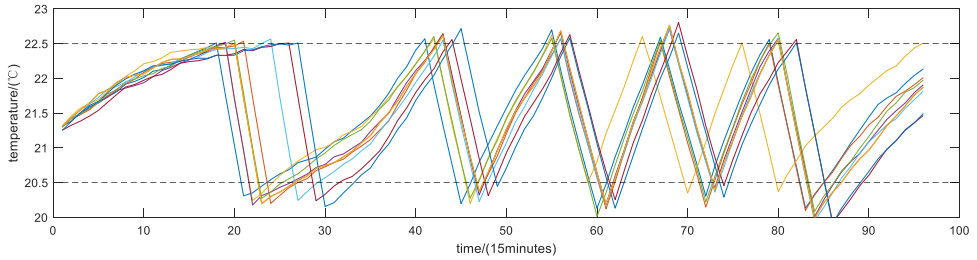

(a) Case 1

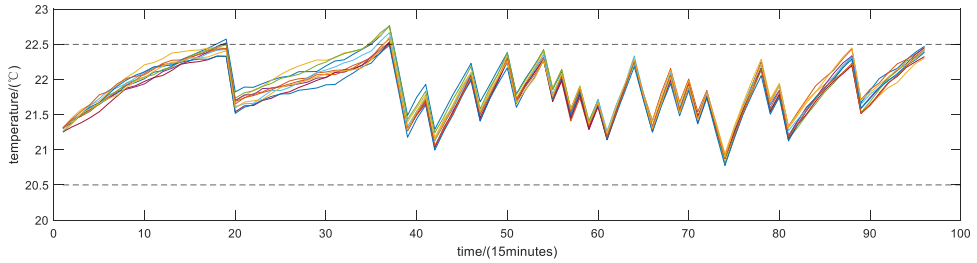

(b) Case 2

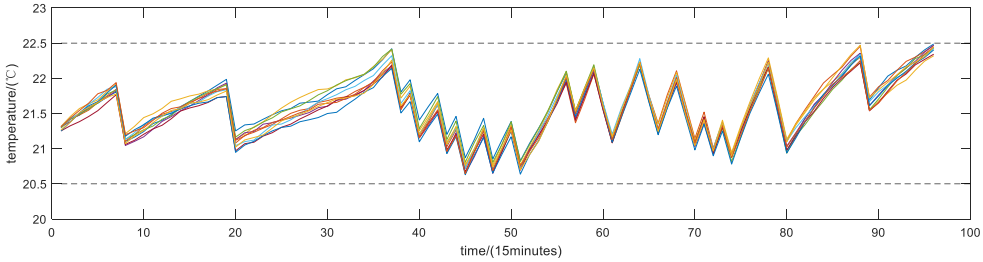

(c) Case 3

Figure 4.7 Indoor temperature of house 1 in different cases.

Figure 4.8 shows the water temperature of house 1 in different cases. The minimum and maximum water temperatures for house 1 are 45.50℃ to 55.50℃, respectively. In Case 1, the water temperature range of house 1 in all the scenarios is from 44.30℃ to 58.90℃. In Case 2, the water temperature range of house 1 in all the scenarios is from 45.73℃ to 55.01℃. In Case 3, the water temperature range of house 1 in all the scenarios is from 45.66 to 55.27℃. Therefore, both the water temperature in Case 2 and Case 3 satisfy the pre-defined limits.

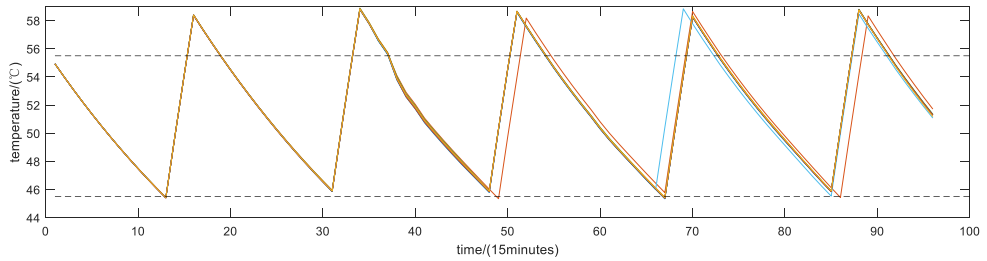

(a) Case 1

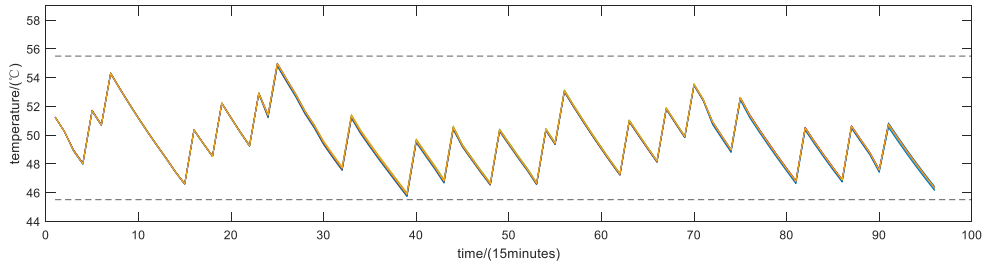

(b) Case 2

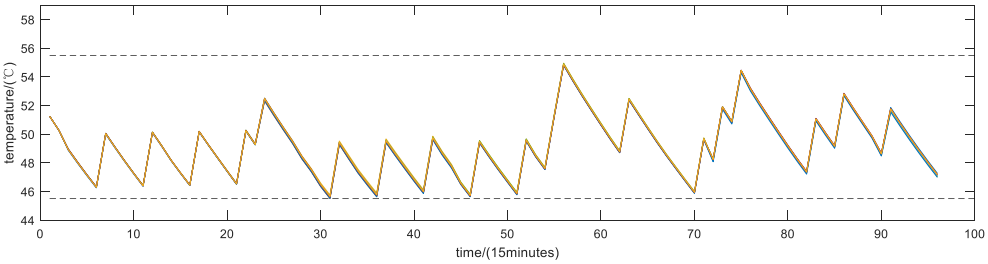

(c) Case 3

Figure 4.8 Water temperature of house 1 in different cases.

4.5.3 Discussions

This section discusses the impact of scenario reduction on optimization results and computational time. First, three test cases are created, with each case having a different number of scenarios. Then the optimal operating schedules for these cases are solved and substituted back to the original 100 samples to evaluate system performance. The results are given in Table 4.9.

Table 4.9 Impact of scenario reduction on results.

No. of scenarios	10	15	20
Avg. peak load (kW)	386.06	380.93	384.63
Avg. load violation (kW)	2.42	0.36	1.08
Avg. discomfort cost ($)	3.68	3.46	3.49
Avg. electricity cost ($)	5.49	6.28	6.01
Avg. total cost ($)	9.37	9.77	9.59

The table shows the average peak load in all three cases are below the 390-kW contracted limit. The average load violations in the three cases are 2.42 kW, 0.36 kW, and 0.18 kW, respectively. Further, when the number of scenarios is 10, residential customers would pay less for electricity costs, but they are also expected to experience more discomfort than in cases with higher numbers of scenarios. From the results, it is concluded that the difference among the results in the three cases is not significant, and therefore setting the number of scenarios to 10 does not much affect the system performance.

Further, the computational time of the proposed approach is given in Table 4.10. The proposed approach takes nine iterations to converge.

Table 4.10 Computational time of the proposed method.

Iteration	1	2	3	4	5	6	7	8	9
DSO (*sec*)	0.34	0.32	0.37	0.33	0.34	0.34	0.33	0.38	0.33
House (*sec*)	304.07	2.07	13.69	5.86	13.70	3.68	11.75	2.34	2.12

Since the house-level optimization is run in parallel, the computational time of each iteration is determined by the house, which has the largest computational time. Also, the house-level model is a mixed-integer quadratic programming problem, and the first iteration has the longest computational time (for initializing the problem). For the utility-level, it only takes around 0.5 seconds to finish the calculation in each iteration. The total computational time for solving the residential DR problem with the SP-ADMM algorithm is 6 minutes 3 seconds. Since the communication delay among different agents is not considered in this chapter, the time consumption in practical applications would be slightly longer than the times in Table 4.10. From the table, it is concluded that the proposed algorithm satisfies the computational time requirements for residential DR applications.

4.6 Chapter Summary

This chapter presents a comprehensive scheduling framework for scalable residential DR programs considering day-ahead and real-time electricity market operations. Due to computational complexity and privacy concerns, the model is not suitable for a DSO to solve as a centralized optimization, especially when multiple uncertain scenarios must be considered in the DR programs. Therefore, this chapter proposes a new algorithm combining SP and ADMM to form the SP-ADMM algorithm, which can decompose the original centralized DR scheduling model to a utility-level problem and a set of house-level sub-problems to distribute the computational complexity and to incorporate multiple uncertain scenarios.

The case study demonstrates that the proposed approach can reduce customers' electricity bills, discomfort, and the peak load at the utility level. Since the optimization model is solved in a distributed manner, increasing the number of houses does not affect the

number of variables. Thus, it does not significantly impact the computing performance. Therefore, the proposed approach is applicable to large scale applications. The information exchange among the utility, LAs, and customers is limited to real and reactive power consumption, dual variables, and the power mismatch in each scenario, which protects customers' privacy. Finally, the results show that the proposed SP-ADMM model can improve residential DR performance and prevent constraint violations as compared to the conventional and deterministic ADMM approaches.

Chapter 5 Deep Deterministic Policy Gradient Based Heating, Ventilation, and Air Conditioning Control Strategy for Residential Demand Response Programs

Model-based residential DR methods can significantly reduce customers' electricity costs and the peak load at the utility level when the thermodynamic behaviors of buildings are accurately modeled. However, it may not always be possible to use functional relationships to describe complex temperature dynamics in the real world. Further, parameters, such as the thermal resistance and thermal capacitance of buildings, are usually not readily available. To overcome these challenges, a DDPG based HVAC control strategy is presented in this chapter for residential DR programs. The proposed approach does not require detailed building models or day-ahead weather forecast information. Rather, it continuously interacts with the environment and determines HVAC control actions based on the current outdoor temperature, current indoor temperature, current time, and non-dispatchable load information. The simulation study is conducted on a one hundred house system, and the results are compared with that of the conventional thermostatic and model-based approaches to demonstrate the performance.

Nomenclature

Sets and Indices

N_N / i	Set/index of residential houses.
j	Index of sample.
k	Index of iteration.

N_T / t	Set / index of time.

Parameters

M	Size of the mini-batch in DDPG.
N_E	Number of episodes.
p_i^{hvac}	Power rating of the HVAC in house i (kW).
$p_{i,t}^{nr}$	Real load of the non-responsive devices in house i at time t (kW).
$\overline{p}^{pcc}$	Maximum contracted load limit at the PCC (kW).
$\underline{T}_i^{in}$	Minimum indoor temperature of house i (°C).
$\underline{T}_i^{in}$	Maximum indoor temperature of house i (°C).
T_i^{ins}	Indoor temperature setpoint of house i (°C).
T_t^{out}	Outdoor temperature at time t (°C).
α	Discomfort weight factor ($/°C).
η^Q	Learning rate of the critic network.
η^π	Learning rate of the behavior network.
λ^{vio}	Peak load violation charge ($/kW).

Variables

$b_{i,t}^{hvac}$	ON/OFF status of the HVAC.
$cost_{i,t}$	Electricity cost of house i at time t ($).
$dis_{i,t}^{hvac}$	Indoor temperature discomfort of customer i at time t (°C).
$p_{i,t}^{cus}$	Real load of house i at time t (kW).
p_t^{pcc}	Aggregated load at the PCC at time t (kW).
p_t^{vio}	Amount of load violation at time t.
Q	Action value.
$r_{i,t}$	Immediate reward of house i at time t
$T_{i,t}^{in}$	Indoor temperature of house i at time t (°C).
π	Policy.
θ	Weight factors in the neural networks.

5.1 Introduction

As the electrical load continues to grow, there is an increasing need to examine opportunities of shifting the peak load to improve the utilization rate of electricity infrastructure. One method to realize this goal is to use some means of storing energy, for example, battery energy storage systems (BESS) [119]. However, building loads such as HVAC can also provide support through thermal energy storage via the building envelope [55]. The use of residential appliances is a potentially lower cost solution compared to the utilization of large ESSs [120].

Existing DR research has primarily focused on deployments for industrial or commercial customers [54]. These customers tend to have large loads that are more easily targetable by energy management systems. However, residential load accounts for 38% of the total electricity consumption in the United States (2013) and represent a significant missed opportunity [121]-[122]. Still, there are challenges to energy shifting for residential loads. Unlike the industrial or commercial load, the residential load is composed of numerous low-power home appliances. In addition, the electricity consumption habits of residential customers are highly varied and dynamic.

Many efforts have been dedicated to investigating load controls and optimizations in residential networks. In [123], a linear relationship among outdoor temperature, indoor temperature, HVAC coefficient of performance, and HVAC power rating is used to calculate the indoor temperature dynamics of residential houses in the direct load control programs. In [124], a HVAC equivalent thermal parameter model is utilized to evaluate the impacts of uncertain parameters (e.g. floor area, thermal resistance, and air change rate) on aggregate DR. In [125], a simplified differential equation is used to simulate HVAC cooling operations,

and formulas for calculating building thermal resistance and the air mass inside a building are provided. In [126], the RC model is employed to define the thermal dynamics of a building zone, where the thermal resistance and capacitance parameters are estimated from the construction data or measurement data by using a parameter identification technique.

The literature review reveals that many researchers assume that the thermal dynamic behaviors of residential houses are accurately modeled. However, it may not always be possible to use the functional relationship to represent the complex temperature dynamics in real-world implementations. Moreover, parameters such as the thermal resistance and thermal capacitance of buildings are usually not readily available.

In recent years, with the development of machine learning algorithms, considerable attention has been focused on using data-driven approaches to solve residential DR problems. In data-driven methods, the agents continuously interact with the environment and learn behaviors from experience to determine the control actions. In [127], model predictive control (MPC) based co-scheduling is compared to data-driven building automation algorithms. The results demonstrate that both approaches can achieve significant energy cost reductions. In [128], a reinforcement learning (RL) based bidding strategy is proposed for the HVAC systems in the double-auction markets, and the data-driven method performs similarly to the model-based bidding strategy. Further, in [129], a deep RL based algorithm is presented for building HVAC controls. The simulation shows that the proposed control strategy can reduce the energy cost while maintaining the indoor temperature within the desired range.

In summary, these works demonstrate the significant potential of using data-driven approaches to reduce residential customers' electricity bills. However, most of the literature

solely focuses on HVAC control within a single building, and lacks a control strategy to coordinate the operations of HVACs over a wide area with multiple residential houses to realize system-level objectives. To address this problem, a DDPG based HVAC control strategy is proposed for residential DR programs in this chapter. The main contributions of this chapter are listed as follows:

1) a distributed system architecture to reduce the action space dimension and ensure the feasibility of the proposed approach for large-scale applications is presented,

2) a RL based approach, which does not require detailed building models or day-ahead weather forecasting to determine the HVAC control actions is proposed

3) the DDPG-based method is compared with conventional thermostat and model-based control approaches to demonstrate the performance.

The rest of this chapter is organized as follows, Section 5.2 formulates the residential DR problem, Section 5.3 explains the HVAC control strategy with the DDPG algorithm, Section 5.4 conducts the case study, and Section 5.5 concludes the paper.

5.2 Problem formulation

5.2.1 System architecture

As illustrated in Figure 5.1, the architecture of the proposed approach is composed of a utility and multiple residential customers. The benefit of using a distributed structure over a centralized structure is that the action space dimension of the agent is significantly reduced when the number of DR participants is large. Therefore, it is more applicable to scalable applications.

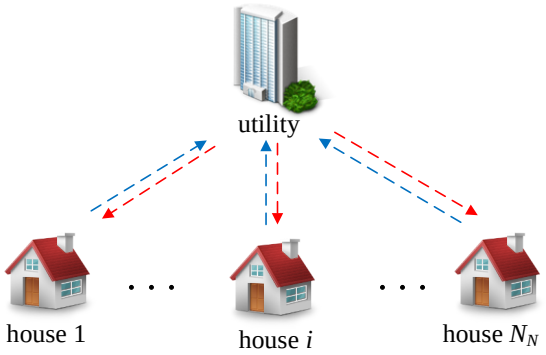

Figure 5.1 Illustration of the communication exchange in the proposed approach.

In addition, the HVAC within each house is identified as a DR resource due to its large power ratings and thermal inertia (changing device operating status does not have a significant impact on customers' comfort in the short term). It is assumed that the HEMS within each house is responsible for communicating with the utility on behalf of customers, providing training for the neural networks, and making HVAC control actions.

5.2.2 Information exchange

Figure 5.2 explains the process of information exchange between the utility and residential customers. Within each training episode, customers first send their non-responsive load information to the utility. Then the utility calculates the aggregated non-responsive load and broadcasts this information to all the customers. After receiving the aggregated non-responsive load messages, the HEMS in each house determines the operation status of the HVAC based on the system state, and reports the total load information to the utility. Finally, the utility calculates the electricity price and broadcasts it to all the customers.

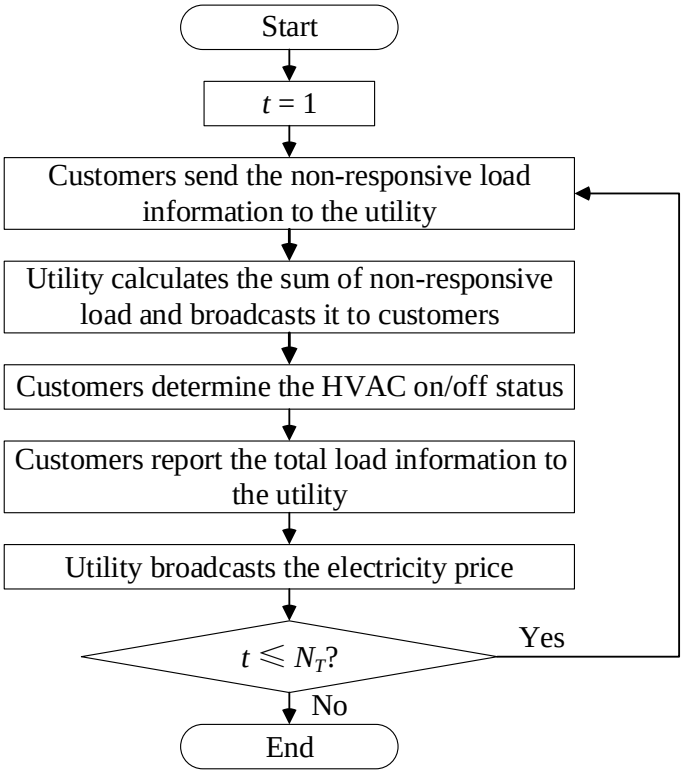

Figure 5.2 Information exchange between the utility and customers in each episode.

5.2.3 System states

The current system state is assumed to only be related to the system state and control action in the last time slot, and it is not related to the system states and actions in the other time slots. Therefore, the HVAC control problem is formulated as a finite Markov decision process [130]. Four features are identified to represent the system states, including:

1) the current outdoor temperature: T_t^{out}

2) the current indoor temperature: $T_{i,t}^{in}$

3) the current time: t

4) the sum of non-responsive load in the system at time *t*: $\sum_{i=1}^{N_N} p_{i,t}^{nr}$.

5.2.4 Control actions

The control actions (switching the HVAC on/off) are determined by the HEMS and based on the system states. Once a control action is made, the HEMS is not allowed to change the HVAC operation status until the next 15-minute time period comes.

5.2.5 Reward function

The objective of the residential DR program is to minimize the sum of electricity cost, discomfort cost, and load violation cost. The immediate reward of customer *i* at time *t* is calculated by:

$$r_{i,t} = -cost_{i,t} - \alpha \cdot dis_{i,t}^{hvac} - \lambda^{vio} \cdot p_t^{vio} / N_N \tag{4.1}$$

where the first term is the electricity cost of customer *i* at time *t*, the second term is the discomfort cost of customer *i* at time *t* due to indoor temperature deviating from the setpoint, the third term represents the peak load violation charge when the peak load exceeds the contracted load limit at the utility level.

The electricity cost term in eq. (4.1) is calculated by:

$$p_{i,t}^{cus} = p_i^{hvac} \cdot b_{i,t}^{hvac} + p_{i,t}^{nr} \tag{4.2}$$

$$cost_{i,t} = p_{i,t}^{cus} \cdot \left(a \cdot p_t^{pcc} + b \right) \tag{4.3}$$

where eq. (4.2) calculates the total load of customer *i* at time *t*, eq. (4.3) calculates the electricity cost of customer *i* at time *t*, $b_{i,t}^{hvac}$ is a binary variable that represents the operation status of the HVAC (1 means ON, and 0 means OFF).

The discomfort in eq. (4.1) is defined as the difference between the actual indoor temperature and the indoor temperature setpoint, as calculated by:

$$dis_{i,t}^{hvac} = \left| T_{i,t}^{in} - T_i^{ins} \right| \tag{4.4}$$

Finally, the amount of peak load violation is calculated by eq. (4.5), and the peak load violation charge is set to \$10/kW in this chapter.

$$P^{vio} = \max\left(P_t^{pcc} - \overline{P}^{pcc}, 0 \right) \tag{4.5}$$

5.3 HVAC control strategy with DDPG

The goal of HVAC control is to maximize the sum of accumulative reward $R_i = \sum_{t=1}^{T} r_{i,t}$ in each house. However, due to the complex thermodynamic behaviors of buildings and ambient weather disturbances, it is challenging to develop a function to describe indoor temperature dynamics with high accuracy. To overcome this challenge, the DDPG algorithm, which is a RL algorithm that combines the deep Q network and deep policy gradient, is applied to solve the HVAC control problem [131].

As illustrated in Figure 5.3, the DDPG is composed of four neural networks, including actor behavior network $\pi(s|\theta^{\pi})$, actor target network $\pi'(s|\theta^{\pi'})$, critic behavior network $Q(s,a|\theta^{Q})$, and critic target network $Q'(s,a|\theta^{Q'})$. The inputs to the actor networks are the system states, and the outputs from the actor networks are deterministic control actions. The inputs to the critic networks are the system states and control actions that are generated by the action network, and the outputs from the critic networks are the action values Q.

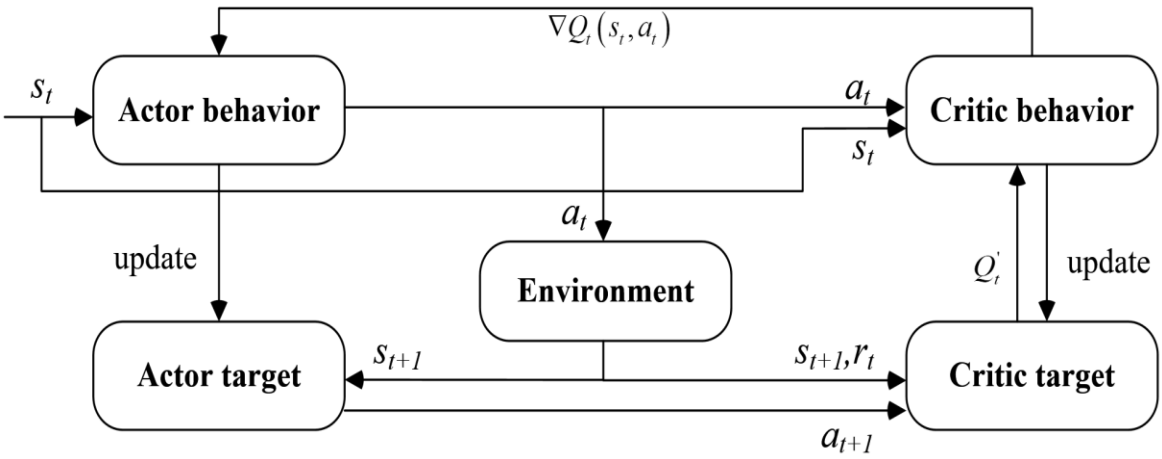

Figure 5.3 Information flow in the DDPG algorithm.

During the training process, the equations for updating the critic networks are given by:

$$y_{i,j,t} = r_{i,j,t} + \gamma \cdot Q'_{i,j,t+1}\left(s_{i,j,t+1}, a_{i,j,t+1} \middle| \theta^{Q'}\right) \tag{4.6}$$

$$L_i\left(\theta_i^Q\right) = \min \sum_{j=1}^{M} \left[Q_{i,j,t}\left(s_{i,j,t}, a_{i,j,t} \middle| \theta^Q\right) - y_{i,j,t} \right]^2 \Big/ M \tag{4.7}$$

$$\theta_{i,k+1}^Q = \theta_{i,k}^Q + \eta^Q \cdot \partial L / \partial \theta_{i,k}^Q \tag{4.8}$$

$$\theta_{i,k+1}^{Q'} = \alpha \cdot \theta_{i,k}^Q + (1-\alpha) \cdot \theta_{i,k+1}^{Q'} \tag{4.9}$$

where eq. (4.6) calculates the target Q value of house *i* at time *t*, eq. (4.7) is the loss function that minimizes the mean square error (MSE) between the target Q value and the behavior Q value, eq. (4.8) updates the weights in the critic behavior network, eq. (4.9) updates the weights in the critic target network, γ is the discounting factor, and η^Q is the learning rate for the critic behavior network.

The equations for updating the actor networks are given by:

$$J_i\left(\theta_i^{\pi}\right)=\max\sum_j Q_{i,j}\left(s_{i,j,t},a_{i,j,t}\left|\theta_i^{Q}\right.\right) \tag{4.10}$$

$$\theta_{i,k+1}^{\pi}=\theta_{i,k}^{\pi}+\eta^{\pi}\cdot\partial J_i/\partial\theta_{i,k}^{\pi} \tag{4.11}$$

$$\theta_{i,k+1}^{\pi'}=\alpha\cdot\theta_{i,k}^{\pi}+\left(1-\alpha\right)\cdot\theta_{i,k+1}^{\pi'} \tag{4.12}$$

where eq. (4.10) is the loss function that maximizes the expected total reward under the policy $\pi(s|\theta_i^{\pi})$, eq. (4.11) updates the weights in the actor behavior network, eq. (4.12) updates the weights in the actor target network, and η^{π} is the learning rate for the actor behavior network.

The details of the DDPG algorithm are provided in Algorithm 1. Within each episode, the actor behavior network first generates the probability distribution of the potential actions according to the current system state, and outputs the HVAC control action based on the logic in eq. (4.13). Then the replay buffer stores the transition ($s_{i,t}$, $a_{i,t}$, $r_{i,t}$, $s_{i,t+1}$) and randomly draw a mini-batch for training. After that, the current system state, the next system state, and the immediate reward are imported to the critic networks to evaluate the Q values. Finally, the weights in the actor networks are updated by the gradient descent method based on eq. (4.8)-(4.9), and the weights in the critic network are also updated by the gradient descent method based on eq. (4.11)-(4.12).

$$a_{i,t}=\begin{cases}0 & \text{if } T_{i,t}^{in}\le\underline{T}_i^{in} \text{ or } \left(T_{i,t}^{in}\ge\underline{T}_i^{in} \text{ and } 0\le\pi_{i,t}\left(s_t\right)\le 0.5\right)\\ 1 & \text{if } T_{i,t}^{in}\ge\overline{T}_i^{in} \text{ or } \left(T_{i,t}^{in}\le\overline{T}_i^{in} \text{ and } 0.5<\pi_{i,t}\left(s_t\right)\le 1\right)\end{cases} \tag{4.13}$$

Algorithm 1: DDPG-based HVAC control strategy for residential demand response

1. Randomly initialize the actor behavior network $\pi_i(s|\theta^{\pi})$ and critic behavior network $Q_i(s,a|\theta^{Q})$ for each house.
2. Initialize the actor target network π_i' and critic target network Q_i' for each house with weights $\theta_i^{\pi} \rightarrow \theta_i^{\pi'}$ and $\theta_i^{Q} \rightarrow \theta_i^{Q'}$
3. **for** episode = 1 to N_E, **do**
4. **for** house = 1 to N_N, **do**
5. Initialize system state $s_i(T_{t=0}^{out}, T_{i,t=0}^{in}, t=0, \sum_i^{N_N} P_{i,t=0}^{nr})$
6. **for** t = 1 to N_T, **do**
7. Action behavior network selects HVAC control action $a_{i,t}$ with $\pi_i(s|\theta^{\pi})$
8. Execute action, receive immediate reward $r_{i,t}$ and the next system state $s_{i,t+1}$
9. Store the transition ($s_{i,t}$, $a_{i,t}$, $r_{i,t}$, $s_{i,t+1}$) in the replay buffer.
10. Collect a minibatch of transitions from the replay buffer
11. Update the critic behavior network by minimizing the MSE in eq. (4.7)-(4.8).
12. Update the actor behavior network by maximizing the expected total reward in eq. (4.10)-(4.11).
13. Update the critic target network and the actor target network based on eq. (4.9) and eq. (4.12), respectively.
14. **end for**
15. **end for**
16. **end for**

By continuously interacting with the environment through offline training, the DDPG algorithm can learn what control actions to take under certain circumstances. Once the neural networks are well trained, the DDPG-based algorithm is used for online implementations.

5.4 Simulation study

In this section, the proposed DDPG-based HVAC control strategy is evaluated in a one-utility one hundred-house test system. The results from the proposed reinforcement learning based approach are compared with the conventional thermostatic and distributed ADMM based controls to demonstrate the performance.

5.4.1 Parameter settings

As shown in Figure 5.4, outdoor temperature data of 29 days in summer (the green lines) is used to train the neural networks in the DDPG, and the outdoor temperature data of another day (the purple line) is used for testing.

The non-responsive load profile is given in Figure 5.5 [97]. Random samples from normal distributions of solar power outputs and non-responsive loads are considered for each house to provide variation [98].

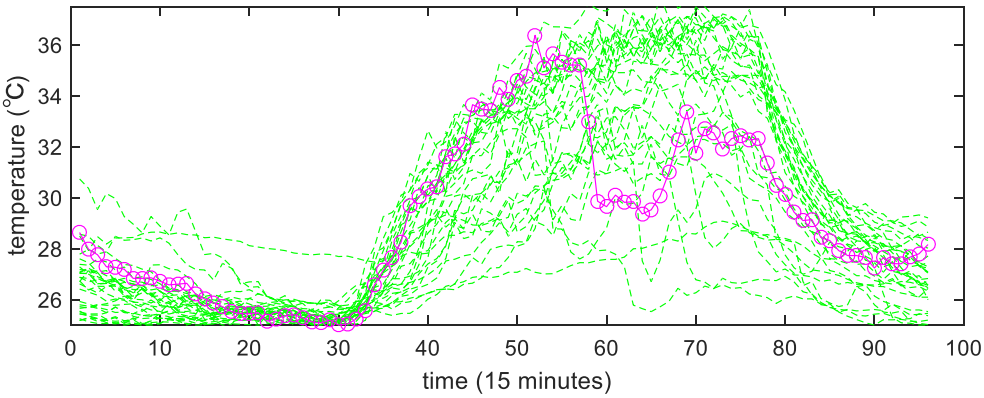

Figure 5.4 Outdoor temperature profiles for training and testing.

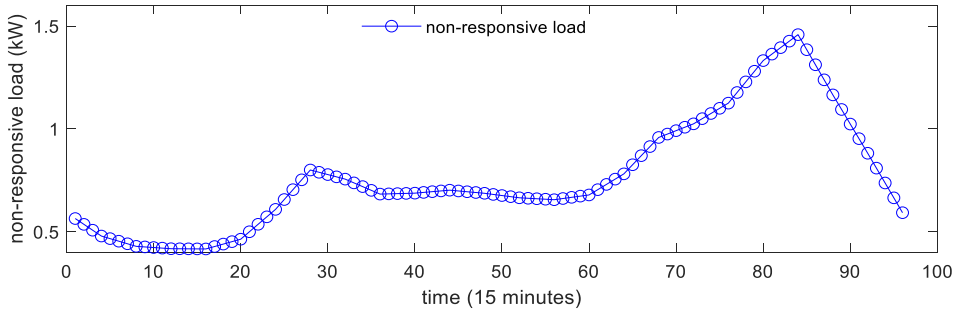

Figure 5.5 Non-responsive load profile.

Table 5.1 DDPG parameter settings.

	Actor network	Critic network
Size of input	[1,4]	[1,5]
No. of hidden layers	2	2
Size of each hidden layer	[4, 20], [20, 20]	[5, 20], [20, 20]
Activation function	ReLU	tanh
Size of output	[20, 1]	[20, 1]
Learning rate	0.01	0.01
Discount factor	n/a	1
Size of mini-batch	96	

The HVAC power rating is set to 3.5 kW. The indoor temperature setpoint of each house is set as a random number between 21℃ and 23℃ to provide variation. The minimum temperature is one degree Celsius below the indoor temperature setpoint and the maximum temperature is one degree Celsius above the indoor temperature setpoint in each house.

The DDPG parameter settings are provided in Table 5.1. There are two hidden layers in both the actor networks and the critic networks. Within each hidden layer, there are 20 neurals. ReLU is selected as the activation function for the actor network, and tanh is selected as the activation function for the critic network. The learning rate is set to 0.01 and the decay factor in the critic network is set to 1. Finally, the number of episodes is set to 600.

5.4.2 Results and discussions

Three test cases are designed to compare the performance of different HVAC control strategies. In Case 1, the conventional thermostatic HVAC control strategy is applied, (i.e. the HVAC would not change their operating status unless the indoor temperature falls out of the pre-specified boundaries). In Case 2, the ADMM approach presented in Chapter 3 is

used to manage the operating schedule of HVACs. Finally, Case 3 implements the proposed DDPG-based HVAC control strategy for residential DR.

Figure 5.6 compares the resulting load profiles in different cases. In Case 1, the peak load at the utility level is 280.39 kW, which exceeds the system contracted load limit of 255 kW. The peak load in Case 1 appears at 6:15 pm. In Case 2, the peak load at the utility level is 254.77 kW, which satisfies the utility-level requirement. The peak load in Case 2 appears at 5:15 pm. In Case 3, the peak load is 256.52 kW, which is slightly above the contracted load limit but still considerably improves the system performance if compared to Case 1. The peak load in Case 3 appears at 7:45 pm.

Table 5.2 compares the average cost of residential customers in different cases. The customers using the ADMM-based control strategy are expected to have greater cost savings and less discomfort than the other two cases, and the load violation charge in Case 2 is $0.

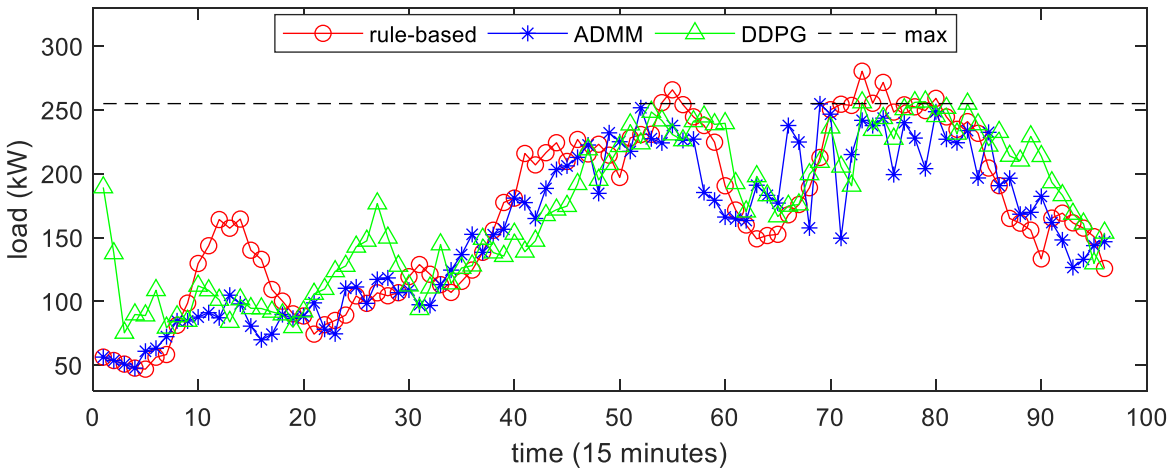

Figure 5.6 Load profiles in different cases.

Table 5.2 Comparison of the average cost in different cases.

	Conventional (Case 1)	ADMM (Case 2)	DDPG (Case 3)
Average electricity cost ($)	3.55	3.27	3.57
Average discomfort cost ($)	2.78	2.57	3.72
Load violation (kW)	25.39	0	1.52
Average load violation cost ($)	2.54	0	0.15
Average total cost ($)	8.87	5.84	7.44

The average electricity cost and average discomfort cost in the DDPG-based approach are the highest among the three approaches. However, since the load violation in Case 3 is much smaller than that in Case 1, the overall performance of the DDPG-based HVAC control is still better than the conventional thermostatic control approach. Therefore, both the ADMM and DDPG based HVAC control strategies can reduce the peak load at the utility, but the costs in the DDPG based approach are higher than that in the ADMM based approach.

Figure 5.7 compares the indoor temperature of house 1 in the three different cases. The indoor temperature setpoint is 22℃. The minimum indoor temperature bound is set to 21℃ and the maximum indoor temperature bound is set to 23℃. From the graph, it is observed that the indoor temperature in Case 2 has the least deviation from the setpoint and is always within the preferred bound, while the indoor temperature in the other two cases may violate the temperature constraints during some time intervals.

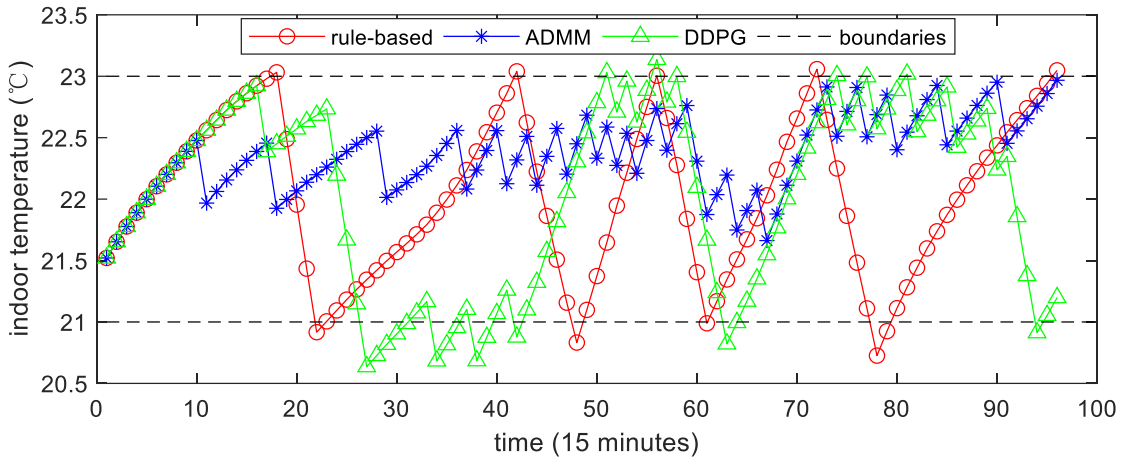

Figure 5.7 Indoor temperature in different test cases.

Table 5.3 Computational time and input data requirements of each approach.

	Conventional (Case 1)	ADMM (Case 2)	DDPG (Case 3)
Building model	No	Yes	No
Temperature forecast	No	Yes	No
Training data	No	No	Yes
Computational time	0 *sec*	129.20 *sec*	2.76 *sec*

Table 5.3 shows the computational time and input data requirements of each approach. From the table, it is concluded that the conventional thermostatic HVAC control strategy has the lowest requirements on input data, and it can instantaneously output the control actions. However, there is no coordination among the responsive devices in this control mode, and therefore it cannot conduct the residential DR.

By contrast, the ADMM approach can significantly reduce the peak load at the utility level and reduces customers' electricity bills, but this method requires accurate building models and the day-ahead outdoor temperature forecasts. The computational time of

ADMM-based HVAC control is also the longest of the three approaches (more than 60 times longer than the reinforcement learning based approach), which restricts its potential for online control applications.

Finally, even though the load profile of the DDPG-based method may slightly exceed the contracted load limit, it can still considerably reduce the peak load at the utility level. The most significant advantage of the DDPG- over the ADMM-based HVAC control strategy is that it significantly reduces the requirements on input data. Furthermore, once the neural networks are well trained, it only takes 2.76 *sec* for the agent in each house to determine the control actions for HVAC. Therefore, the DDPG-based HVAC control strategy is applicable to online HVAC controls or the cases where accurate building models or weather forecast information is not available.

5.5 Chapter Summary

In this chapter, a DDPG-based HVAC control strategy is presented for residential DR programs. The proposed approach does not require detailed building models or the day-ahead outdoor temperature forecasting. Rather, it uses the current outdoor temperature, current indoor temperature, current time, and non-responsive load information as the inputs to generate the HVAC control actions. A simulation study on a one hundred-house system demonstrates that the DDPG-based control strategy has high computational efficiency and the ability to reduce the peak load at the utility level after the neural networks are well trained. Therefore, the proposed approach is applicable to online residential DR programs or applications where accurate building models or weather forecast information is not available.

Chapter 6 Conclusions and Future Works

Power system congestion and uncertainty management with residential DR is a promising research topic owning to the increasing penetration of renewable energy and the development of transactive energy. In this dissertation, Chapter 1 briefly introduces network congestion evaluation and management approaches.

Chapter 2 proposes an interval optimization model to evaluate the ATC in power systems. The inputs of the model are the lower and upper boundaries of uncertain wind power, rather than a detailed PDF. Both the duality theory and artificial binary variables are introduced to convert the NP-hard pessimistic model to a single-level maximization problem for efficient calculation. Case studies demonstrate that increasing the number of time intervals or system size does not significantly affect the computational time, hence validating the feasibility of the proposed algorithm in practical applications. This chapter also studies the impacts of forecasting error and weighting factors on optimization results.

Chapter 3 presents a distributed and scalable residential DR management model. The proposed approach has a hierarchical network structure, which is composed of utility, LAs, and residential customers. The ADMM is applied as the solution algorithm to decompose the centralized model into a utility-level sub-problem and a set of house-level sub-problems. Case studies demonstrate that the proposed approach not only reduces the peak load at the utility level, but also reduces the electricity bills for customers without significantly affecting their discomfort level. Since the optimization model can be decomposed and solved in a distributed manner, the proposed approach is applicable to distribution networks with large numbers of houses. Finally, the information exchange among the utility, LAs, and customers

is limited to power consumption, the dual variable of the power balance equation, and power mismatch, such that the customers do not have to release the ON/OFF status of their devices to the public.

Chapter 4 further investigates the impacts of uncertainty on residential DR programs. A new algorithm combining scenario-based SP and ADMM is proposed to solve the residential DR problem. The proposed model considers both the day-ahead and real-time electricity markets. Similar to Chapter 3, the centralized social welfare maximization model is decomposed to utility-level and house-level sub-problems to reduce computational burden. The results demonstrate that the proposed approach of a SP-based model can improve system performance and prevent constraint violations as compared to the conventional thermostatic and deterministic control approaches when considering weather and customers' behavior uncertainties.

Chapter 5 proposes a DDPG for residential DR programs. The benefit of this RL based control scheme is that it does not require the thermodynamic models of buildings or day-ahead weather forecast information. Once the neural networks within each house are well trained, control actions can be calculated within a short period of time according to the current system states. Therefore, this approach can be applied to real-time controls or cases where accurate building model or weather forecast information is not available.

Future works will focus on further including EWHs and ESSs into the RL-based HVAC control strategy for residential DR programs and continue to study the impacts of parameter settings on the DDPG algorithm to improve the system performance.

Appendix

A. Converting max-min to max with strong duality theory

The feasibility of converting the original max-min problem to a maximization problem can be proved based on the definition of the strong duality theory. According to ref. [132], p^* denotes the optimal value for the optimization problem in (A.1)-(A.3) with $f_0(x), \ldots, f_m(x)$ convex, and d^* denote the optimal value for its dual problem. If $d^* = p^*$, then the strong duality holds.

$$min\ f_0(x) \tag{A.1}$$

$$s.t.\ f_i(x) \le 0, i = 1,\ldots,m \tag{A.2}$$

$$Ax = b \tag{A.3}$$

In Chapter 2, since both the objective function and the constraints in the primary model are linear, the strong duality theory applies and d^* is equal to p^*. Therefore, the proposed transformation will not change the optimal objective function value. The corresponding dual problem for the problem in eq. (2.15)-(2.18) can be expressed as:

$$\max_{\lambda,\nu,\gamma^L,\gamma^U} \ -[\underline{b}_i, \bar{b}_i]^T \lambda_i - \underline{d}_i^T \nu_i + L^T \gamma_i^L - U^T \gamma_i^U \tag{A.4}$$

$$A_i^T \lambda + E_i^T \nu - \gamma_i^L + \gamma_i^U = -c_i \tag{A.5}$$

$$\nu_i \ge 0;\ \gamma_i^L \ge 0;\ \gamma_i^U \ge 0 \tag{A.6}$$

B. Using the RC model to calculate the indoor temperature dynamics

In the literature, there are two main types of modeling approaches for residential buildings: model-based and data-driven. In Chapter 3 and Chapter 4, a simplified RC model was used to capture indoor temperature dynamics. For more information on the detailed RC model, refer to [79]. The RC model is constituted with an electrical analog pattern with resistance (R) and capacitance (C), which are obtained from historical data by using linear regressions. It has a "visible" model structure and therefore can be used for optimal control of HVAC systems. The input parameter for the HVAC model is the day-ahead forecasted outdoor temperature. The HVAC model is represented by:

$$C_i^{house} \frac{dT_{i,t}^{in}}{dt} = (T_t^{out} - T_{i,t-1}^{in}) / R_i^{house} - b_{i,t}^{hvac} \cdot p_i^{hvac} \quad \text{(B.1)}$$

where eq. (B.1) is a first-order differential equation to represent the indoor temperature dynamics of house *i*, C_i^{house} is the thermal capacitance of house *i*, $T_{i,t}^{in}$ is the indoor temperature of house *i* at time *t*, $T_{i,t}^{out}$ is the outdoor temperature at time *t*, $b_{i,t}^{hvac}$ is the on/off status of the HVAC in house *i* at time *t*, and p_i^{hvac} is the power rating of the HVAC in house *i*.

The discrete-time version of eq. (3) for calculating the indoor temperature of house *i* at each time step *t* is represented by:

$$T_{i,t}^{in} = T_{i,t-1}^{in} + [(T_{i,t}^{out} - T_{i,t-1}^{in}) / R_i^{house} - B_{i,t}^{hvac} \cdot P_i^{hvac} \cdot \Delta t] / C_i^{house} \quad \text{(B.2)}$$

References

[1] National Academy of Sciences, National Academy of Engineering, and National Research Council. 2009. America's Energy Future: Technology and Transformation. Washington, DC: The National Academies Press. https://doi.org/10.17226/12091.

[2] L. Bai, J. Wang, C. Wang, et al, "Distribution locational marginal pricing (DLMP) for congestion management and voltage support," *IEEE Transactions on Power Systems*, vol. 33, no. 4, pp. 4061-4073, Jul. 2018.

[3] Q. Zhang, W. Feng, M. Kamel, et al, "Extended LMP under high-penetration wind power," *IEEE/PES Transmission and Distribution Conference and Exposition Latin America*, pp. 1-5, Sep. 2018.

[4] A. Pillay, S. Prabhakar Karthikeyan, and D. P. Kothari, "Congestion management in power systems — A review," *International Journal of Electrical Power and Energy Systems*, vol. 70, pp. 83-90, 2015.

[5] California ISO, "Available Transfer Capability Implementation Document," [Online] Availabl e: https://www.caiso.com/Documents/AvailableTransferCapabilityImplementationDocument.pdf.

[6] New York ISO, "Available Transfer Capability Implementation Document ATC ID MOD-001 -1a," [Online] Available: https://www.nyiso.com/documents/20142/2268529/CurrentAvailableTransferCapabilityImplementationDocumentATCID.pdf.

[7] North American Electric Reliability Council, "Standard MOD-001-2 — modeling, data, and analysis — Available transmission system capacity," Feb. 2014.

[8] H. Chen, T. Jiang, X. Li, et al, "Available transfer capability calculations considering demand response," *IEEE Power & Energy Society General Meeting*, pp. 1-5, Jul. 2017.

[9] B. Wang, X. Fang, X. Zhao, H. Chen, "Bi-level optimization for available transfer capability evaluation in deregulated electricity market," *Energies*, vol. 8, no. 12, pp. 13344-13360, Nov. 2015.

[10] G. C. Ejebe, J. Tong, J. G. Waight, et al., "Fast calculation of linear available transfer capability," *IEEE Transactions on Power Systems*, vol. 15, no. 3, pp. 1112-1116, Aug. 2000.

[11] M. Patel, and A. Girgis, "New iterative method for available transfer capability calculation," *IEEE Power & Energy Society General Meeting*, pp. 1-6, Jul. 2011.

[12] M. Kim, D. Kim, Y. Yoon, et al, "Determination of available transfer capability using continuation power flow with fuzzy set theory," *IEEE Power & Energy Society General Meeting*, pp. 1-7, Jun. 2007.

[13] O. Mohammed, M. Mustafa, D. Mohammed, et al, "Available transfer capability calculation method: a comprehensive review," *International Transactions on Electrical Energy Systems*, in-press.

[14] Y. Du, F. Li, J. Li, et al, "Achieving 100x acceleration for N-1 contingency screening with uncertain scenarios using deep conventional neural network," *IEEE Transactions on Power Systems*, vol. 34, no. 4, pp. 3303-3305, Jul. 2019.

[15] X. Fang, F. Li, and N. Gao, "Available transfer capability of photovoltaic generation incorporated system," *IEEE Power & Energy Society General Meeting*, pp. 1-5, Jul. 2014.

[16] Y. Xiao, and Y. Song, "Available transfer capability (ATC) evaluation by stochastic programming," *IEEE Power Engineering Review*, vol. 20, no. 9, pp. 50-52, Sep. 2000.

[17] N. Avila, and C. Chu, "Distributed probabilistic ATC assessment by optimally conditions decomposition and LHS considering intermittent wind power generation," *IEEE Transactions on Sustainable Energy*, vol. 10, no. 1, pp. 375-385, Jan. 2019.

[18] Y. Gu, H. Jiang, J. Zhang, et al, "Multi-timescale three-phase unbalanced distribution system operation with variable renewable generations," *IEEE Transactions on Smart Grid*, vol. 10, no. 4, pp. 4497-4507, Jul. 2019.

[19] Y. Zhang, J. Dong, T. Kuruganti, et al, "Distributionally robust building load control to compensate fluctuations in solar power generation," in *American Control Conference*, pp. 1-7, Jul. 2019.

[20] T. Jiang, X. Li, H. Chen, et al, "Optimal energy storage siting and sizing to mitigate voltage deviation in distribution networks," *IEEE Power & Energy Society General Meeting*, pp. 1-5, Aug. 2019.

[21] Y. Du, and F. Li, "Intelligent multi-microgrid energy management based on deep neural network and model-free reinforcement learning," *IEEE Transactions on Smart Grids*, vol. 11, no. 2, pp. 1066-1076, Mar. 2020.

[22] T. Wijaya, M. Vasirani, and K. Aberer, "When bias matters: an economic assessment of demand response baselines for residential demand response," *IEEE Transactions on Smart Grid*, vol. 5, no. 4, pp. 1755-1763, Jul. 2014.

[23] U.S. Environmental Protection Agency, "About the U.S. electricity system and its impact on the environment," [Online] Available: https://www.epa.gov/energy/about-us-electricity-system-and-its-impact-environment.

[24] Rethink technology research, "Residential demand response 2019-2025 – executive summary," [Online] Available: https://rethinkresearch.biz/report/residential-demand-response-2019-2025-executive-summary-free-download/.

[25] P. Yi, X. Dong, A. Iwayemi, et al., "Real-time opportunistic scheduling for residential demand response," *IEEE Transactions on Smart Grid*, vol. 4, no. 1, pp. 227-234, Mar. 2013.

[26] S. Vandael, B. Claessens, M. Hommelberg, et al., "A scalable three-step approach for demand side managemtn of plug-in hybrid vehicles," *IEEE Transactions on Smart Grid*, vol. 4, no. 2, pp. 720-728, May 2013.

[27] W. Pei, Y. Du, H. Xiao, et al., "Optimal operation with photovoltaics and gas turbines in demand responses," *International Conference on Power System Technology (POWERCON)*, pp. 3058-3063, Oct. 2014.

[28] P. Khajavi, H. Abniki, and A. Arani, "The role of incentive based demand response programs in smart grids," *10th International conference on Environment and Electrical Engineering*, pp. 1-4, May, 2011.

[29] V. Stagliano, J. Hayden, "The electric transmission paradox," *Electricity Journal*, vol. 17, no. 2, pp. 37-46, Mar. 2004.

[30] A. Kumar, and S.C. Srivastava, "AC power transfer distribution factors for allocating power transactions in a deregulated market," *IEEE Power Engineering. Review*, vol. 22, no. 7, pp. 42-43, Jul. 2002.

[31] Y. Ou, and C. Singh, "Assessment of available transfer capability and margins," *IEEE Transactions on Power Systems*, vol. 17, no. 2, pp. 463-468, May 2002.

[32] R. Zhang, G. Li, H. Chen, "Study of probabilistic available transfer capability by improved particle swarm optimization," *International Conference on Power System Technology*, pp. 1-6, Oct. 2006.

[33] X. Fang, F. Li, N. Gao, "Probabilistic available transfer capability evaluation for power systems with high penetration wind power," *International Conference on Probabilistic Methods Applied to Power Systems*, pp. 1-6, Jul. 2014.

[34] Y. Cui, Z. Bie, and X. Wang, "Study on calculation of probability available transfer capability," *Proceedings of International Conference on Power System Technology*, vol. 4, pp. 2052-2056, Oct. 2002.

[35] Y. Xiao, Y. Song, and Y. Sun, "Application of stochastic programming for available transfer capability enhancement using FACTS devices," *IEEE Power Engineering Society Summer Meeting*, pp. 1-8, Aug. 2002.

[36] A. Rodrigues, and M. Silva, "Probabilistic Assessment of Available Transfer Capability Based on Monte Carlo Method with Sequential Simulation," *IEEE Transactions on Power Systems*, vol. 22, no. 1, pp. 484-492, Jan. 2007.

[37] Y. Xiao, Y. H. Song, "Available transfer capability (ATC) evaluation by stochastic programming," *IEEE Transactions on Power Systems*, vol. 20, no. 0, pp. 50-52, Sep. 2000.

[38] T. Ding, F. Li, X. Li, et al., "Interval radial power flow using extended DistFlow formulation and Krawczyk iteration method sparse approximate inverse preconditioner," *IET Generation, Transmission & Distribution*, vol. 9, no. 14, pp. 1998-2006, Oct. 2015.

[39] C. Zhang, H. Chen, Z. Liang, "Reactive power optimization under interval uncertainty by the linear approximation method and its modified method," *IEEE Transactions on Smart Grid*, vol. PP, no. 99, pp. 1-1, Feb. 2017.

[40] T. Ding, C. Huang, R. Bo, et al., "Interval arithmetic based optimal curtailment for infeasible SCED considering wind power uncertainties," *IEEE Power & Energy Society General Meeting*, pp. 1-5, Jul. 2015.

[41] ISO New England, "ISO New England calculation of TTC for external interfaces and ATC for PTF interfaces," [Online] Available: http://www.oasis.oati.com/NU/NUdocs/iso_ne_ttc_atc_method.doc, Mar. 2009.

[42] Midcontinent Independent System Operator (MISO), "Available transfer capability implement ation document," [Online] available: http://www.oasis.oati.com/woa/docs/MISO/MISOdocs/TP-OP-005-r20_Available_Transfer_Capability_Implementation_Document.pdf, Dec, 2017.

[43] P. Du, W. Li, X. Ke et. al., "Probabilistic-based available transfer capability assessment considering existing and future wind generation resources," *IEEE Transactions on Sustainable Energy*, vol. 6, no. 4, pp. 1263-1271, Oct. 2015.

[44] T. Ding, R. Bo, F. Li, et al., "Interval power flow analysis using linear relaxation and optimality-based bounds tightening (OBBT) methods," *IEEE Transactions on Power Systems*, vol. 30, no. 1, pp. 177-188, Jan. 2015.

[45] H. Chen, X. Fang, R. Zhang, et al., "Available transfer capability evaluation in a deregulated electricity market considering correlated wind power," *IET Generation, Transmission & Distribution*, vol. 12, no. 1, pp. 53-61, Feb. 2018.

[46] Federal Energy Regulatory Commission, "Reactive power requirements for non-synchronous generation," June 2016.
[47] T. Ding, R. Bo, W. Gu, et al., "Absolute value constraint based method for interval optimization to SCED model," *IEEE Transactions on Power Systems*, vol. 29, no. 2, pp. 980-981, Mar. 2014.
[48] A. Saric, and A. Stankovic, "An application of interval analysis and optimization to electric energy markets," *IEEE Transactions on Power Systems*, vol. 21, no. 2, pp. 515-523, May 2006.
[49] X. Kou, F. Li, and W. Feng, "Transmission constrained economic dispatch via interval optimization considering wind uncertainty," *IEEE Power & Energy Society General Meeting*, pp. 1-5, Aug. 2018.
[50] O. Ma, N. Alkadi, P. Cappers, et al., "Demand response for ancillary services," *IEEE Transactions on Smart Grid*, vol. 4, no. 4, pp. 1988-1995, Dec. 2013.
[51] Y. Chen, M. Hu, and Z. Zhou, "A data-driven analytical approach to enable optimal emerging technologies integration in the co-optimized electricity and ancillary market," *Energy*, vol. 122, pp. 613-626, Mar. 2017
[52] Q. Shi, F. Li, Q. Hu, and Z. Wang, "Dynamic demand control for system frequency regulation: Concept review, algorithm comparison, and future vision," *Electric Power System Research*, vol. 154, pp. 75-87, Jan. 2018.
[53] Y. Baek, S. Hadley, R. Uria-Martinez, et al., "Eastern interconnection demand response potential," Oak Ridge National Laboratory, ORNL/TM-2012/303, 2012.
[54] M. Starke and N. Alkadi, "Assessment of industrial load for demand response across US regions of the western interconnect," Oak Ridge National Laboratory, ORNL/TM-2013/407, 2013.
[55] X. Kou, F. Li, J. Dong, et al., "A distributed energy management approach for residential demand response," *3rd International Conference on Smart Grid and Smart Cities*, pp. 1-6, June 2019.
[56] D. Han and J. Lim, "Design and implementation of a smart home energy management systems based on ZigBee," *IEEE Transactions on Consumer Electronics*, vol. 56, no. 3, pp. 1417-1425, Nov. 2010.
[57] H. Zandi, E. Vineyard, J. Sanyal, et al., "Home energy management retrofit control platform," *12th IEA Heat Pump Conference*, pp. 1-10, May 2017
[58] X. Wu, J. He, Y. Xu, et al., "Hierarchical control of residential HVAC units for primary frequency regulation," *IEEE Transactions on Smart Grid*, vol. 9, no. 4, pp. 3844-3856, July 2018.
[59] Z. Wu, S. Zhou, J. Li, et al., "Real-time scheduling of residential appliances via conditional risk-at-value," *IEEE Transactions on Smart Grid*, vol. 5, no. 3, pp. 1282-1291, May 2014.
[60] Q. Shi, F. Li, G. Liu, et al, "Thermostatic load control for system frequency regulation considering daily demand profile and progressive recovery," *IEEE Transactions on Smart Grid*, vol. 10, no. 6, pp. 6259-6270, Nov. 2019
[61] S. Gottwalt, J. Garttner, H. Schmeck, et al., "Modeling and valuation of residential demand flexibility for renewable integration," *IEEE Transactions on Smart Grid*, vol. 8, no. 6, pp. 2565-2574, Nov. 2017.

[62] M. Pedrasa, T. Spooner, and I. MacGill, "Coordinated scheduling of residential distributed energy resources to optimize smart home energy services," *IEEE Transactions on Smart Grid*, vol. 1, no. 2, pp. 134-143, Sep. 2010.

[63] S. Pal and R. Kumar, "Electric vehicle scheduling strategy in residential demand response programs with neighbor connection," *IEEE Transactions on Industrial Informatics*, vol. 14, no. 3, pp. 980-988, Mar. 2018.

[64] W. Zheng, W. Wu, B. Zhang, et al., "Distributed optimal residential demand response considering operational constraints of unbalanced distribution networks," *IET Generation, Transmission & Distribution*, vol. 12, no. 9, pp. 1970-1979, May 2018.

[65] K. Worthmann, C. Kellett, P. Braun, et al., "Distributed and decentralized control of residential energy systems incorporating battery storage," *IEEE Transactions on Smart Grid*, vol. 6, no. 4, pp. 1914-1923, July 2015.

[66] F. Gazijihani and J. Salehi, "Game theory-based profit maximization model for microgrid aggregators with presence of EDRP using information gap decision theory," *IEEE Systems Journal*, vol. 13, no. 2, pp. 1767-1777, June 2019.

[67] P. You, S. Low, W. Tushar, et al., "Scheduling of EV battery swapping—part I: Centralized solution," *IEEE Transactions on Control of Network Systems*, vol. 5, no. 4, pp. 1886-1897, Dec. 2018.

[68] P. You, S. Low, W. Tushar, et al, "Scheduling of EV battery swapping—part II: Distributed solution," *IEEE Transactions on Control of Network Systems*, vol. 5, no. 4, pp. 1920-1930, Dec. 2018.

[69] R. Takapoui, N. Moehle, S. Boyd, et al., "A simple effective heuristic for embedded mixed-integer quadratic programming," *International Journal of Control*, vol. 93, no. 1, pp. 2-12, 2020.

[70] N. Gatsis, and G. Giannakis, "Residential load control: Distributed scheduling and convergence with lost AMI messages," *IEEE Transactions on Smart Grid*, vol. 3, no. 2, pp. 770-786, Jun. 2012.

[71] S. Boyd, N. Parikh, E. Chu, et al., "Distributed optimization and statistical learning via the alternating direction method of multipliers," *Foundations and Trends in Machine Learning*, vol. 3, no. 1, pp. 1-122, 2011.

[72] S. Kim and G. Giannakis, "Scalable and robust demand response with mixed-integer constraints," *IEEE Transactions on Smart Grid*, vol. 4, no. 4, pp. 2089-2099, Dec. 2013.

[73] X. Fang, B. Hodge, H. Jiang, et al, "Decentralized wind uncertainty management: alternating direction method of multipliers based distributionally-robust chance constrained optimal power flow," *Applied Energy*, vol. 239, pp. 938-947, Apr. 2019.

[74] S. Tsai, Y. Tseng, and T. Chang, "Communication-efficient distributed demand response: A randomized ADMM approach," *IEEE Transactions on Smart Grid*, vol. 8, no. 3, pp. 1085-1095, May 2017.

[75] Y. Wang, L. Wu, and S. Wang, "A fully-decentralized census-based ADMM approach for DC-OPF with demand response," *IEEE Transactions on Smart Grid*, vol. 8, no. 6, pp. 2637-2647, Nov. 2017.

[76] Z. Li, Q. Guo, H. Sun, et al., "ADMM-based decentralized demand response method in electric vehicle virtual power plant," *IEEE Power & Energy Society General Meeting*, pp. 1-5, Jul. 2016.

[77] L. Zhang, V. Kekatos, and G. Giannakis, "Scalable electric vehicle charging protocols," *IEEE Transactions on Power Systems*, vol. 32, no. 2, pp. 1451-1462, Mar. 2017.

[78] M. Farviar, R. Neal, C. Clarke, et al., "Optimal inverter VAR control in distribution systems with high PV penetration," arXiv: 1112.5594v1, Dec. 2011.

[79] B. Cui, F. Chen, J. Munk, et al., "A hybrid building thermal modeling approach for predicting temperatures in typical, detached, two-story houses," *Applied Energy*, vol. 236, pp. 101-116, Feb. 2019.

[80] J. Dong, M. Olama, T. Kuruganti, et al, "Adaptive building load control to enable high penetration of solar photovoltaic generation," *IEEE Power & Energy Society General Meeting*, pp. 1-5, Jul. 2017.

[81] A. Levitt, "Comparing RTO market framework Rules in DER context," [Online] Available: http://www.pjm.com/~/media/committees-groups/committees/mrc/20160824-special/20160824-item-02-der-rto-benchmarking.ashx.

[82] R. Henriquez, G. Wenzel, D. Olivares, et al., "Participation of demand response aggregators in electricity markets: Optimal portfolio management," *IEEE Transactions on Smart Grid*, vol. 9, no. 5, pp. 4861-4871, Feb. 2017.

[83] PJM, "How does PJM make money," [Online] Available: https://learn.pjm.com/who-is-pjm/how-does-pjm-make-money.aspx.

[84] C. Li, X. Yu, W. Yu, et al., "Efficient computation for sparse load shifting in demand response management," *IEEE Transactions on Smart Grid*, vol. 8, no. 1, pp. 250-261, Jan. 2017.

[85] K. Ma, Y. Yu, B. Yang, et al., "Demand-side energy management considering price oscillation for residential building heating and ventilation system," *IEEE Transactions on Industrial Informatics*, vol. 15, no. 8, pp. 4742-4782, Aug. 2019.

[86] B. Rajasekhar, N. Pindoriya, W. Tushar, et al., "Collaborative energy management for a residential community: A non-cooperative and evolutionary approach," *IEEE Transactions on Emerging Topics in Computational Intelligence*, vol. 3, no. 3, pp. 177-192, Jun. 2019.

[87] L. Gan and S. Low, "An online gradient algorithm for optimal power flow on radial networks," *IEEE Journal on Selected Areas in Communication*, vol. 34, no. 3, pp. 625-638, Mar. 2016.

[88] Q. Peng and S. Low, "Distributed optimal power flow algorithm for radial networks, I: Balanced single phase case," *IEEE Transactions on Smart Grid*, vol. 9, no. 1, pp. 111-121, Jan. 2018.

[89] J. Jian, C. Zhang, L. Yang, et al., "A hierarchical alternating direction method of multipliers for fully distributed unit commitment," *International Journal of Electrical Power & Energy Systems*, vol. 108, pp. 204-217, 2019.

[90] G. Liu, T. Jiang, T. Ollis, et al., "Distributed energy management for community microgrids considering network operational constraints and building thermal dynamics," *Applied Energy*, vol. 239, pp. 83-95, 2019.

[91] D. Nguyen, T. Narikiyo, and M. Kawanishi, "Optimal demand response and real-time pricing by a sequential distributed consensus-based ADMM approach," *IEEE Transactions on Smart Grid*, vol. 9, no. 5, pp. 4964-4974, Sep. 2018.

[92] J. Qin, Y. Wan, X. Yu, et al., "Consensus-based distributed coordination between economic dispatch and demand response," *IEEE Transactions on Smart Grid*, vol. 10, no. 4, pp. 3709-3719, Jul. 2019.

[93] GAMS Development Corporation, General Algebraic Modeling System (GAMS) Release 27.1.0, Fairfax, VA, USA, 2019.
[94] M. Baran, and F. Wu, "Network reconfiguration in distribution system for loss reduction and load balancing," *IEEE Transactions on Power Delivery*, vol. 4, no. 2, pp. 1401-1406, Apr. 1989.
[95] National Renewable Energy Laboratory, "National solar radiation data base 1991-2005 update: typical meteorological year 3," [Online] Available: https://rredc.nrel.gov/solar/old_data/nsrdb/1991-2005/tmy3/.
[96] National Renewable Energy Laboratory, "User manual for TMY3 data sets," [Online] Available: https://www.nrel.gov/docs/fy08osti/43156.pdf.
[97] OpenEI, "Commercial and residential hourly load profiles for all TMY3 locations in the United States," [Online] Available: https://openei.org/datasets/files/961/pub/.
[98] A. Piazza, M. Piazza, and G. Vitale, "Statistical processing of data coming from a photovoltaic plant for accurate energy planning," *Renewable Energy & Power Quality Journal*, DOI: 10.24084/repqj06.400, Mar. 2008.
[99] E. Burger and S. Moura, "Generation following with thermostatically controlled load via alternating direction method of multipliers sharing algorithm," *Electric Power Systems Research*, vol. 146, pp. 141-160, May 2017.
[100] G. Pillo and F. Giannessi, Nonlinear optimization and related topics, Boston, MA, USA: Springer, 2000.
[101] S. Mhanna, G. Verbic, and A. Chapman, "Adaptive ADMM for distributed AC optimal power flow," *IEEE Transactions on Power Systems*, vol. 34, no. 3, pp. 2025-2035, May 2019.
[102] F. Chen, F. Li, W. Feng, et al., "Reliability assessment method of composite power system with wind farms and its application in capacity credit evaluation of wind farms," *Electric Power Systems Research*, vol. 66, pp. 73-82, Jan. 2019.
[103] B. Qin, J. Ma, W. Li, et al, "Decomposition-based stability analysis for isolated power systems with reduced conservativeness," *IEEE Transactions on Automation Science and Engineering*, in-press.
[104] Y. Du, and F. Li, "A Hierarchical Real-time Balancing Market Considering Multi-microgrids with Distributed Sustainable Resources," *IEEE Transactions on Sustainable Energy*, vol. 11, no. 1, pp. 72-83, Jan. 2020.
[105] U.S. Environmental Protection Agency, "About the U.S. electricity system and its impact on the environment," [Online] Available: https://www.epa.gov/energy/about-us-electricity-system-and-its-impact-environment.
[106] H. Han, S. Gao, Q. Shi, et al, "Security-based active demand response strategy considering uncertainties in power systems," *IEEE Access*, vol. 5, pp. 16953-16962, Aug. 2017.
[107] X. Fang, Q. Hu, F. Li, et al, "Coupon-based demand response considering wind power uncertainty: a strategic bidding model for load serving entities," *IEEE Transactions on Power Systems*, vol. 31, no. 2, pp. 1025-1037, May 2015.
[108] C. Eksin, H. Delic, and A. Ribeiro, "Demand response management in smart grids with heterogeneous consumer preferences," *IEEE Transactions on Smart Grid*, vol. 6, no. 6, pp. 3082-3094, Nov. 2015.

[109] W. Pei, Y. Du, W. Deng, et al, "Optimal bidding strategy and intramarket mechanism of microgrid aggregator in real-time balancing market," *IEEE Transactions on Industrial Informatics*, vol. 12, no. 2, pp. 587-596, Apr. 2016

[110] X. Kou, and F. Li, "Interval optimization for available transfer capability (ATC) evaluation considering wind power uncertainty," *IEEE Transactions on Sustainable Energy*, vol. 11, no. 1, pp. 250-259, Dec. 2018.

[111] M. Diekerhof, F. Peterssen, and A. Monti, "Hierarchical Distributed Robust Optimization for Demand Response Services," *IEEE Transactions on Smart Grid*, vol. 9, no. 6, pp. 6018-6029, Nov. 2018.

[112] M. Shafie-Khah, and P. Siano, "A stochastic home energy management system considering satisfaction cost and response fatigue," *IEEE Transactions on Industrial Informatics*, vol. 14, no. 2, pp. 620-6029, Nov. 2018.

[113] Z. Chen, L. Wu, and Y. Fu, "Real-time price-based demand response management for residential appliances via stochastic optimization and robust optimization," *IEEE Transactions on Smart Grid*, vol. 3, no. 4, pp. 1822-1831, Dec. 2012.

[114] EPCOR, "Terms and conditions for distribution connection services," Alberta, Canada, 2016.

[115] K. Ma, Y. Yu, B. Yang, et al, "Demand-side energy management considering price oscillations for residential building heating and ventilation systems," *IEEE Transactions on Industrial Informatics*, vol. 15, no. 8, pp. 4742-4782, Aug. 2019.

[116] Y. Chen, and M. Hu, "Swarm intelligence-based distributed stochastic model predictive control for transactive operation of network building clusters," *Energy and Buildings*, vol. 198, no. 1, pp. 207-215, Sep. 2019.

[117] S. Raschka, "Data preprocessing and machine learning with Scikit-Learn," [Online] Available: https://sebastianraschka.com/pdf/lecture-notes/stat479fs18/05_sklearn_slides.pdf.

[118] X. Wang, Z. Hu, M. Zhang, et al, "Two-stage stochastic optimization for unit commitment considering wind power based on scenario analysis," *China International Conference on Electricity Distribution*, pp. 1-5, Aug. 2016.

[119] T. Jiang, H. Chen, X. Li, et al, "Optimal sizing and operation strategy for hybrid energy storage systems considering wind uncertainty," *IEEE Power & Energy Society General Meeting*, pp. 1-5, Aug. 2018.

[120] C. Li, X. Yu, W. Yu, et al., "Efficient computation for sparse load shifting in demand side management," *IEEE Transactions on Smart Grid*, vol. 8, no. 1, pp. 250-261, Jan. 2017.

[121] U.S. Environment Protection Agency, "Electricity consumers," [Online] Available: https://www.epa.gov/energy/electricity-customers.

[122] W. Li, C. Yuen, N. Hassan, et al., "Demand response management for residential smart grid: from theory to practice," *IEEE Access*, vol. 3, pp. 2431-2440, Nov. 2015.

[123] A. Molina, A. Gabaldon, J. A. Fuentes, et al, "Implementation and assessment of physically based electrical load models: application to direct load control residential programmes," *IEE Proceedings – Generation, Transmission and Distribution*, vol. 150, no. 1, pp. 61-66, Jan. 2003.

[124] Y. Sun, M. Elizondo, S. Lu, et al, "The impact of uncertain physical parameters on HVAC demand response," *IEEE Transactions on Smart Grid*, vol. 5, no. 2, pp. 916-923, Mar. 2014.

[125] A. Tascikaraoglu, N. Paterakis, O. Erdinc, et al, "Combining the flexibility from shared energy storage systems and DLC-based demand response of HVAC units for distribution system operation enhancement," *IEEE Transactions on Sustainability Energy*, vol. 10, no. 1, pp. 137-148, Jan. 2019.

[126] E. Rezaei, and H. Dagdougui, "Optimal real-time energy management in apartment building-integrating microgrid with multi-zone HVAC control," *IEEE Transactions on Industrial Informatics*, in press.

[127] T. Wei, X. Chen, X. Li, et al, "Model-based and data-driven approaches for building automation and control," *IEEE/ACM International Conference on Computer-Aided Design*, pp. 1-8, Nov. 2018.

[128] Y. Sun, A. Somani, and T. E. Carroll, "Learning based bidding strategy for HVAC systems in double auction retail energy markets," *American Control Conference*, pp. 1-6, Jul. 2015.

[129] T. Wei, Y. Wang, and Q. Zhu, "Deep reinforcement for building HVAC control," *ACM/EDAC/IEEE Design Automation Conference*, pp. 1-6, Jun. 2017.

[130] L. Yu, W. Xie, D. Xie, et al, "Deep reinforcement learning for smart home energy management," *IEEE Internet of Things Journal*, vol. 7, no. 4, pp. 2751-2762, Dec. 2019.

[131] T. Lillicrap, J. Hunt, A. Pritzel, et al, "Continuous control with deep reinforcement learning," arXiv: 1509.02971, Jul. 2019.

[132] S. Boyd, and L. Vandenberghe, Convex Optimization. Cambridge, U.K.: Cambridge University Press, 2004.

Publications

Journal papers

[J1] **X. Kou**, and F. Li, "Available transfer capability (ATC) evaluation considering wind power uncertainty," *IEEE Transactions on Sustainable Energy*, vol. 11, no. 1, pp. 250-259, Jan. 2020.

[J2] **X. Kou**, F. Li, J. Dong, M. Starke, J. Munk, Y. Xue, M. Olama, and H. Zandi, "A scalable and distributed algorithm for managing residential demand response programs using alternating direction method of multipliers (ADMM)," *IEEE Transactions on Smart Grid*, in press.

[J3] O. Ozmen, J. Nutaro, M. Starke, J. Munk, L. Roberts, **X. Kou**, P. Im, J. Dong, F. Li, T. Kuruganti, and H. Zandi, "Power system simulation testbed for transactive energy management systems," *Sustainability*, in press.

[J4] X. Li, T. Jiang, L. Bai, **X. Kou**, F. Li, H. Chen, and G. Li, "A general optimization model for tracking voltage security region boundary in bulk power grids," *CSEE Journal of Power and Energy Systems*, in revision.

[J5] **X. Kou**, F. Li, J. Dong, M. Olama, M. Starke, Y. Chen, and H. Zandi, "A comprehensive scheduling framework using SP-ADMM for residential demand response with weather and consumer uncertainties," *IEEE Transactions on Power Systems*, under review.

Conference papers:

[C1] Y. Chen, **X. Kou**, M. Olama, H. Zandi, C. Liu, S. Kassaee, B. Smith, A. Abu-Heiba, and A. Momen, "Bi-level optimization for electricity transaction in smart community with modular pump hydro storage," in *ASME International Design Engineering Technical Conferences & Computers and Information in Engineering Conference*, St. Louis, MO, USA, pp. 1-10, Aug. 2020.

[C2] Y. Chen, M. Olama, **X. Kou**, K. Amasyali, J. Dong, and Y. Xue, "Distributed solution approach for Stackelberg pricing game of aggregated demand response," in *IEEE Power & Energy Society General Meeting*, Montreal, QC, Canada, pp. 1-5, Aug. 2020.

[C3] C. Rooks, **X. Kou**, and F. Li, "Interval optimization for robust economic dispatch in active distribution networks considering uncertainty," in *International Conference on Smart Energy Systems and Technologies (SEST)*, pp. 1-6, Porto, Portugal, Sep. 2019

[C4] **X. Kou**, F. Li, J. Dong, M. Starke, J. Munk, T. Kuruganti, H. Zandi, "A distributed energy management approach for residential demand response," in *3rd International Conference on Smart Grid and Smart Cities (ICSGSC)*, Berkeley, CA, USA, pp. 170-175, Jun. 2019.

[C5] T. Jiang, X. Li, H. Chen, R. Zhang, G. Li, **X. Kou**, M. Wang, and F. Li, "Optimal energy storage sizing and siting to mitigate voltage deviation in distribution networks," *in IEEE Power & Energy Society General Meeting*, Atlanta, GA, USA, pp. 1-5, Aug. 2019.

[C6] **X. Kou**, F. Li, and W. Feng, "Transmission constrained economic dispatch via interval optimization considering wind uncertainty," in *IEEE Power & Energy Society General Meeting*, Portland, OR, USA, pp. 1-5, Aug. 2018.

[C7] T. Jiang, H. Chen, X. Li, R. Zhang, **X. Kou**, F. Li, "Optimal sizing and operation strategy for hybrid energy storage systems considering wind uncertainty," in *IEEE Power & Energy Society General Meeting*, Portland, OR, USA, pp. 1-5, Aug. 2018.

[C8] W. Feng, **X. Kou**, Q. Zhang, and F. Li, "Impact of neutral current on cable overloading," in *IEEE PES T&D Conference and Exposition* Denver, CO, USA, pp. 1-9, Apr. 2018.

[C9] Y. Du, F. Li, **X. Kou**, and W. Pei, "Coordinating multi-microgrid operation within distribution system, a cooperative game approach," in *IEEE Power & Energy Society General Meeting*, Chicago, IL, USA, pp. 1-5, Jul. 2017.

[C10] H. Chen, T. Jiang, X. Li, G. Li, X. He, **X. Kou**, L. Bai, F. Li, and X. Fang, "Available transfer capability calculations considering demand response," in *IEEE Power & Energy Society. General Meeting*, Chicago, IL, USA, pp. 1-5, Jul. 2017.

[C11] **X. Kou**, and F. Li, "PQ curve based voltage stability analysis considering wind power," in *4th International Conference on Control, Decision and Information Technologies (CoDIT)*, Barcelona, Spain, pp. 1180-1184, Apr. 2017.

Vita

Xiao Kou joined Dr. Fangxing (Fran) Li's group at The University of Tennessee at Knoxville in January 2016 to pursue his Ph.D. degree in Electrical Engineering. He received his B.S. degree from Beihang University, Beijing, China, in 2012, and his M.S. degree from the University of Denver, Denver, CO, in 2015. His research interests include electricity markets, demand response, and renewable energy integration.